2011

Vibration diagnosis of elastic shafts with a transverse crack

Cai Zhongyi
Edith Cowan University

Edith Cowan University

Copyright Warning

SCHOOL OF ENGINEERING

FACULTY OF COMPUTING, HEALTH AND SCIENCE

EDITH COWAN UNIVERSITY

Vibration Diagnosis of Elastic Shafts with A Transverse Crack

By

Zhongyi Cai

November 2011

This thesis is presented in fulfilment of the requirements for the degree of

Master of Engineering Science

USE OF THESIS

The Use of Thesis statement is not included in this version of the thesis.

ABSTRACT

Detection of the shaft crack in a rotating machine is one of the most challenging problems in equipment predictive maintenance. In the available literature, various crack detection methods have been applied to study the dynamic behaviour of a cracked shaft.

This study sought to attempt a vibration-based method. Elastic shafts with three different types of transverse cracks, including experimentally-induced fatigue crack, welded shaft crack, and wire-cut crack, were fabricated, and used to analyse the bending stiffness and frequency response in the vertical direction. The results from the cracked shafts were compared with that of an intact shaft.

Bending stiffness of different shafts was measured as a function of rotation angle of the shafts. Among the three different crack types, the bending stiffness of the fatigue crack shaft showed a typical breathing behaviour, which was consistent with the previous theoretical results. The welded shaft crack also demonstrated opening and closing characteristics, but the stiffness was found to be much lower compared with that of a fatigue cracked shaft. As for the wire-cut crack, no breathing mechanism was observed for any rotational angle, due to the big width of the gap. Therefore, it is concluded that the fatigue induced crack is the most accurate method to evaluate the vibration characteristics of cracked shafts. Our results also indicated that existing switching model and harmonic models cannot describe the periodic stiffness of a transverse shaft crack accurately.

Modal analysis was carried out on the intact shaft, as well as the three types of cracked shafts. Frequency responses in the X-axis direction were obtained. The correlation between the bending stiffness and the resonant frequency was examined, and it was experimentally proved that the decrease in resonant frequency was almost proportional to the reduction in the stiffness. Also, the amplitude of vibration response was found to be amplified by the crack element. The cause and implications of these results were analysed, and they are expected to deepen our understanding of crack diagnosis using vibration method.

DECLARATION

I certify that this thesis does not, to the best of my knowledge and belief:

- incorporate without acknowledgement any material previously submitted for a degree or diploma in any institution of higher education;
- contain any material previously published or written by another person except where due reference is made in the text; or
- contain any defamatory material.

I also grant permission for the Library at Edith Cowan University to make duplicate copies of my thesis as required.

Date: 8 November 2011

ACKNOWLEDGEMENS

Foremost, I would like to express my deepest gratitude to my supervisor *Dr Helen Wu,* and associate supervisor *Dr Xiaoli Zhao* who steered me in the right direction, guided and supported me throughout this research period. Without their kind assistance and encouragement, this study would have never been accomplished.

A large vote of thanks to the research writing consultants - *Dr Greg Maguire* and *Dr Jo Mcfarlane*, both of them rendered great helps in improving my academic writing skills and made my thesis look presentable.

A special word of appreciation goes to the IT staff, *Mr. Kourosh* and Zhi *Huan Yu*, for their unrelenting support at all times and stages in the development of my thesis. I thank *Mr. Slavko Nikolic* for his assistance in preparation of my research specimens. Also, I would like to thank our library staff - *Mrs Maria Woodhouse* and *Mrs Lyn Leslie* for their great support in searching my research reference material.

Finally, I wish to thank *Professor Daryoush Habibi* for his encouragement and inspiring. Also I would like to acknowledge the supported and invaluable suggestions from my colleagues. Personally, I thank my family for their cooperation and support.

CONTENTS

NOTATION

Basic SI units are given in parentheses.

B	shaft thickness (m)
D	shaft diameter (m)
E	Young's Modulus (N/m^2)
I	shaft cross sectional area moment of inertia (m^4)
K	shaft stiffness (N/m)
K_C	bending stiffness of wire-cut shaft (N/m)
K_F	bending stiffness of fatigue cracked shaft (N/m)
K_{Ic}	metallic materials' fracture toughness ($N/m^{3/2}$)
K_{max}	maximum stress-intensity factor ($N/m^{3/2}$)
k_0	intact shaft stiffness (N/m)
K_R	stiffness matrix of rotating shaft (N/m)
K_W	bending stiffness of welding cracked shaft (N/m)
k_η	shaft stiffness in η direction (N/m)
k_ξ	shaft stiffness in ξ direction (N/m)
L	shaft length (m)
l	crack location from one end of shaft (m)
n	number of cycles for fracture test
P	cyclic bending force (N)
P_{max}	maximum cyclic force (N)
S	support span between two bearings (m)
s	shaft bending stress (N/m^2)
W	support span of the three point bending fixture for fatigue crack (m)
x	X-axis
y	Y-axis
α	shaft crack depth (m)
θ	shaft rotating angle (degree)
σ	applied stress (N/m^2)

LIST OF TABLES

LIST OF FIGURES

CHAPTER 1

INTRODUCTION

1.1 Importance of crack detection

The Diagnosis of shaft cracks in rotating machinery has been a research challenge for both industry and academia for several decades. Such cracks can cause total shaft failure and enormous costs in down time. Accordingly, owners of critical plant machinery are particularly interested in early detection of symptoms that can lead to in-service failure of machinery and equipment. Safe and reliable operation of equipment relies on proactive maintenance aided by newly emerging diagnostic technologies.

There are several predictive maintenance techniques used to monitor and analyse critical rotating machines and equipment in a typical plant. Such as vibration analysis, ultrasonics, thermography, tribology, process monitoring, visual inspection, and other non-destructive analysis techniques (Mobley, 1999). Of these techniques, vibration analysis is the dominant predictive maintenance technique used with maintenance management programs, as it is non-destructive and doesn't interfere with the machine's normal operation.

In the field of vibration condition monitoring, the diagnostics of rotating machinery has been gaining importance in recent years. Shafts are basic components in most high-performance rotating equipment and utility plant, such as high-speed compressors, steam and gas turbines, generators and pumps. Although usually quite robust and well designed, serious defects can develop in shafts without much apparent warning. Total shaft failure can be catastrophic. This study focuses on the characteristic of cracked shafts, and their vibration dynamic behaviour.

There are a few types of shaft cracks which can develop during the operation of rotating machines. The transverse crack remains the most important type of crack as the machine safety is significantly influenced by its occurrence. The study of transverse cracks has been extensive because, being perpendicular to the shaft they reduce the cross-sectional area and result in significant damages to rotors. Many factors can influence the occurrence of shaft cracks. (Please see Chapter 2 and Sabnavis *et al*, 2004). A transverse crack caused by material fatigue (Fig. 1.1.) is a very common defect in rotating equipment that operates for extended periods under heavy load. A rotating shaft is subjected to different types of mechanical stresses, such as bending, torsional, shear, and static radial loads. A crack will be initiated in the local region where stresses exceed the yield strength of the shaft material, which may have already been reduced due to fatigue. As the crack grows to a certain depth, the shaft cannot support the static and dynamic loading any more. Consequently, the shaft would often experience a sudden fracture, causing enormous costs in down time and possible injuries to people.

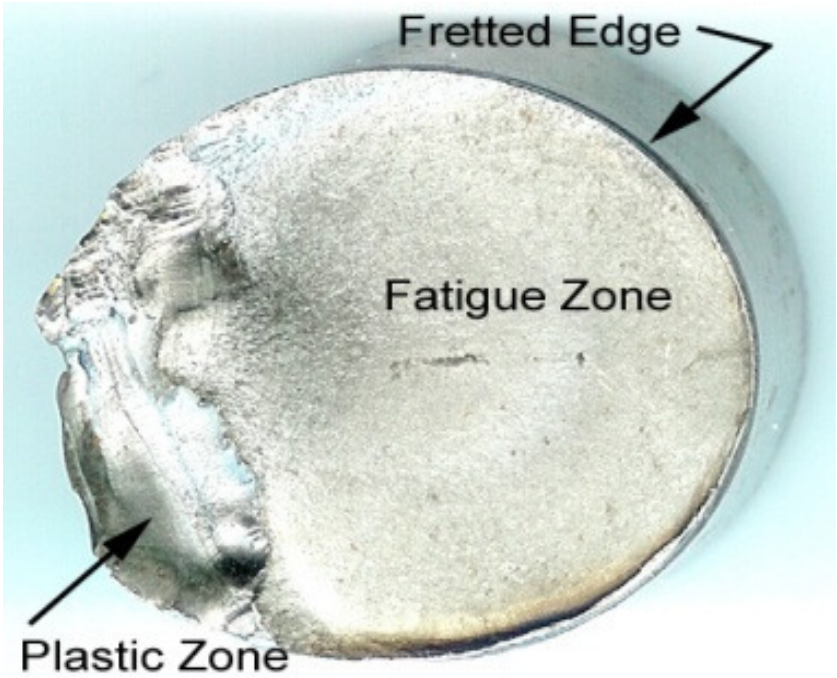

Fig.1.1.The cross-sectional view of a shaft with fatigue crack

1.2 Crack detection techniques

Shaft crack detection techniques adopted in the literature can be broadly grouped into two methods: vibration-based and model-based methods (Papadopoulos, 2008).

The former relies on detecting changes in vibration signals as a crack in a structure tends to modify its dynamic characteristics such as the natural frequencies and mode shapes. Conversely, through monitoring the trend changes in measurements of the natural frequencies and mode shapes of a rotating shaft over time, a crack present in the shaft could be predicted. The stiffness of a shaft is reduced by a crack and consequently the shaft's Eigen-frequencies decline. Measuring these changes can help with identifying an early stage crack (Sekhar and Prabhu, 1992). Unfortunately, the available indicators cannot reliably differentiate a cracked shaft from other problems that create similar vibration spectra and waveforms, such as a misaligned or unbalanced shaft. Thus, to develop more reliable diagnostic methods, a thorough understanding of periodical stiffness of a cracked shaft is necessary.

The model-based methods are based on analytical or numerical models to simulate the behaviour of cracked shafts during rotation. In model-based identification, the fault-induced change in the rotor system is taken into account by equivalent loads in the mathematical model. These equivalent loads are virtual forces and moments acting on the linear undamaged system to generate a dynamic behaviour identical to that measured in the damaged system. However, the approximations and assumptions used in the model-based approaches could lead to large errors for the analysis of cracked shaft dynamic behaviour. Specifically in consideration of cracked shaft stiffness, the stiffness parameters used in some of the models do not really reflect its periodic change at different rotation angles.

1.3 Objectives and Scope of the Present Work

In available literature, various crack detection methods have been applied to study the dynamic behaviour of a cracked shaft and major progress has been made during the past 40 years (Kumar and Rastogi 2009). Many crack detection diagnostic techniques have been developed based on linear fracture mechanics and rotor dynamics theories. Specifically, the dynamic behaviour of cracked shafts has helped predict the presence of a crack in a rotating system. However, a more accurate and reliable technique is required to predict the generation and propagation of a crack in a rotating shaft. One limitation is that there is no universal method or algorithm to identify a specific type of shaft crack. The damaged shafts used for studying vibration characteristics in many papers did not reflect real world fatigue cracks. Few model analysis methods are based on true "online" operating conditions. Instead, numerical or analytical studies, based on mathematical models are used and rarely involve subsequent experimental verification.

Analysing the periodic variation of a cracked shaft's stiffness is the key step in understanding its dynamic behaviour (Al-Shudeifat and Butcher 2011). When a cracked shaft rotates, the crack opens and closes during each revolution, that is, it breathes. And this creates stiffness variation of the shaft at various rotational angles (Dimarogonas 1996). Accurate stiffness values for a cracked element is essential for simulating the vibration responses of a cracked shaft, or for establishing a more accurate cracked rotor model. However, there has been insufficient experimental investigation of how the shaft crack breathing mechanism interacts with the change of stiffness during each revolution.

This work uses AISI 1030 steel as the specimen shaft material, and generates three different types of elastic shaft specimens with a transverse crack depth of 40% of the shaft diameter along the radial direction. It involves a detailed study of the characteristics of cracked shafts by measuring the variation in stiffness during each revolution, and analysing the vibration behaviour of the elastic cracked shafts, and then comparing these results with data for an intact

shaft. The aim is to identify a unique vibration signal that will be able to reflect the dynamic behaviour of a cracked shaft. An attempt is made to develop a more effective cracked shaft monitoring technique that can detect emerging problems and avoid catastrophic failures. The major objectives of this study are to:

- Conduct a critical review of the literature relating to vibration detection techniques for cracked shafts in rotating machinery.
- Create three different types of elastic cracked shaft specimens, and specifically a fatigue crack.
- Measure and investigate the stiffness of different types of elastic cracked shafts from different rotational angles at a quasi-static loading in a three-point bending fixture using an Instron 5569 machine.
- Perform vibration signal analysis on the shafts using a Spectraquest's rotor Machinery Fault Simulator (MFS). This will involve multiple tasks:

    - Applying the latest Modal Test Consultant (MTC) program with hammer excitation tool, to measure and record data from multiple channels of frequency responses and time domains, such as transfer function, acceleration signals in different directions;
    - Using the Brüel & Kjær PULSE software package to define, analyse and contrast the first natural frequency of cracked shafts;
    - Comparing these results with equivalent data of an intact shaft.

1.4 Publications

During the progress of research work, attempts have been made to prepare the manuscripts of research papers based on the thesis work for publication in journals/conference proceedings. The details of the accepted papers are as follows:

Helen Wu, Zhongyi Cai, Keqin Xiao (2011). An Experimental Study of Breathing Mechanism for the Transversely Cracked Shafts. *Advanced Materials Research* (in print).

Zhongyi Cai, Helen Wu, Xiaoli Zhao and Jianping Zhang (2011). Bending Stiffness Analysis of Elastic Shafts with three Types of Transverse Cracks. *Advanced Materials Research* (in print).

1.5 Organisation of Thesis

The general details of the thesis are described in this chapter. Chapter 2 presents a critical review of the literature on the types of shaft cracks, their causes, the characteristics of cracked shafts and the different methods that have been applied for shaft crack diagnosis. The review establishes the need for this research and the appropriateness of methods chosen. The configuration and preparation of the three different types of cracked shaft specimens are described in Chapter 3. Details of experimental study of the bending stiffness of the cracked and intact shafts are reported in Chapter 4. Vibration signal analysis of the dynamic behaviour of cracked and intact shafts is presented in Chapter 5, to help provide a basis for practical maintenance programs. The summary and general conclusions along with future recommendations are presented in Chapter 6.

CHAPTER 2

LITERATURE REVIEW

2.1 General

Cracks in shafts have long been identified as one of the main safety problems of operating turbo-machines (Dimarogonas 1970). Crack generation in a shaft is a process in which fractures grow slowly. If a shaft crack goes undetected in an operating machine, it grows continuously, so that the reduced cross section of the rotor eventually is unable to withstand the dynamic loads applied to it. When this happens, the rotor will very rapidly fail in a brittle fracture mode once the crack reaches a critical size. This sudden failure releases a large amount of energy that is stored in the rotating system. This can sometimes result in serious injury or costly disruptions to the process. Clearly, detecting shaft cracks is an important issue.

In spite of the great advances made in the areas of metallurgy, manufacturing and design, cracked shafts still pose a great threat in manufacturing / process plants. This has stimulated ongoing research into cracked shaft detection and diagnostics, with more than 500 technical papers having been published in English alone in the past 30 years (Sabnavis *et al*. 2004). Various on-line and off-line analysis techniques have been developed to effectively detect cracks before they cause failure.

"The dynamic behaviour of a rotating shaft with a transverse crack" has been studied since the late 1960's (Dimarogonas and Papadopoulos 1983). The approaches for detecting cracked shafts during the operation of equipment in the power industry were initiated about forty years ago in response to a very damaging systems failure. (Dimarogonas 1996) and are ongoing.

Some of the excellent review papers that have appeared, include Wauer (1990), who reviewed the dynamics of a cracked rotor, modelled the cracked portion within the structure, and developed detection methods for diagnosing fracture damage.

Similarly, Gasch (1993) provided a comprehensive survey based on a simple Laval rotor (one disk on an elastic shaft), this included the stability behaviour of a rotating shaft with a crack, the forced vibrations due to imbalance and the crack, and potential early crack detection.

Dimarogonas (1996) reviewed the vibration of cracked structures and reported that the vibration response of a cracked structure was affected due to the greater flexibility occurring around such faults. Two new harmonics were found in addition to the second rotational harmonic and the sub-harmonic at critical speed. Moreover, the opening and closing mechanism of cracks in a rotating shaft is highlighted as an area that warrants further investigation.

In Sabnavis *et al.* (2004) literature review paper, they summarized the information and papers on cracked shaft detection and diagnostics developed after 1990. The types and causes of shaft cracks were addressed. Different shaft crack detection methods were grouped and briefly outlined.

Carden and Fanning (2004) reviewed vibration-based condition monitoring in terms of its applications and relevance to structural engineering. The two common vibration analysis techniques, for structural damage or degradation, were based on natural frequencies or mode shape. The former yielded encouraging results with filtering out the effects from the environment. However, it was argued that techniques involving identification algorithms were usually more successful when structural damage was limited to a few locations. Moreover, the most effective applications have been limited to small structures that have been tested in a laboratory. It is not suitable for the frequency shifts alone for damage identification in whole structures, as the result was not promising. The latter usually compared two sets of mode shapes either by the

Modal Assurance Criteria (MAC) or Coordinate Modal Assurance Criterion (COMAC). The MAC value can be used for indicating the level of similarity between two mode shapes. A 1 value is a perfect match and 0 indicates complete dissimilarity. Thus, a reduction of the MAC value may indicate damage. "The COMAC is a point-wise measure of the difference between two sets of mode shapes and takes a value between 1 and 0. A low COMAC value would indicate discordance at a point and therefore is a possible damage location indicator."

Carden and Fanning argued that it was more efficient to compare mode shapes than to analyse changes in natural frequencies, associated with cracks. Their review revealed numerous and diverse algorithms for vibration based condition monitoring, which utilized data from time, frequency and modal domains. They suggested that using more sensors to enhance this data set would improve crack damage detection.

Papadopoulos (2008) reviewed linear fracture mechanics and rotor dynamic theories for modelling cracks in rotors, including the Strain Energy Release Rate (SERR) theory developed by the founder of fracture mechanics, Alan Arnold Griffith. "The SERR is the amount of energy, perunit length along the crack edge that is supplied by the elastic energy in the body and by the loading system in creating the new fracture surface area." (See page 763). The key formula for connecting fracture stress to crack size for brittle materials, the foundation of fracture mechanics, was

$$\sqrt{GE} = \sigma\sqrt{\pi\alpha} \qquad (2.1)$$

where E is Young's Modulus, G is SERR, σ is the applied stress, and α is half the crack length.

The SERR approach has been widely applied over 30 years to calculate the compliance flexibility that leads to a transverse crack in a rotating shaft. To model the exact position of the crack, the local compliance has been further applied to the shaft and rotor for six degree of freedoms (DOFs).

However, the SERR approach does not take into account any friction and the impact on the cracked area, as the crack breathes under load while the shaft rotates. “The hysteretic damping of the rotor and the temperature near the crack tip are expected to be influenced by the crack propagation, especially under medium and high stresses” (See Papadopopous, 2008). Moreover, it is hysteretic damping in that the retarding force is proportional to the velocity and inversely related to the frequency of the vibration.

Most recently, Kumar and Rastogi (2009) briefly reviewed the dynamics of a cracked rotor. The different modelling approaches that have been applied to a cracked rotor were addressed, including, the Hilbert- Huang Transform (HHT); Wavelet Transform and the Finite Element Approach. Some of the new analytical techniques included were, extended lagrangian mechanics, genetic algorithm analysis, and a least squares identification method. The two key conclusions made were that the crack breathing mechanism is the crucial element for modelling in an accurate crack model; and that the finite element method addresses the local compliance matrix more effectively. The latter has been applied by various researchers to study the dynamic behaviour of a shaft with different types of crack, for example, transverse crack, helicoidal crack and slant crack.

2.2 Cause of shaft cracks

The initiation and propagation of a shaft crack is a complex process that arises from machining imperfections. “Cracks may be caused by mechanical stress raisers, such as sharp keyways, abrupt cross-sectional changes, heavy shrink fits, dents and grooves, or factors such as fretting and/or metallurgical factors such as forging flaws, inclusions, porosity and voids.” (Sabnavis *et al*. 2004).

A rotating shaft is always subjected to different types of stresses such as bending, torsional, shear, and static radial loads. When shafts are rotating under a continuous heavy load, cracks will be initiated in the local region where stresses exceed the yield strength of the shaft material, which may have been impaired by fatigue. In most rotor systems, the stress field contains a mixture of bending and

torsional stresses. If the shaft is subjected only to bending stresses, it is possible that a transverse crack will be developed. If there is a pure torsional stress, most probably a helicoidal crack will be formed. However, in rotating machinery, bending stress is usually the dominant component, thus a transverse crack will occur.

When a crack is initiated, a few factors will affect the crack growth rate. In certain conditions, crack propagation can be accelerated by:

- Thermal stresses;
- Environmental: such as exposure to corrosive mediums;
- Welding heat affected zones(HAZs) in the rotor material;
- The presence of any residual stresses or non-homogeneity in the rotor material;
- Operating faults.

2.3 Types of shaft cracks

In the literature, based on the crack geometries, cracks are broadly classified into the following three groups:

- **Transverse cracks** (Fig. 2.1) This type of crack is perpendicular to the shaft axis. They reduce the shaft cross-sectional area and result in significant damages to rotors. These are the most serious and most common defects. Thus, they have been extensively studied by the most past and current researchers ((Gasch 1993), (Dirr 1994), (Han 2007) and (Al-Shudeifat and Butcher 2011)).

- **Longitudinal cracks**. This type of crack is parallel to the shaft axis and is relatively rare and less serious.

- **Slant cracks**. This type of crack is at an angle to the shaft axis. It doesn't occur very frequently, but could appear in industrial machine shafts. Slant cracks are the same as "helicoidal cracks" (Bachschmid*et al*. 2008) and

mainly influence the torsional behaviour of the rotor in a manner quite similar to the effect of transverse cracks on the lateral bending behaviour. A previous researcher (Sekhar *et al.* 2005) concluded that the slant crack's effect on lateral vibration is less than that of a transverse crack.

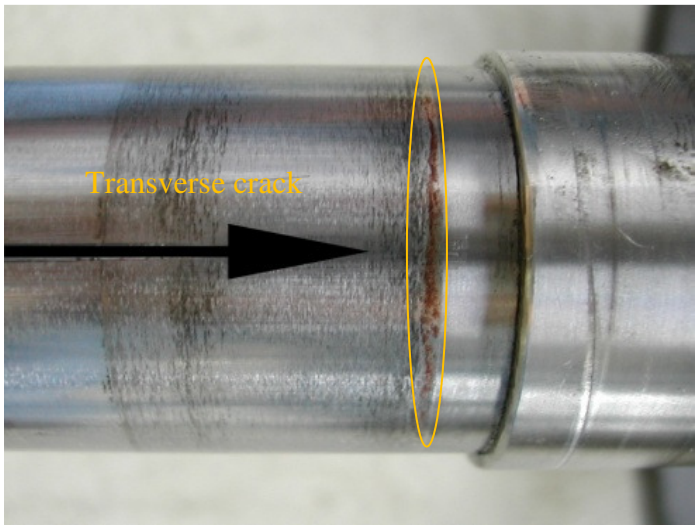

Fig.2.1. A transverse crack

There are some other crack names used by earlier researchers. The "circumferential crack" (Dimarogonas and Papadopoulos 1983), "Gaping cracks" in some journal papers refer to cracks that always remain open. These are more correctly called "Notches". The open crack model presented in (Papadopoulos 2008) was based on a gaping crack. The crack was defined as remaining open in each revolution. Some previous researchers experimentally studied a shaft crack through generating a notch on a shaft specimen. The results were debated since it may not reflect the real shaft crack's nature.

Another name frequently seen in the literature is "crack breathing". When the shaft is rotating, the crack opens and closes according to the stresses developed around the cracked surface (Al-Shudeifat and Butcher 2011). The crack remains open when the affected part of the material is subjected to extensive stresses; the reverse occurs under compressive stresses. This is known as the crack breathing mechanism. In recently published journal papers about

cracked shaft detection diagnostics (Han 2007), the breathing mechanism of a transverse crack in an elastic shaft has been extensively researched.

In this work, three different types of transverse cracked shaft specimens were explored experimentally by investigating how the shaft crack breathing mechanism interacted with the changes in shaft stiffness during each revolution.

2.4Characteristics of a cracked shaft

Crack breathing is one of the popular approaches for studying the dynamics of a cracked shaft by many researchers (Sekhar 2005). During each revolution, the crack opens and closes gradually, in other words, it breathes during shaft rotation. In large industrial turbine-generator rotors, static deflection often dictates shaft vibration patterns. If any cracks are present in this kind of rotor, the crack will open and close according to the shaft rotation (Pennacchi *et al.* 2006).

Crack breathing behaviour lead to changes in one of the shaft mechanical properties-stiffness (Mayes and Davis 1984). An intact shaft's stiffness normally remains the same value at different angles of rotation. However, when a shaft has a crack, the shaft stiffness will change periodically at different rotational angles. At a certain angle, when the stresses on a crack surface are compressive, the crack remains closed and the shaft has almost the same stiffness as an intact shaft. When the stress becomes extensive, the crack will open, in which case the stiffness of the shaft is reduced significantly. (Papadopoulos 2008) also addressed an intermediate situation between the fully open and fully closed state. That is, a partially opened or partially closed crack.

This breathing phenomenon is one of the crucial characteristics of the cracked shaft. It attracts many researchers to focus on it for the study of cracked shaft diagnostics. However, it is not yet fully understood how partial crack closure interacts with changes in shaft stiffness, and further, to key variables of the crack detection problem. "Crack breathing mechanism plays an important role in the analysis of dynamic behaviour of a cracked rotor. This breathing phenomena must

be modelled accurately to detect the crack in a rotor" as per Kumar and Rastogi (2009).

2.5 Identification methods

In the references, shaft crack identification methods are generally divided into three groups:

- Vibration-based approaches;
- Model-based approaches;
- Other approaches.

In Sabnavis *et al*. (2004) review, the emphasis was on crack detection in shafts by using (1) vibration-based methods (direct signal measurement or set up a crack model), (2) modal testing (through measuring mode shape or natural frequency changes, response to special input excitation, any changes of these measurements could be associated with crack development.) and (3) non-traditional methods (fuzzy logic, genetic algorithms, etc.).

2.5.1. Vibration-based approaches

This signal based method can be broadly categorized as follows:

a) Frequency measurements-based identification;
b) Mode shape or response-based identification;
c) Harmonic excitation or external excitation-based identification;
d) Wavelet transforms;
e) Others.

In vibration-based identification, a common non-destructive evaluation procedure for detecting a crack location and size is to measure the natural frequency response of the structure with cracks. As mentioned previously, a cracked structure will have reduced stiffness and increased damping. As

mentioned in vibration theory, the stiffness reduction is related to the decrease in natural frequencies observed and modified the vibration modes of the structure.

A significant portion of the published literature on crack detection and diagnostics focuses on this direct signal measurement technique. Sekhar and Prabhu (1992) applied vibration analysis in their paper- "crack detection and vibration characteristics of cracked shafts". And they claimed that the significant changes of natural frequencies and the differential of these could be applied to crack detection. They also found that the results are more appreciable for cracked shafts with low slenderness ratio L/D.

Bachschmid *et al*. (2000) promoted a method for assessing the location and depth of a transverse crack in a shaft, by using vibration measurements. The literature and field experience support the conclusion that a transverse crack modifies the dynamic behaviour of the rotor, by generating periodic vibration, with 1x, 2x and 3x revolution components in a horizontal axis shaft. The crack's location is identified using a modal technique in the frequency domain. "The crack depth is calculated by comparing the static bending moment, due to the rotor weight and to the bearing alignment conditions, to the identified 'equivalent' periodic bending moment, which simulates the crack." The authors validated this method through experimental results obtained on a test-rig.

Some authors combined the natural frequency data with a Finite Element Model (FEM) for a better result. Lee and Chung (2000) presented the basic method by comparing the contour graph of the first two structural natural frequencies to analyse the crack depth and location, using the FEM method. This was done by defining the intersecting point of the highest amplitude that corresponded to the measured Eigen-frequency variations caused by the crack presence.

Mode shape and response-based identification are other vibration signal approaches adopted by many published papers for shaft crack identification.

Mohiuddin and Khulief (2002) have presented a signal-based method through analysis of the Dynamic Response of a cracked shaft.

Dong *et al*. (2004) studied the open crack of a static state rotor through vibration analysis using a continuous model and parameter identification. Under the conditions that the cracked rotor has a circular cross-section, fracture mechanics methods were applied to model the cracked region as a local flexibility. They reported that the crack location and depth can be predicted "by measuring the deflection at two symmetric points and using the contour method of identification."

Identification based on harmonic or external excitation was achieved by Collins *et al*. (1991) who presented an axial impulse methodology for identifying cracks in rotating shafts. They presented the coupled equations of motion of a rotating shaft due to the presence of the crack. The system of differential equations of motion with cyclic axial impulses as excitations was then solved. Their proposed methodology for the detection of cracks was based on the difference of an axial frequency spectrum of a cracked rotating shaft, compared to an un-cracked shaft. Their study, however, did not include the time response or frequency response of the shaft due to any excitation in the bending directions.

Ishida and Inoue (2006) have reported a harmonic excitation method for "detection of a rotor crack based on nonlinear vibration diagnosis." In their paper, a harmonic excitation force was applied to the cracked rotor and its excitation frequency responses were investigated, and the nonlinear resonances due to the crack were analysed.

Wavelet transforms is another signal-based method that has been widely adopted by many authors. Prabhakar *et al.* (2001) have applied a continuous wavelet transform (CWT) to diagnose cracks in a rotor from time domain signals. Zou *et al.* (2002) through the continuous wavelet time—frequency transform, compared the wavelet time-frequency properties of the un-cracked rotor and the cracked rotor, and the difference in wavelet time-frequency properties of the

cracked to the un-cracked rotor was discussed. However, Nagaraju *et al.* (2009) considered that most of the crack detection works reported in the literature used either 1D wavelets or 2D wavelets (CWT). The crack detection from the signals is dependent on time as well as frequency. So, even the 2D wavelets are not efficient enough to detect a crack. The authors presented a 3D wavelet (CWT) which proved to be less sensitive to noise disturbance, as extra noise in the signal may affect the result's accuracy. By doing that, they claimed a better signal was achieved. The time and frequency features of the crack were clearly identified.

Others signal-based applications like Guo and Peng (2007) used the Hilbert-Huang transform to detect and monitor a small transverse crack in a rotor during the start-up phase by capturing transient responses. Sinha (2007) presented another signal processing tool -Higher order spectra (HOS) for identifying the presence of a breathing transverse crack. The principle of this method is based on the higher harmonics in a signal. This is typical of non-linear dynamic behaviour in mechanical systems. A transverse crack which breathes during shaft rotation also exhibits non-linear behaviour. However, as the author comments, the experiments were conducted on a small rig, the test results obtained need an enhancement to increase the confidence level in the diagnosis.

Prabhakar *et al.* (2001) suggested measuring mechanical impedance for detecting and monitoring cracks in rotor-bearing systems. The authors found that the mechanical impedance changes substantially due to the crack and follows definite trends with the crack parameters (depth and location) and force location. The normalized mechanical impedance of a rotor system is more sensitive to a breathing crack than an open crack. Sudden changes in mechanical impedance are observed at multiples of the running frequency for the breathing crack.

2.5.2. Model-based approaches

Model-based identification methods differ from signal-based monitoring systems, in that continuously recorded vibration signals are used. These methods can be used individually or in combination (A. S. Sekhar 2004). Many model-based

approaches have been reported in the literature for modelling cracks in rotating shafts. These methods applied analytical or numerical models to simulate the dynamic behaviour of cracked shafts during rotation. In model-based methods, equivalent loads are incorporated in the mathematical model to simulate the fault-induced change in the rotor system. "These equivalent loads are virtual forces and moments acting on the linear undamaged system to generate a dynamic behaviour identical to that measured in the damaged system." (Papadopoulos 2008).

The main idea in modelling the crack is to introduce a local compliance Matrix. Penny and Friswell (2003) presented the three well-known simple crack models- (1) The hinge model, (2) The Mayes model and (3) The Jun *et al*. Model. Based on a Jeffcott rotor, they analysed the stiffness matrix of a rotating shaft when the crack was at the open and closed states.

In the hinge model, it is assumed that the crack changes abruptly between closed to open states when the shaft rotates, and vice-versa. The stiffness matrix in rotational coordinates (ξ, η), due to a crack is

$$\mathrm{K}_R = \begin{bmatrix} k_\xi(\theta) & 0 \\ 0 & k_\eta(\theta) \end{bmatrix} \tag{2.2}$$

Thus, in the hinge model the variable stiffness $k_\xi(\theta)$ and $k_\eta(\theta)$ are defined by

$$k_\xi(\theta) = \begin{cases} k_0, & -\frac{\pi}{2} \le \theta < \frac{\pi}{2} \\ k_\xi, & \frac{\pi}{2} \le \theta < \frac{3\pi}{2} \end{cases} \tag{2.3a}$$

and

$$k_\eta(\theta) = \begin{cases} k_0, & -\frac{\pi}{2} \le \theta < \frac{\pi}{2} \\ k_\eta, & \frac{\pi}{2} \le \theta < \frac{3\pi}{2} \end{cases} \tag{2.3b}$$

Where θ is the angular position of the crack, k_0 is the stiffness of the shaft when the crack is closed and k_ξ and k_η are the stiffness in the ξ and η directions when

the crack is open. When the crack is closed, its stiffness is equal to that of an equivalent intact shaft.

In the Mayes model, the stiffness $k_\xi(\theta)$ and $k_\eta(\theta)$ are defined as follows:

$$k_\xi(\theta) = \tfrac{1}{2}\left(k_0 + k_\xi\right) + \tfrac{1}{2}\left(k_0 - k_\xi\right)\cos\theta \tag{2.4a}$$

And

$$k_\eta(\theta) = \tfrac{1}{2}\left(k_0 + k_\eta\right) + \tfrac{1}{2}\left(k_0 - k_\eta\right)\cos\theta \tag{2.4b}$$

The Jun *et al.* Model (cited by Penny and Friswell, 2003) applied the equations of motion for a simple rotor with a breathing crack. Based on fracture mechanics, the cross coupling stiffness and the direct stiffness are estimated when the crack opens and closes. Thus, the stiffness matrix in rotational coordinates were rewritten as

$$\mathrm{K}_R = \begin{bmatrix} k_{\xi\xi}(\theta) & k_{\xi\eta}(\theta) \\ k_{\eta\xi}(\theta) & k_{\eta\eta}(\theta) \end{bmatrix} \tag{2.5}$$

In these three crack models, stiffness variation was considered as a function of the opening and closing of the crack. However, for both the hinge model and Mayes model, no direct relationship between the shaft stiffness and the depth of crack was reported. Although the Jun *et al.* model has improved on this defect at a particular rotation angle by taking into account the shaft length and diameter, the modulus of elasticity of the shaft material, the depth of the crack and the lateral force. The three models simplified the breathing crack model to a switching crack model (crack switched from open state to closed state abruptly). There is a lack of investigation into the breathing crack in a partially open and partially close state. It is clear that the switching crack model cannot reflect the real nature of crack stiffness variation with rotational angles, as the crack remains in a partially open (or closed) state most of the time during rotation.

Most recently, an actual breathing mechanism of the breathing crack model has been proposed by Al-Shudeifat and Butcher (2011). A new breathing function of the breathing crack was reported. This new model applied the finite element method, established the correct periodically time-varying stiffness matrix, and formulated and incorporated it into the global stiffness matrix. This approach drew on Mayes and Davis's (1984) concept of a local reduction of the crack area moment of inertia.

Sekhar (2004) has also promoted a model-based approach for identifying cracks in a rotor system. In this paper, the finite element method has been used to model the rotor, while the crack was indicated by changes in local flexibility.

Pennacchi *et al.* (2006) applied a model-based approach to identify the dynamical behaviour of a cracked shaft, experiments were conducted on a large test rig to validate this method. The results obtained, according to the authors, are more accurate. However, the artificial cracks they generated cannot reasonably represent the dynamic behaviour of a fatigue crack.

Investigation through the Finite Element Method (Fig.2.2) is another popular modal-based approach, which has been widely adopted in the published literature. Dirr *et al.* (1994) focused on "detection and simulation of small transverse cracks in rotating shafts." In their work, a finite element model was developed for numerical simulation of the dynamic behaviour of a cracked rotor.

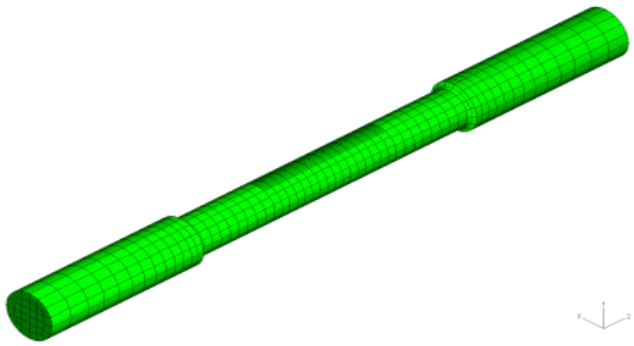

Fig.2.2.A shaft Finite Element Model (FEM)

Chan and Lai (1995) presented the FE-based simulation of a shaft with a transverse crack. They analysed different cases of cracked and un-cracked shafts, and claimed the results can be used as a reliable indicator for shaft crack detection in symmetric rotors.

Darpe (2007) presented an investigation of the dynamics of a simple Jeffcott rotor model for a slant crack. A flexibility matrix of such a cracked rotor was developed. In the equations of motion, the stiffness coefficients based on the flexibility values were used. Slant and transverse cracks can be compared via flexibility and stiffness coefficients and the unbalanced response characteristics. The author concluded that the rotor with a slant crack was "stiffer in lateral and longitudinal directions, but more flexible in torsion compared to the transverse cracked rotor."

2.5.3. Other approaches

Other than the above mentioned techniques, there are some non-traditional techniques and methodologies reported in the literature for analysing the dynamics of a cracked rotor.

He *et al.* (2001) applied a genetic algorithm method together with finite element methods to detect cracks in a shaft. As the authors state, genetic algorithms avoid some of the weaknesses of traditional gradient based analytical search methods including the difficulty in constructing well-defined mathematical models directly from practical inverse problems. They also claimed that the genetic algorithm method can predict shaft crack locations.

Lebold *et al.* (2004) used a non-intrusive torsional vibration analysis as a synergistic method for crack detection in rotating equipment.

Yu *et al.* (2006) presented an artificial neural network with a back-propagation learning algorithm and modal analysis via finite element model of a

cracked rotor system. They claimed that this method is a fast and highly accurate identification technique for a crack fault in rotating machinery.

Strategies based on Lagrangian mechanics are rarely reported, yet, they provide remarkable insight into the dynamics of a cracked rotor system. This approach uses classical Lagrangian equations as an extension of Noether's theorem (Kumar and Rastogi 2009).

A combined approach (vibration signal-based and model-based) for crack detection has been proposed by A. S. Sekhar (2004). This approach modelled the rotor using FEM, while the fault nature and symptoms of the model are characterized using a Fast Fourier Transform (FFT) or an advanced signal processing tool- Continuous Wavelet Transform (CWT). It was found that the accuracy for shaft crack identification with this method has been improved.

Other methods, such as neural networks, fuzzy logic, borescope inspection and sophisticated signal processing techniques, etc, were reviewed and summarized in the review by Sabnavis *et al.* (2004).

2.6 Concluding remarks

A brief literature review on types of cracks, causes of cracks, the unique characteristics of the crack breathing mechanism and various crack identification methods has been attempted in the above. It indicates that the area of crack detection is active and continuously evolving. However, there is no accepted algorithm or technique, which can be applied to detect all the different types of cracks in rotating equipment. Updated methods are emerging as further insight and new knowledge are gained in the machine condition monitoring field.

Although many analytical, numerical and experimental investigations of shaft cracks have been reported in the literature, a comprehensive crack detection theory has yet to emerge. Many technical challenges remain unresolved, especially for how the closing and opening of a crack affects the shaft stiffness

during rotation. Moreover, accurate modelling techniques are needed for the crack breathing mechanism, so that the actual fatigue that leads to a crack in a rotating shaft is incorporated.

In contrast with the model-based methods, the vibration-based methods rely on hardware such as sensors, and analysers. With the latest technologies developed in this area, an effort is made by current researchers to search for an efficient way of shaft crack detection. In the present study, the vibration signal identification method is explored by conducting experiments using a SpectraQuest's rotor Machinery Fault Simulator (MFS), and the latest analysis program (Brüel & Kjær PULSE Modal Test Consultant (MTC) with hammer excitation tool). With these available powerful tools, cracked shaft vibration diagnosis can be conducted both online and offline. This system allows up to 10 replicate analyses. The results are expected to be more feasible and applicable. Also, an Instron universal testing machine will allow robust exploration of the interaction between the breathing mechanism of a transverse crack shaft and it's bending stiffness.

CHAPTER 3

CREATION OF SHAFT CRACKS

3.1 General

3.1.1 Shaft material selection

The material used for generating the cracked shaft specimens in this work was AISI 1030 carbon steel (Fig. 3.1.). The basic material properties of AISI 1030 carbon steel are shown in (Table 3.1, 3.2 & 3.3) [BOHLER UDDEHOLM's materials data sheet].

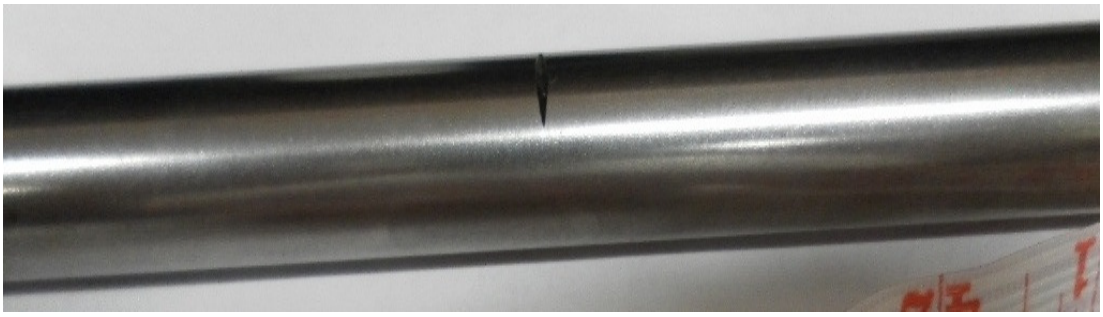

Fig.3.1. AISI 1030 carbon steel shaft specimen

TABLE 3.1 AISI 1030

Category	Steel
Class	Carbon steel
Type	Standard
Designations	*Germany*: DIN 1.1172 *Italy*: UNI CB 35 *United States*: ASTM A108, ASTM A512, ASTM A682, ASTM E399, FED QQ-S-635 (C1030), FED QQ-S-700 (1030).

TABLE 3.2 Material compositions

Element	C	Si	Mn	P	S
Weight %	0.30	0.25	0.75	0.04	0.04

TABLE 3.3 Mechanical properties

Properties		**Condition** (Temp.°C)
Density (× 1000 Kg/m^3)	7.7 - 8.03	25
Poisson's Ratio	0.27 - 0.30	25
Elastic Modulus (GPa)	190 - 210	25
Tensile Strength (MPa)	463.7	25
Yield Strength (Mpa)	341.3	25
Elongation (%)	31.2	25

This material was chosen based on the following criteria: firstly it was referred to by the American Society for Testing and Materials (ASTM) as the standard for shaft material (0.3-0.6% Carbon); secondly, its application is widely reported in journal papers on crack detection and vibration analysis.

3.1.2 Shaft dimension and crack allocation

The specimen shaft will be fixed into a SpectraQuest's rotor Machinery Fault Simulator (MFS, Fig. 3.2.) for vibration analysis. Therefore, the shaft dimension will be based on an actual rotor shaft size, with a total of length $L = 542mm$, and a shaft diameter of$D = 15.875\ mm$.

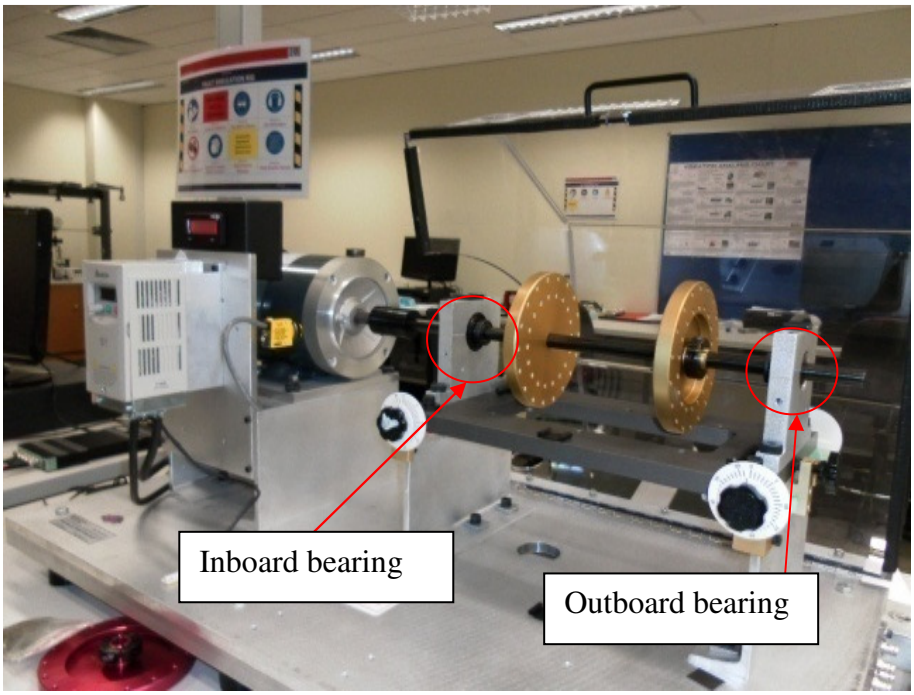

Fig.3.2. SpectraQuest's rotor Machinery Fault Simulator

The crack was located at the centre of the two bearing support span. The distance between the two bearings was $S = 364mm$. The crack location was $l = 300mm$ from one end of the shaft as shown in the shaft schematic diagram (Fig. 3.3) below.

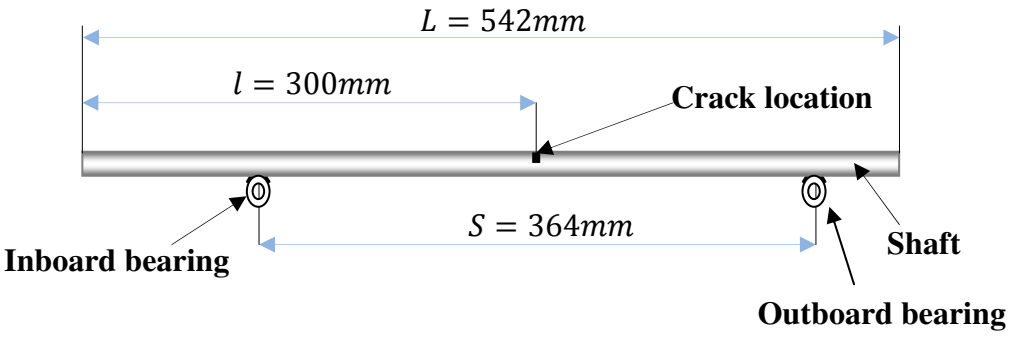

Fig.3.3. Shaft specimen's schematic diagram

3.1.3 Shaft crack shape and depth

As discussed in previous chapters, a transverse crack is the most common and detrimental defect in a rotating shaft. This type of crack has a priority for study in industrial applications. Therefore, this work will focus on transverse crack shaft analysis.

Previous studies indicated that, no significant decrease in shaft stiffness was observed for quasistatic loading of shafts containing closed fatigue cracks smaller than approximately 20% of shaft diameter, (LISSENDEN *et al.*, 2007).Shallow cracks, which have a depth less than 25% of the shaft diameter, will not be able to stimulate the breathing effect (Gasch, 2008). In particular, when conducting vibration natural frequency signal analysis, no significant difference could be observed between a shaft with a shallow crack and an intact shaft. On the other hand, there is little practical significance to detect the deep cracks of more than 50% of the shaft diameter, which would be too late for the purpose of predictive maintenance. As such, the crack used in this study had a depth of 40% diameter along the radial direction of the specimen shaft.

In this work, cracks in elastic shafts were generated using three different experimental methods, i.e., fatigue induced, welded shaft, and wire cutting. The three types of cracks, generated from different processes, will be studied and the results compared.

3.2 Generation of fatigue crack

Usually fatigue cracks could be initiated at the point which has the maximum local stress and the minimum local strength. The local stress pattern is determined by the shape of the shaft, as well as the type and magnitude of the loading (Boyer, 2006). Creating a fatigue crack was one of the most challenging tasks in the present study. It was time consuming and required special knowledge and skills of metallic materials and their fatigue and fracture characteristics.

First, a cut needed to be generated so as to concentrate stress locally. According to ASTM E399 specifications for fatigue pre-cracks, a V-notch (Fig. 3.4.) was seeded at the designated location, in order for a crack to be initiated at this point. The size of the V-notch was $1mm$ in width and $0.5mm$ in depth as per ASTM E-399 requirement.

Fig.3.4.V-notch

The V-notch was machined using an Okuma CNC milling machine in the ECU engineering workshop. To achieve a successful transverse fatigue crack, the shape of the notch played an important role, in particular, the bottom edge of the notch. A sharp edge was used in order to promote the growth of the crack in the perpendicular direction during the fatigue crack process. As the notch was small, the minimum size milling tool was selected, and a few tests were carried out before the required shape and size of notch were obtained.

The specimen shafts with the most satisfactory V-notches were then submitted to the fatigue crack generation process using a dynamic Instron cyclic machine (Instron 8501), with a standard three-point bending fixture that was designed and fabricated at ECU.

Specimens Size, Configuration and Preparation

Test Machine:	Instron 8501 (Fig. 3.5)
Test method:	Three point bending (Fig. 3.6)
Test condition:	Room temperature, 25 ℃
Specimens:	Rotating Shafts
Material:	AISI 1030 Steel
Length:	$542mm$
Diameter:	$15.875mm$

Fig.3.5. Dynamic Instron 8501 machine

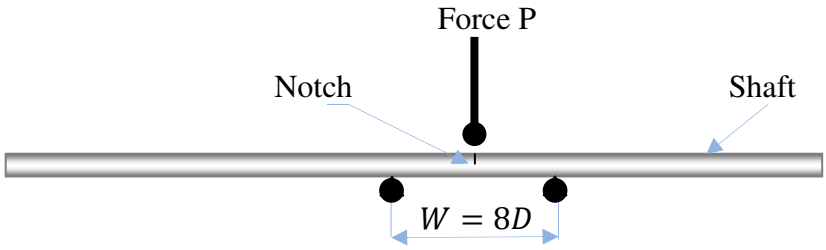

Fig.3.6. Shaft three-point bending schematic diagram

- Notch located at 300mm distance from left end
- $D = 15.875mm$ (Shaft diameter)
- W =the support Span, 8 times of specimen shaft diameter D

The most critical part of the crack generation process was to ensure that the shaft did not have permanent bending deformation. A deformation would affect the accuracy of the results in the next step - measuring the bending stiffness within elastic limit. The control parameter was the applied load. If the load was too high, the shaft would be damaged, but if the load was too low, the crack would not be initiated within a reasonable number of cycles (Approximately 10^4-10^6 cycles, with reference to ASTM E399 standard test method for Linear-Elastic Plane-Strain Fracture Toughness). Thus, it was important to estimate the correct load value to be applied to the shaft for generating the pre-crack (initial crack).

TABLE 3.4 Intact shaft experimental results, Load vs. displacement

Displacement (mm)	**Load** (N)
0	0
0.0645	500.25
0.12137	1003.42
0.21869	1999.90
0.3055	3000.19
0.38438	4000.26
0.45838	5000.25
0.52713	6000.02
0.58969	7000.16
0.648	8000.43
0.70256	9000.15
0.75556	9999.60
0.808	11000.29
0.86025	12000.18
0.91331	12999.89
0.96788	14000.12
1.02319	14999.05
1.07875	16004.08
1.14188	17002.66
1.32444	18001.70

A quasi-static 3-point bending pre-test was conducted to study the elastic limit of a specimen shaft. This would provide a reference range for the fatigue initial force selection. The results are given in Table 3.4.

A force-displacement curve (Fig.3.7) was plotted based on the raw data from the table. As indicated in the figure, when the force reached $16000N$, the specimen began noticeable plastic deformation. Fatigue tests were carried out under repeated (cyclical) loading, therefore, the applied force for generating the fatigue crack needed to be significantly below $16000N$.

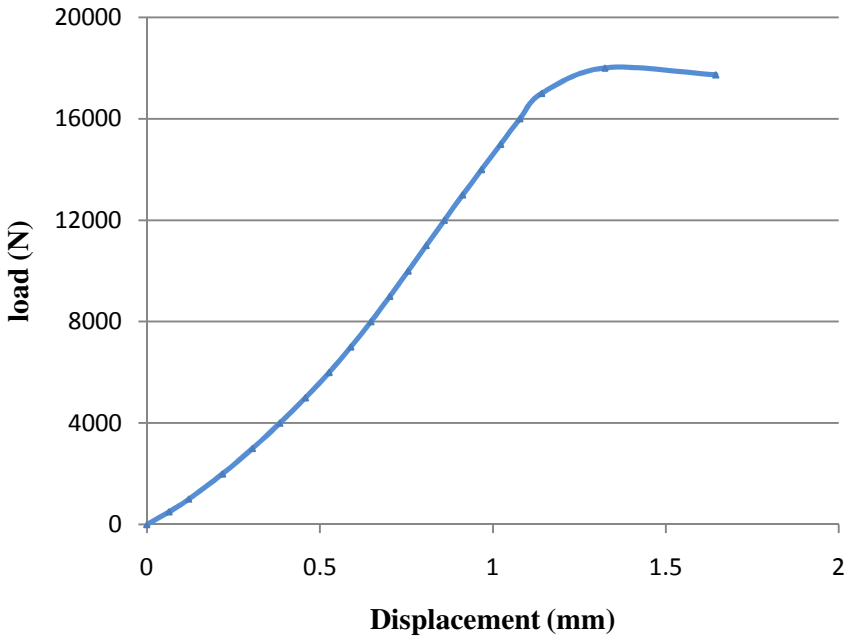

Fig.3.7. Intact shaft 3-point bending, load vs. displacement

A fatigue test could be done by either applying an axial load, or by bending, thus only tensile or compressive stresses on the shaft can be produced (Boyer, 2006). Normally the applied stress is in a cyclical mode. In the present work, the bending load was cycled through a sinusoidal waveform (Fig.3.8).

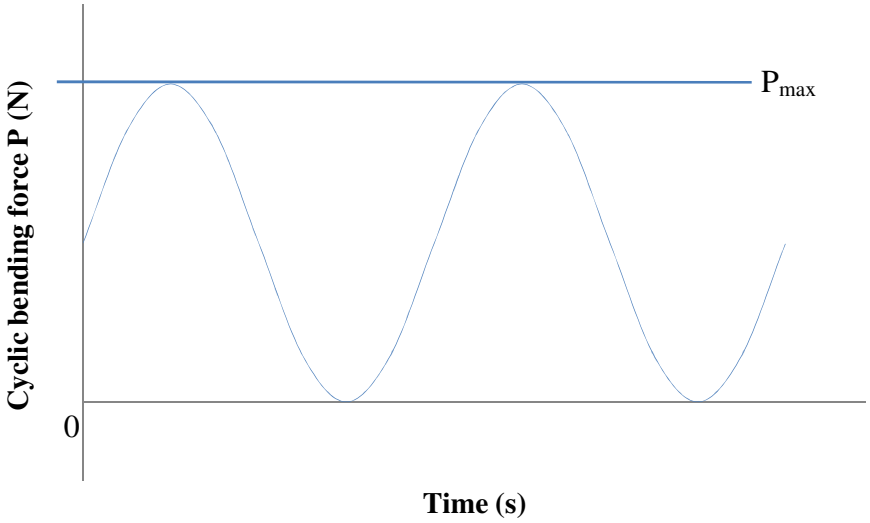

Fig.3.8. Cyclic bending force vs. time

An $s-n$ **Curve** (Fig.3.9) in [ref Howard's book] is reproduced here. From this curve the combination of cyclical load value and the number of cycles required could be obtained.

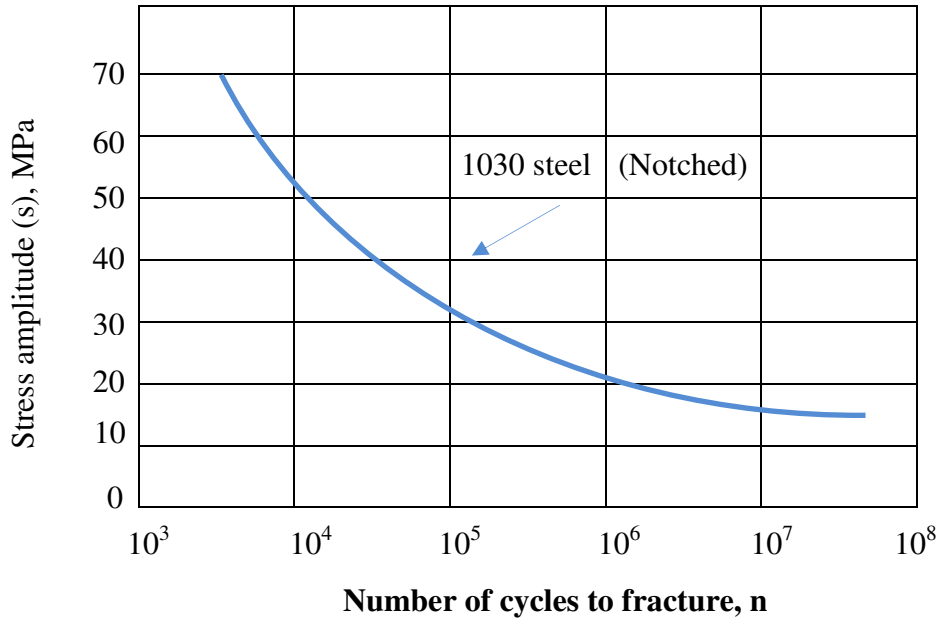

Fig. 3.9 Typical $s-n$ **Curve** for constant amplitude and sinusoidal loading

The maximum cyclical force for a pre-fatigue crack can be estimated through the formula [ref: ASTM E399-08 pages 519]:

$$K_{max} = \frac{P_{max}W}{2BD^{\frac{3}{2}}} f(\frac{a}{D}) \quad (3.1)$$

In the equation:

$$f(\frac{a}{D}) = 0.326 + 30.318\frac{a}{D} - 59.905\left(\frac{a}{D}\right)^2 + 68.889\left(\frac{a}{D}\right)^3 \quad (3.2)$$

where:

P_{max} =Maximum cyclical force, N
W = Support span, in this case $W = 8D$
B = Specimen thickness (shaft diameter), $B = D$
$a = 0.5mm$, crack depth as pre-determined.
K_{max} = maximum stress- intensity factor, according to ASTM E399-08, K_{max} should not be larger than 80% of K_{Ic} (fracture toughness). As a guideline, K_{Ic} = 11Mpa in normal laboratory environments.

Our calculation result provided a guideline, with the maximum cyclical force estimated as $8KN$. However, even with the reference range, it was still difficult to define the individual steel material fracture toughness K_{Ic}. A few dynamic bending tests were attempted to finalize the initial loading force. A maximum cyclic force $P_{max} = 13KN$ was applied on the first test. The sample was damaged because of overloading that caused the shaft to be permanently deformed. The load was then reduced to $P_{max} = 8KN$, but after ten hours and more than 10^6 bending cycles, a crack was still not initiated.

The final set up configuration was determined in the end using a trial-and-error method in order to achieve a successful fatigue pre-crack shaft specimen (Table 3.5).

TABLE 3.5 Data for fatigue crack initiation

Pre-crack test			
Load (KN)	Frequency (Hz)	Cycles (n)	Crack growth (mm)
10	5	40,000	Nil
11	5	35,648	0.5

A pre-crack of $0.5mm$ was observed (measured from the notch tip) after 35,648 cycles with a maximum cyclic load of $11KN$ applied in a sinusoidal waveform with a frequency of 5 Hz at room temperature.

After the crack initiation process, the crack propagation was controlled by further cycling using a lower maximum load. The entire test was conducted using various loading forces ranging from a maximum of $5KN$ to a minimum of $1KN$.In each test, different loading force ranges were applied for a large number of cycles (Table 3.6). Note that, for a normal unloaded condition, the crack is closed. Thus, the crack is invisible and its location or depth could not be determined. The crack can only be observed while the shaft was under a static lateral load in the 3-point bending fixture (Fig.3.10). Crack growth was closely monitored in this way during each fatigue test by using an Olympus optical microscope. At the end stage, the loading force was reduced to $1KN$. The test was finally stopped when the crack reached 40% of the shaft diameter.

TABLE 3.6 Data for fatigue crack propagation

Crack propagating test			
Load (KN)	Frequency (Hz)	Cycles (n)	Crack growth (mm)
5	5	140,250	0.89 +
4	5	93,800	1.5 +
3.5	5	76,500	2.05 +
3	5	61,600	2.75 +
2.5	5	50,000	3.43 +
2	5	40,500	4.05 +
1.5	5	60,410	4.63 +
1	5	110,417	5.65

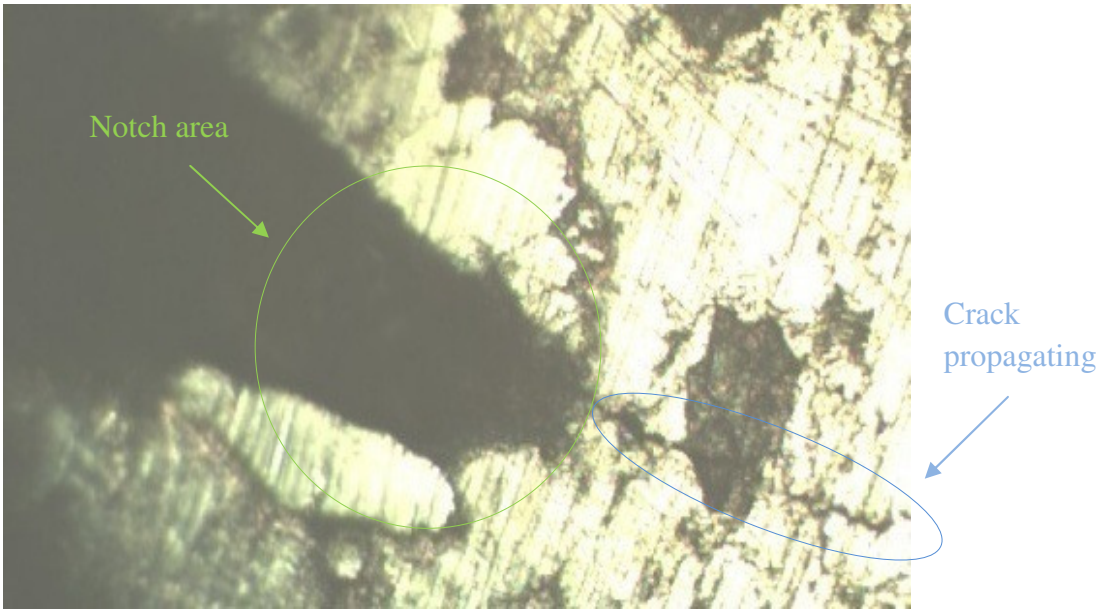

Fig.3.10. Fatigue crack observed under a static bending load

These experiments were performed by the author at the University of Western Australia (UWA). Before operating the Instron 8501 Machine, the author had to attend a one-day safety induction training course (which included safe evacuation procedures), conducted by the Lab technical personnel from the department of Mechanical and Chemical Engineering (UWA). During each test session, the safe operational guidelines were strictly followed and closely supervised by the lab technician. As this dynamic machine produced a loud noise during its operation, each experimental session was conducted in a confined room to avoid the noise affecting the surrounding environment.

3.3 Generation of Welded Shaft Crack

The test specimens for this type of cracked shaft were developed by perfectly welding two pieces of steel rods together using a water cooled TIG welder. A schematic diagram of the fabricating process is shown in Fig.3.11. The material was first cut into two pieces at a point $300mm$ from one end of the shaft. Each side was machined by an OKUMA CNC (Model MX55 VB Year 2000) milling

machine at the two faces to be joined, in order to form a smooth surface contact. The two shaft pieces were then butted together within a jig plate with screws to adjust the alignment. From each shaft half, 30mm of material was removed from around the joint top by a CNC mill until a contact crack was formed for 40% of the shaft diameter.

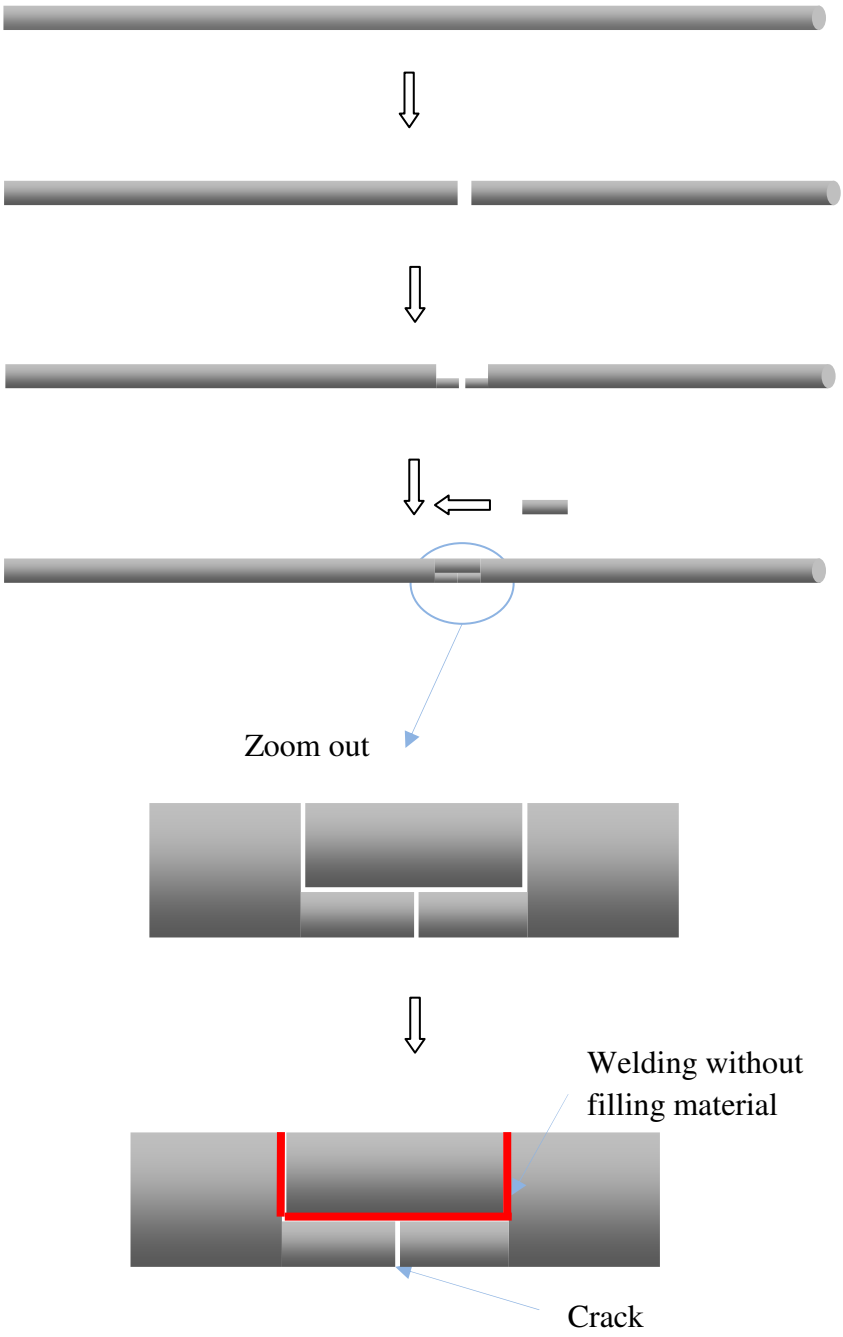

Fig.3.11. A schematic of welded shaft crack fabricating process

A replacement filler block was fabricated from the same material as the two half shaft specimens. The dimensions and shape of the block were the same as those formed by the machined gap when the two half specimens were joined together. The replacement block was then used to join the two pieces of shaft by TIG welding (without filling material) to create one uniform material structure with a crack depth of 40% of the shaft diameter.

The welding conditions, including the welding current and time, were tested carefully in order to produce a uniform weld joint without significantly melting into the replacement block or the two joined shaft pieces while keeping the shaft crack intact. The shaft was left in the jig plate to cool down slowly to ensure a minimal heat treatment effect on the metal. Finally, the shaft was tested using a manual lathe with a live centre at high speed (2500 RPM) to make sure there was no shaft misalignment caused during the welding process.

The location and depth of the crack on these specimens were the same as those for the fatigue-cracked shaft test set. The welded shaft cracks could only be observed under a Moticam 2300 microscope (Fig. 3.12) as the crack gap was so small. It was also expected that the breathing of the crack could be observed during shaft rotation.

Generation of the welded shaft crack specimens were completed in the mechanical workshop at ECU, with the assistance of the workshop technical staff.

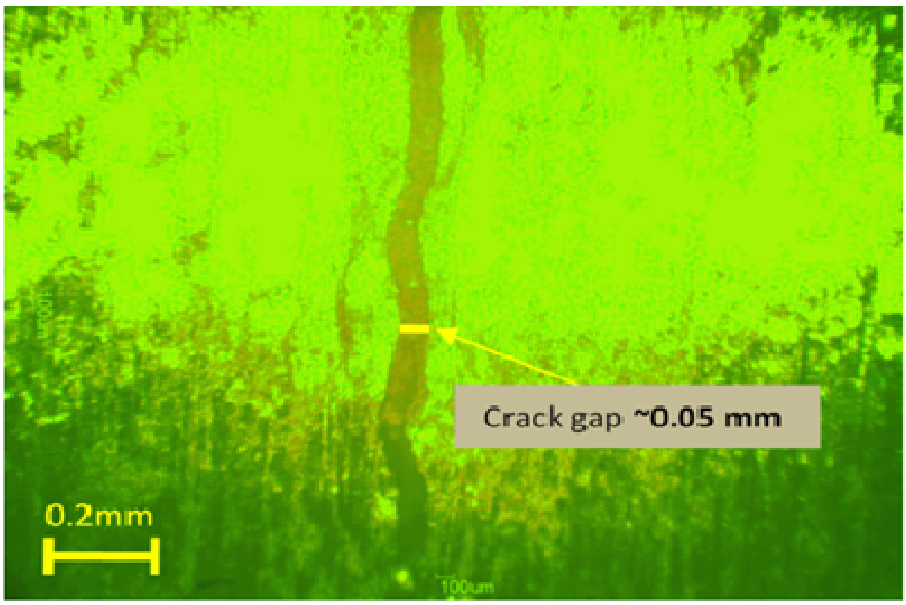

Fig.3.12. Welded shaft crack observed under Moticam 2300 microscope.

3.4 Generation of wire-cut crack

A transverse slot was also generated by an electro-erosion process. The location and depth of the crack were identical to those of the fatigue-cracked shafts.

The wire cut crack was fabricated using a CNC wire cutting machine. The cutting process is known as EDM (Electrical Discharge Machining) which is an electro thermal production process. In this process a thin (0.1 mm) single strand brass wire, in conjunction with de-ionised water, was used. The wire cuts through the shaft by the heat generated from an electrical current, and then instantaneously cooled by the de-ionised water.

Due to its high precision, EDM is an ideal choice to produce a very thin cut. Another advantage of this process was that it did not apply a force to the material during the cutting process, which meant a low possibility of deformation or residual stress.

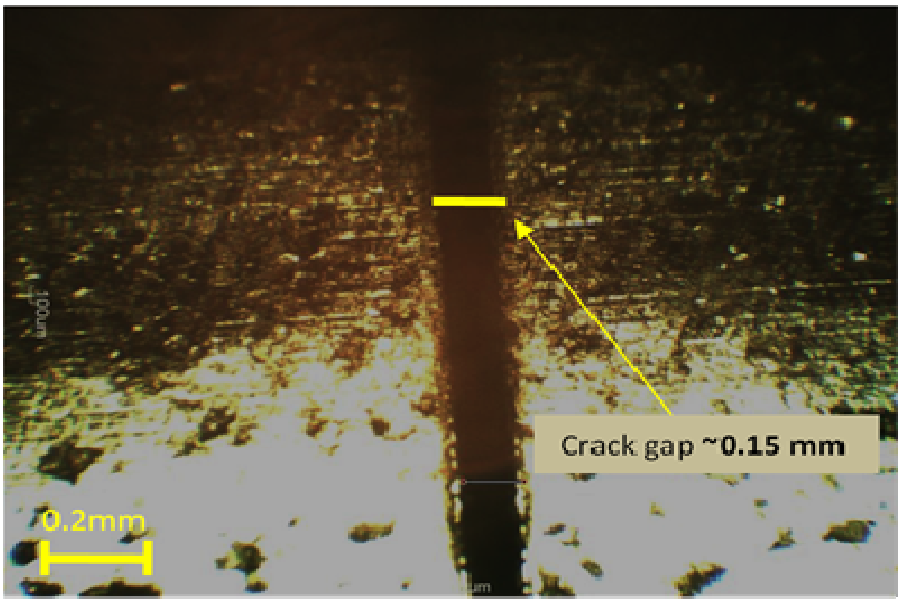

Fig.3.13. Wire-cut crack observed under Moticam 2300 microscope.

The wire cut EDM equipment was guided by OKUMA CNC instruments which controlled the brass wire through a three dimensional axis by reading a G-code software program created from a SolidWorks drawing by using SolidCAM software. Similar to the welded shaft crack, the wire-cut crack could be observed under a Moticam 2300 microscope (Fig. 3.13).

The wire-cut specimens were also fabricated in the mechanical workshop at ECU, with the assistance from the workshop technical staff.

3.5 Conclusions

Developing a crack diagnostic technique required the proper generation of cracked shaft test specimens. This chapter provides the detailed steps of specimen preparation processes for the three different types of cracks. Four specimens were created for each type. All shaft specimens were labelled and stored for the next step of study in which measurements of bending stiffness were to be carried out.

CHAPTER 4

BENDING STIFFNESS MEASUREMENT

4.1Measurement configuration and procedures

In this chapter, the procedures used for stiffness measurement on the cracked shaft specimens will be discussed, and the results presented.

The tests were carried out in the material laboratory at Edith Cowan University (ECU). A model 5569 Instron universal testing machine (Fig.4.1) was used to conduct the bending stiffness measurements, under a quasi-static load at room temperature.

Fig.4.1. Quasi-static Instron 5569 machine

On the shaft an applied bending load simulated the effect of a disc gravity loading while a centrifugal force resulted from disc rotation. In chapter 5, the vibrational analysis on the rotating shaft with a single disc centrally mounted in between the two support bearings and next to the crack location, will be presented. A schematic is illustrated in Figure 4.2. This model is most widely adopted by researchers in the study of basic rotordynamics phenomena. It is normally referred to as the Jeffcott Rotor (Chen and Gunter 2005).

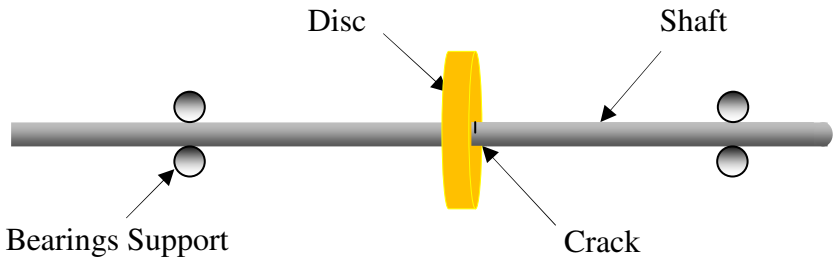

Fig.4.2. A schematic of the arrangement of cracked shaft, disc and bearings

A three point bending fixture was designed and fabricated, based on the actual arrangement of the rotor shaft, disc and bearings. The dimensions of the set up are shown below (Fig.4.3.).

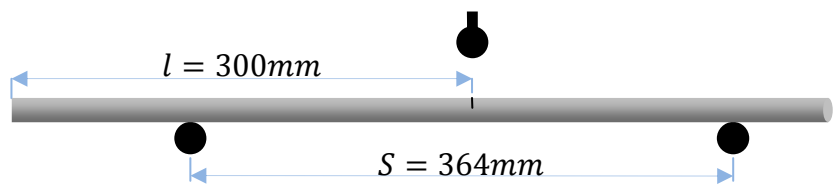

Fig.4.3. The configuration of a 3-point bending stiffness measurement

A three point bending compression program was set up using Instron's Bluehill software. The bending load used here was different from the cyclical dynamic load used in chapter 3 for fatigue crack generation. The load was increased through software control, in a quasi-static mode. A load vs. displacement curve was obtained at the end of each test.

As mentioned in the previous chapter, the bending test on the cracked shaft should be kept within elastic limit so as no plastic deformation could occur. Due to the different set up from that described in chapter 3, a cracked welded shaft was selected for pre-test to estimate the maximum load before plastic deformation. The data obtained was recorded in Table 4.1.

TABLE 4.1 Welded shaft experimental results, Load vs. displacement

Load (N)	**Displacement** (mm)
0	0
125.6594	0.31938
250.4154	0.59419
375.1218	0.84712
500.4795	1.09010
625.7670	1.32713
750.0641	1.55700
875.3305	1.77919
1000.75	2.00356
1125.49	2.22688
1250.64	2.44906
1375.32	2.66963
1500.19	2.89256
1625.30	3.11806
1750.13	3.34800
1875.55	3.58413
2000.12	3.82956
2125.62	4.08656
2250.16	4.36213
2375.43	4.66606
2500.03	5.00950
2625.38	5.41838
2750.80	5.94656
2875.52	6.70119
3000.01	7.89813

A force-displacement curve (Fig.4.4) was plotted based on the raw data from table 4.1. As can be seen from the graph, the specimen began plastic deformation when the force reached 2000N and above, as the slope of the curve started to decline in this region. Therefore, as a guideline, the maximum force applied to a cracked shaft for the bending stiffness test was limited to below2000N.

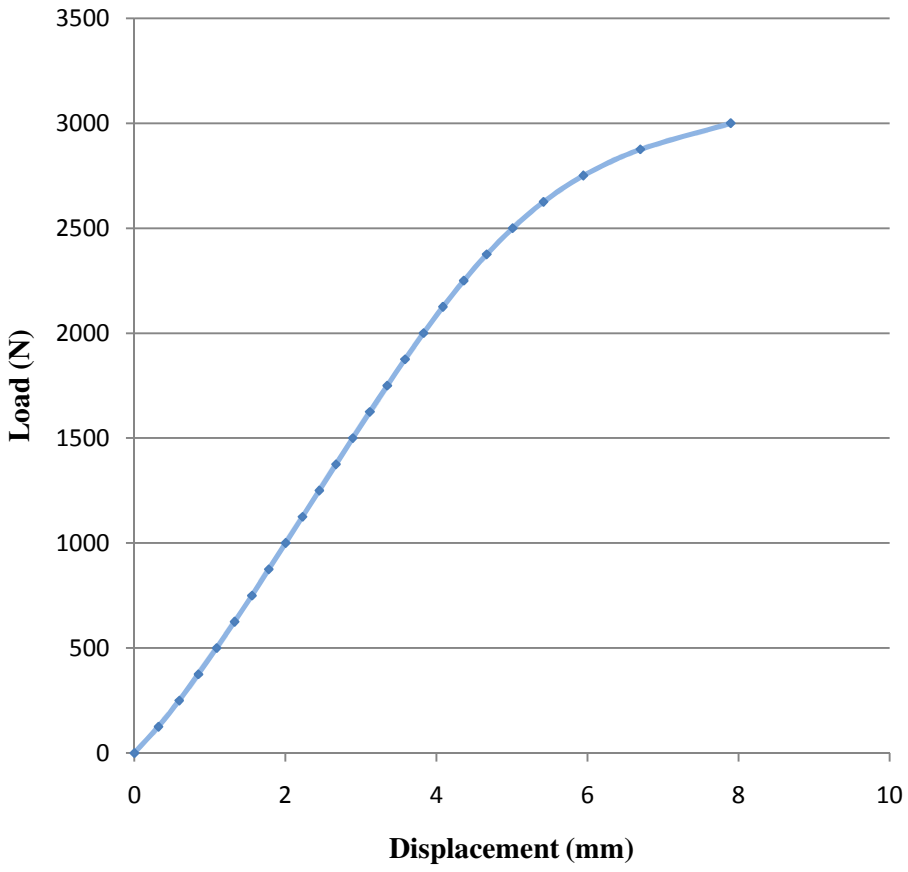

Fig.4.4. Load vs. displacement of a cracked welded shaft

In order to simulate the bending stiffness variation during shaft rotation, each specimen shaft was rotated and measured at 13 different angular positions from 0°to 360° with a 30° increment. The relative position between crack direction and loading axis in a shaft cross sectional view is shown in Figure.4.5.

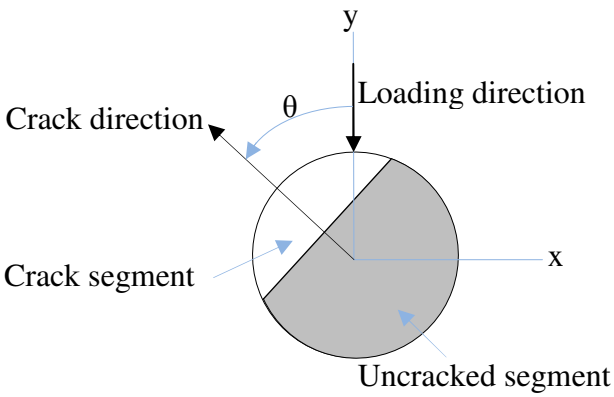

Fig.4.5. A cross-sectional view of rotating angle (θ) between crack and loading axis

The angular positions of the crack for each measurement point was determined accurately by fixing a flexible measuring tape with unit markings around the crack edge on the shaft (Fig.4.6) and then subdividing equally the circumference of the shaft into 12 sections, each having a 30^0 angular interval.

Fig.4.6. Shaft rotating angle measurement with a flexible tape

For each measurement point a small initial force was applied to the shaft to stabilise the measuring process before recording the data. This was to minimize

the error in the displacement caused by fixture backlash or other set up errors. The loading rate was set at 50 N/min. For safety reasons, a maximum force limit of 2 KN was programmed, in order to prevent the shaft from accidentally overloading and being damaged. Load and displacement data were recorded progressively during the measurement tests, and then processed subsequently using Microsoft Excel. Stiffness was calculated from the slope of the load vs. displacement curve.

4.2 Measurement Results

4.2.1 Intact shaft

For comparison purposes, an intact shaft was also measured 13 times at the designated rotation angles. The results obtained averaged the data from three tested intact shafts specimens. At each angle, a load vs. displacement curve was recorded and drawn, thus producing a total of 13 curves shown in Figure 4.7.

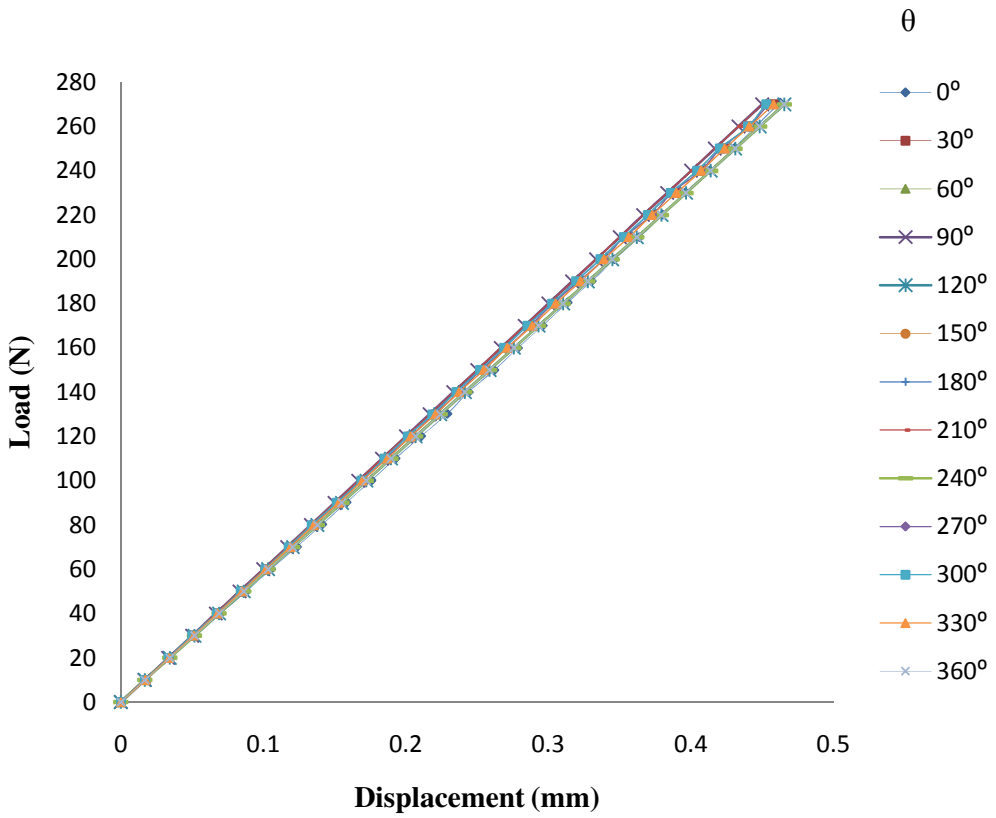

Fig.4.7. Load vs. displacement of an intact shaft, measured at different angular positions

Through calculating the slope of each curve in the above diagram, the stiffness of the intact shaft at 13 different rotating angles was obtained.

Theoretically, the stiffness at the mid-span of the shaft due to bending could be calculated based on the area moment of inertia of the mid-span cross section. The formula (Chen and Gunter 2005, Han 2007) can be rewritten as:

$$K = \frac{48EI}{S^3} \tag{4.1}$$

where $E = 200 \times 10^9 N/m^2$ is the Young's Modulus of the steel, and $S = 364\ mm$ is the width of the support span, , and I is the area moment of inertia.

For a intact shaft,

$$I = \frac{\pi D^4}{64} \tag{4.2}$$

where $D = 15.875\ mm$ is the shaft diameter.

Using the parameters given, we have,

$$I = \frac{3.1415 \times 0.015875^4}{64} = 3.1175 \times 10^{-9} m^4 \tag{4.3}$$

Thus the theoretical stiffness of the intact shaft is:

$$K = \frac{48 \times 200 \times 10^9 \times 3.1175 \times 10^{-9}}{0.364^3} = 620.55\ N/mm \tag{4.4}$$

Table 4.2 shows the comparison between the theoretical and experimental stiffness of the intact shaft at various angular positions. The errors are also given.

TABLE 4.2 Intact shaft stiffness at 13 different angular positions.

Rotating angle θ (degree)	**Stiffness $K_0(N/mm)$**		**Error**(%)
	Experimental results	**Theoretical results**	
0°	592.46	620.55	−4.5
30°	585.32	620.55	−5.7
60°	590.75	620.55	−4.8
90°	588.16	620.55	−5.2
120°	595.80	620.55	−4.0
150°	587.29	620.55	−5.4
180°	588.91	620.55	−5.1
210°	580.94	620.55	−6.4
240°	584.13	620.55	−5.9
270°	600.08	620.55	−3.2
300°	597.44	620.55	−3.7
330°	595.23	620.55	−4.1
360°	593.66	620.55	−4.3

Fig. 4.8 shows the diagram derived from the data in table 4.2. It can be seen that the experimental results were in good agreement with the theoretical results with an overall error being less than 5%. The slightly larger error observed in two of the results are likely due to an inaccurate Young's Modulus value used in the calculations.

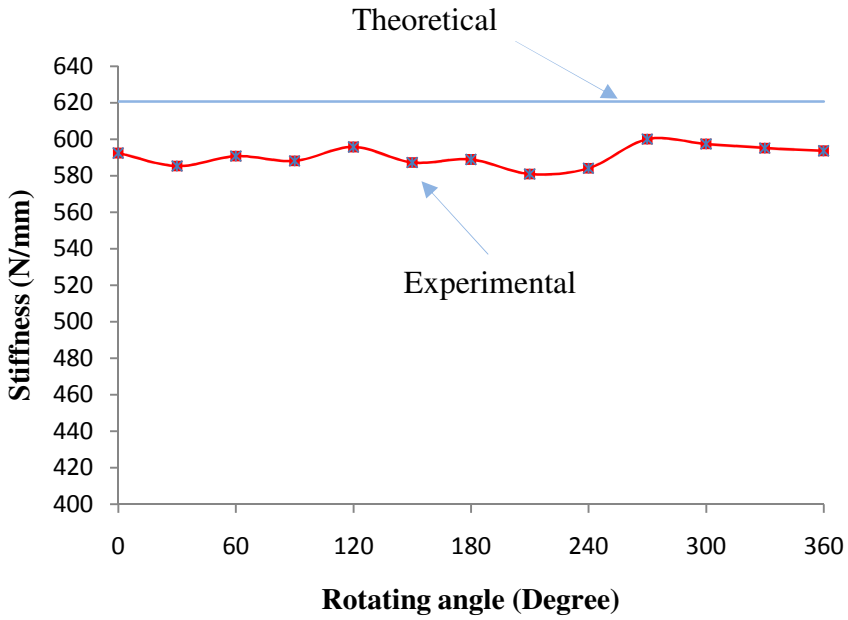

Fig.4.8. An intact shaft's stiffness at different angular positions.

4.2.2 Fatigue cracked shaft

The initial set up and subsequent test procedures used for this specimen set were similar to those used for the intact shafts. Each fatigue cracked shaft was measured 13 times by rotating the shaft anticlockwise to gain each data point, with the first measurement angle θ=0° having the crack in the vertical position as shown in Fig. 4.9a. The angular positions for 90°, 180°, 270° and 360° are illustrated in Figure 4.9b, c, d, and e, respectively.

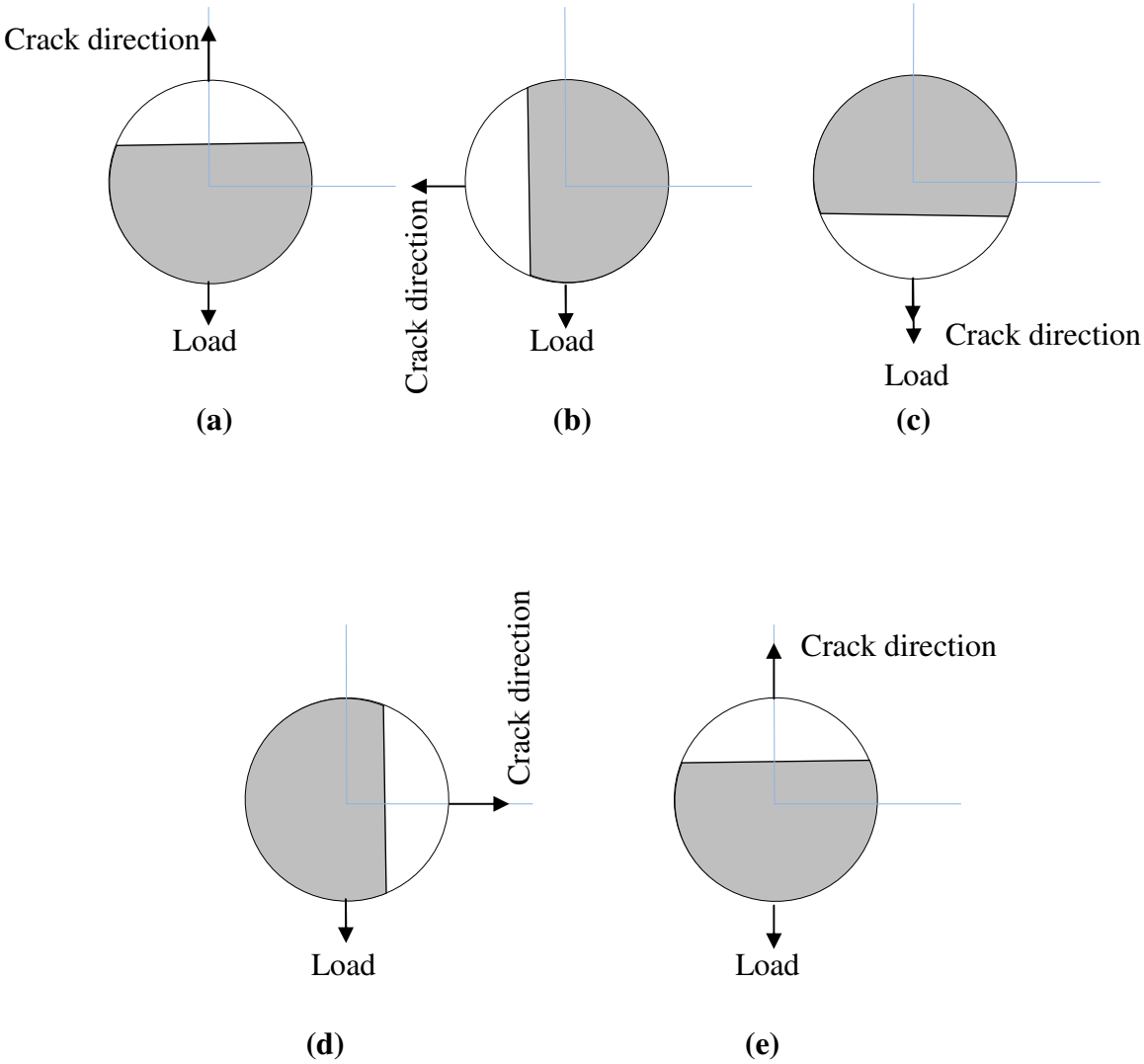

Fig.4.9. A cross-sectional view of a fatigue cracked shaft at different angular positions, (a) θ=0°, (b) θ= 90°, (c) θ= 180°, (d) θ= 270°, (e) θ= 360°.

The measurements were carried out at each defined angle and the results recorded and processed further using Microsoft Excel. Thirteen load vs. displacement curves were produced and plotted in Fig.4.10 below.

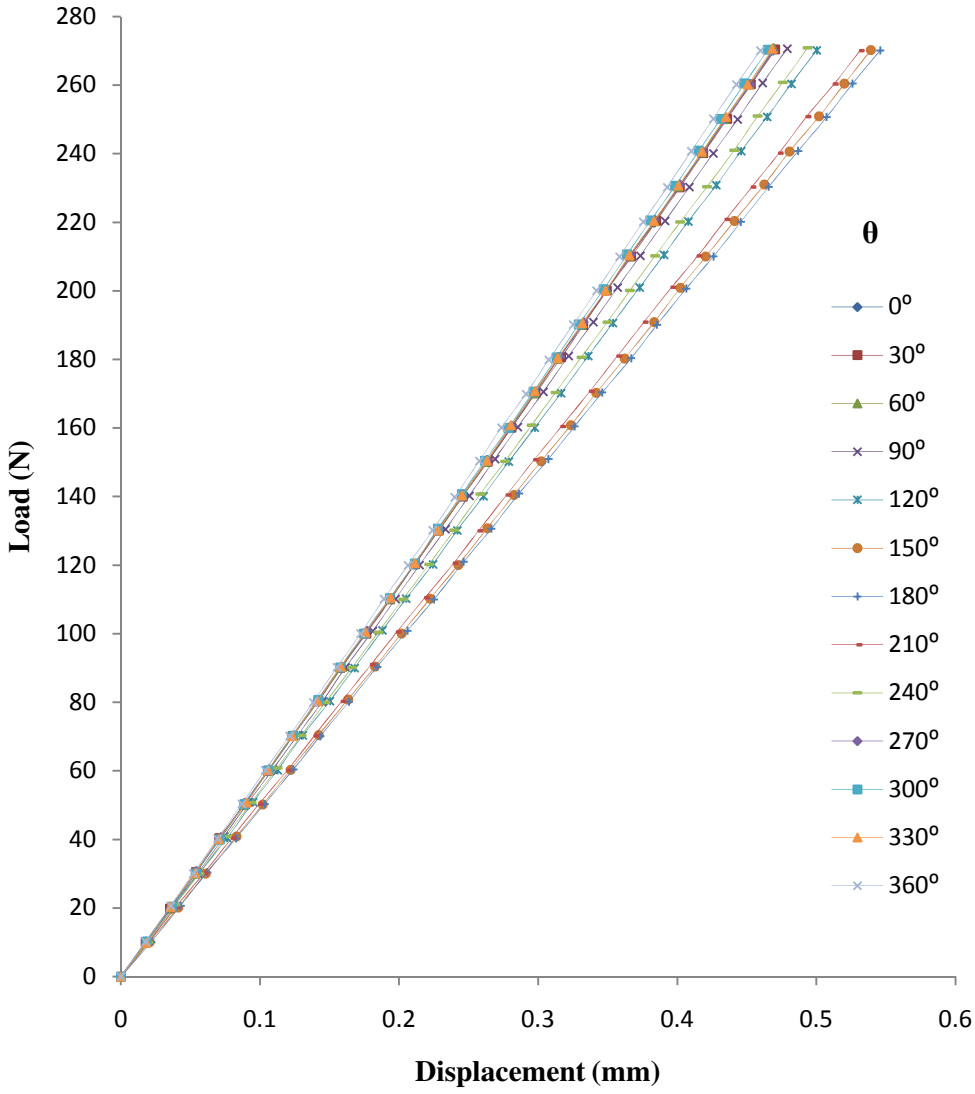

Fig.4.10. Load vs. displacement of a fatigue cracked shaft, measured at different angular positions.

The derived bending stiffness of the fatigue cracked shaft at 13 angular positions was summarised in the Table 4.3 and the curve plotted in Fig.4.11.

TABLE 4.3 Fatigue cracked shaft stiffness at 13 different angular positions.

Rotating angle θ (degree)	**Stiffness $K_F(N/mm)$**
0°	576.4485
30°	574.4269
60°	577.483
90°	565.8069
120°	540.6642
150°	507.1876
180°	495.7687
210°	508.3235
240°	548.74
270°	576.415
300°	582.6316
330°	577.7393
360°	580.4392

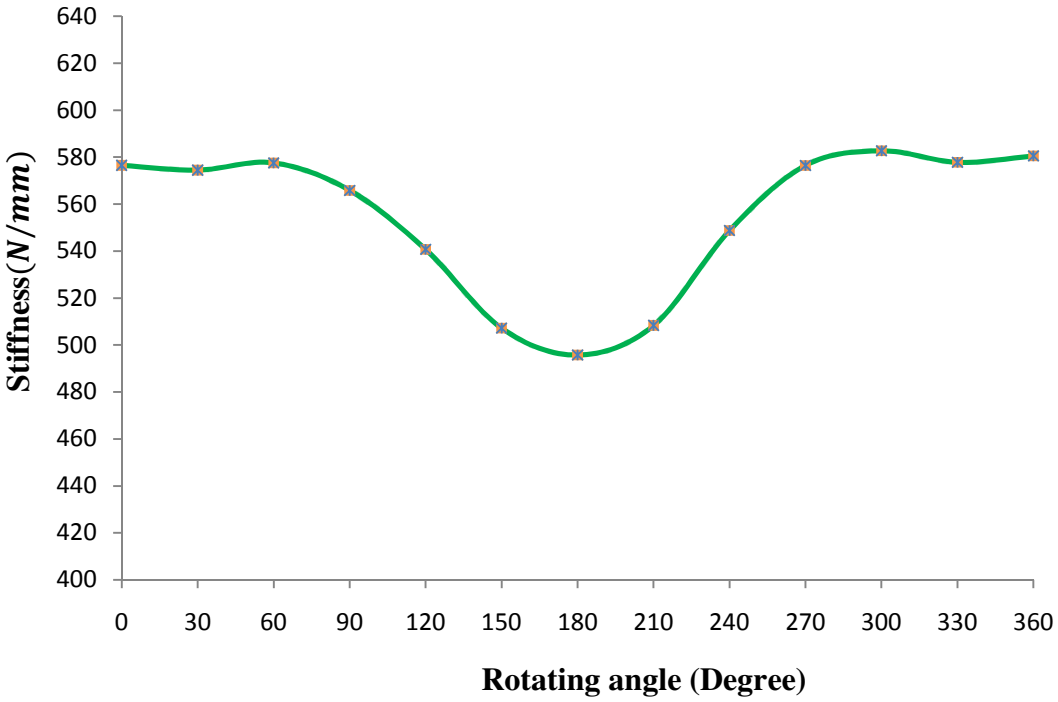

Fig.4.11. A fatigue cracked shaft's stiffness at different angular positions.

4.2.3 Cracked Welded Shaft

The measurement procedures were similar to those used for the fatigue crack experiment. The Load vs. displacement curve (Fig. 4.12), the stiffness values (Table 4.4) and the stiffness diagrams (Fig. 4.13) are presented below.

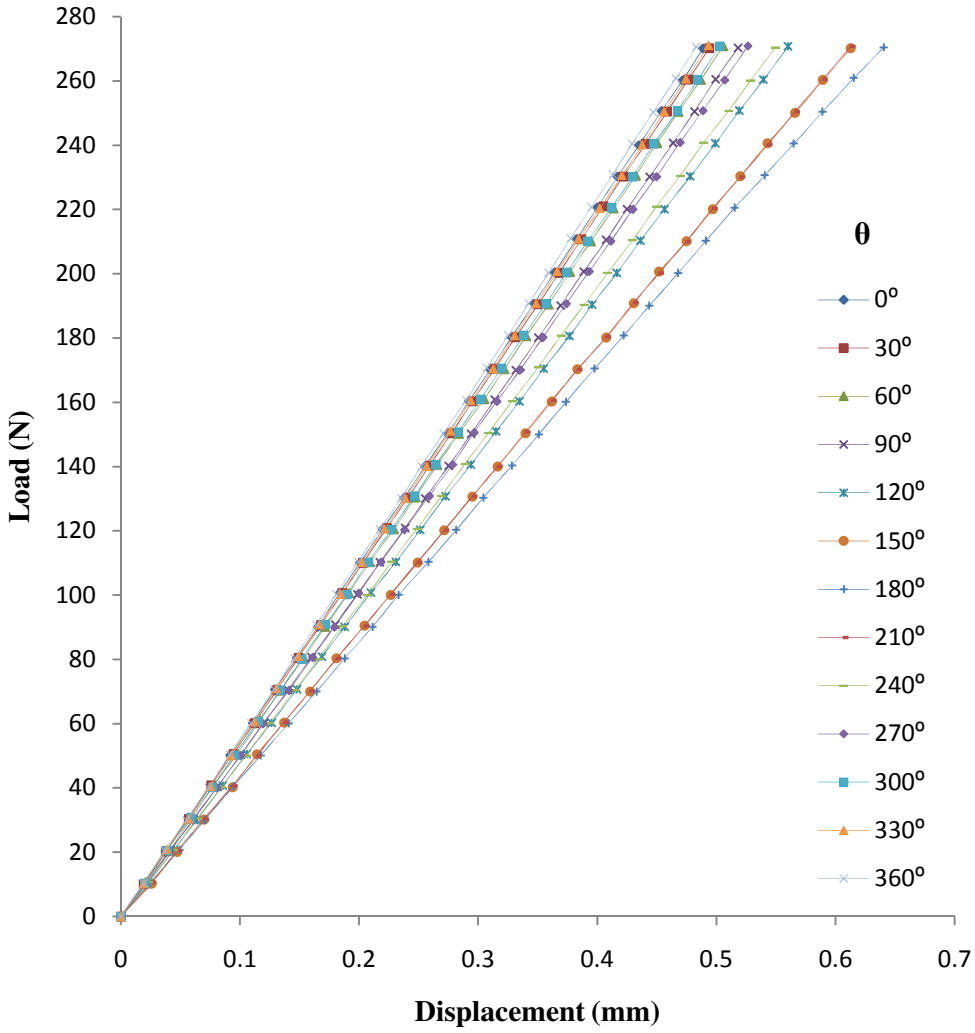

Fig.4.12. Load vs. displacement of a cracked welded shaft, measured at different angular positions.

TABLE 4.4 Cracked welded shaft stiffness at 13 different rotating angles

Rotating angle θ (degree)	**Stiffness $K_W(N/mm)$**
0°	553.3588
30°	547.4188
60°	536.0891
90°	522.6832
120°	483.3428
150°	442.1368
180°	425.7931
210°	443.7361
240°	493.9175
270°	515.3128
300°	538.949
330°	550.6282
360°	560.9558

Thus, the stiffness curve is:

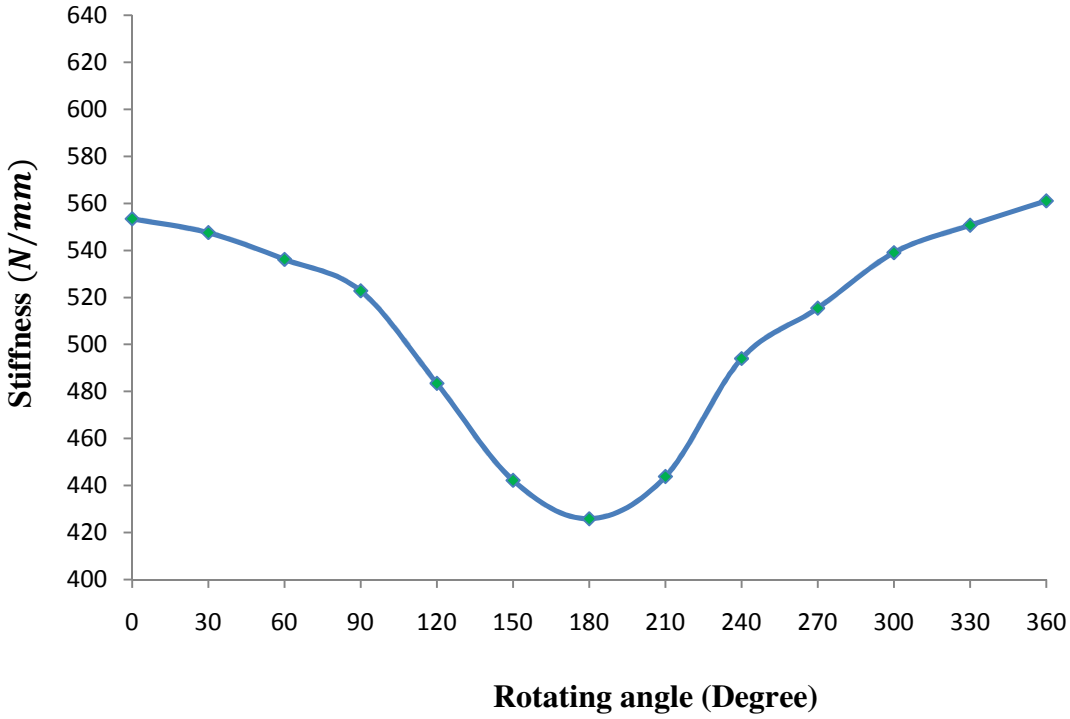

Fig.4.13.A cracked welded shaft stiffness at different angular positions.

4.2.4 Wire-cut cracked shaft

Again the measurement procedures were similar to those of the fatigue crack experiment. The Load vs. displacement curve, the stiffness values, and the stiffness plot are shown in Fig. 4.14, Table 4.5, and Fig 4.15 respectively.

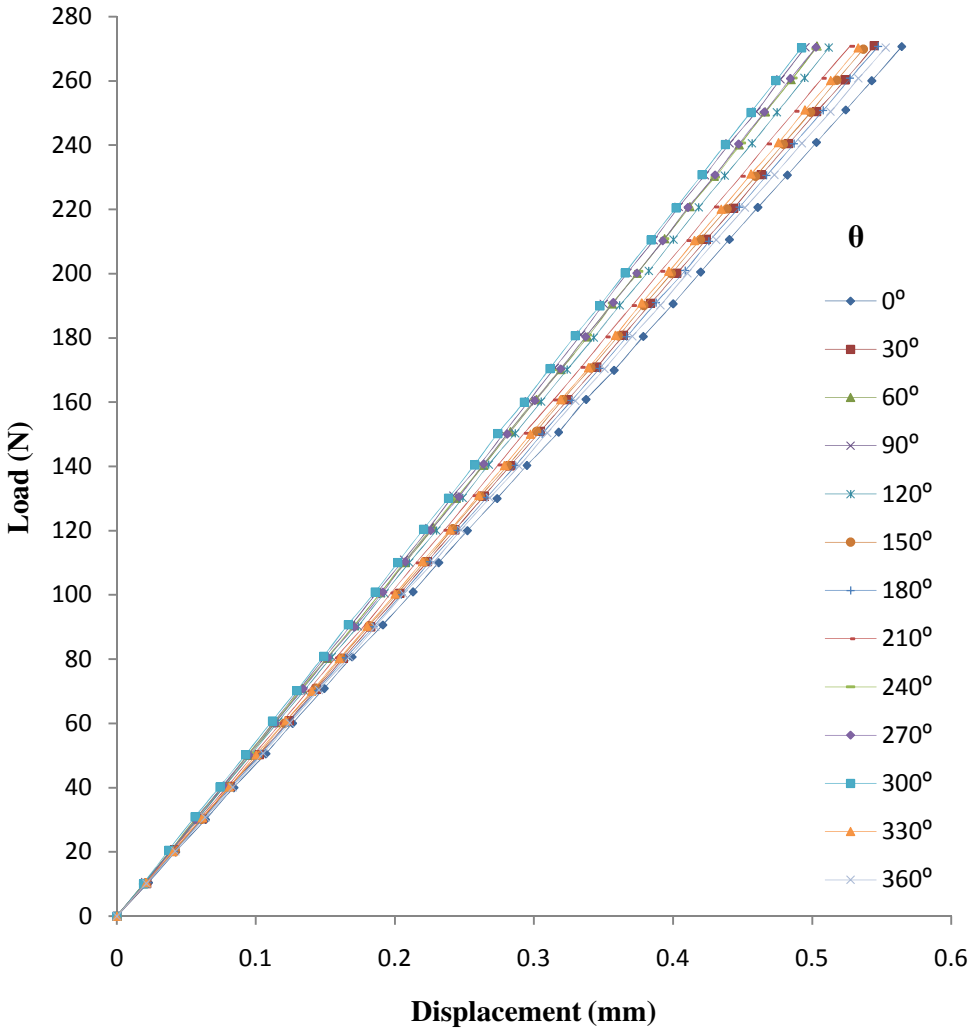

Fig.4.14. Load vs. displacement of a wire-cut cracked shaft, measured at different angular positions

The stiffness value table:

TABLE 4.5 Wire-cut cracked shaft stiffness at 13 different angular positions

Rotating angle θ (degree)	**Stiffness K_C**(N/mm)
0°	479.8141
30°	498.1326
60°	538.1936
90°	547.5442
120°	528.5705
150°	503.217
180°	494.2546
210°	514.4496
240°	537.1212
270°	538.5435
300°	549.259
330°	507.7466
360°	489.4919

And the stiffness diagram,

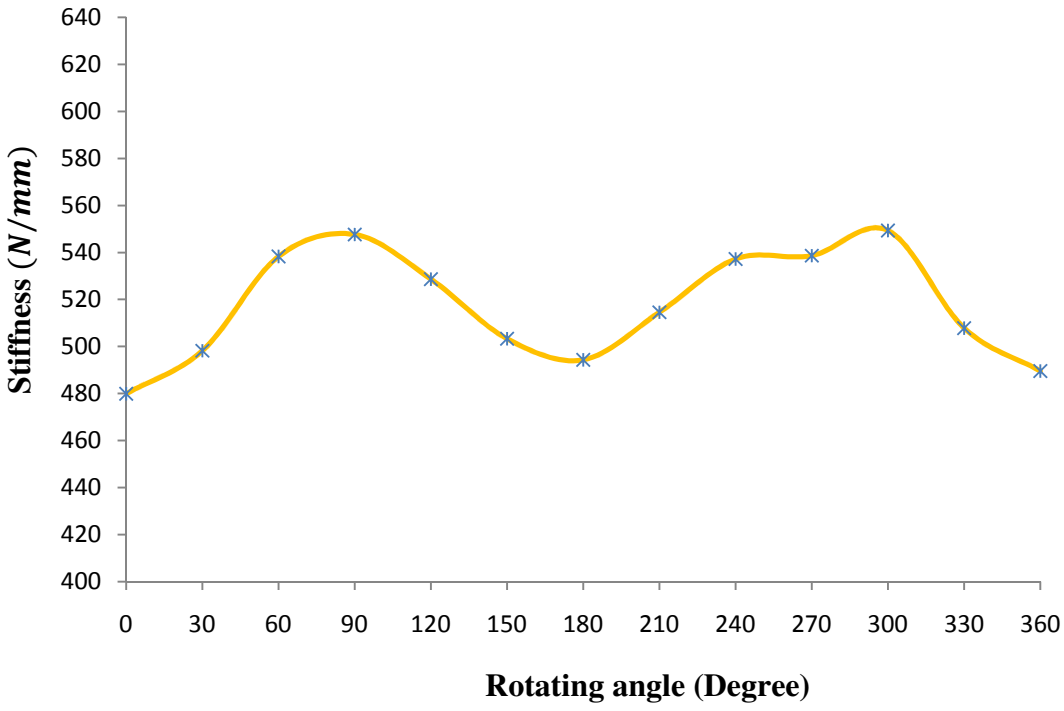

Fig.4.15.A wire-cut cracked shaft's stiffness (N/mm) at different angular positions.

4.3 Discussion

As demonstrated in Figures 4.7, 4.10, 4.12 and 4.14, for all the four types of shaft specimens with different cracks, the load force/displacement curves were linear. On the other hand, for the fatigue crack and welded shaft crack, the corresponding slope of the curve decreased as the crack rotated gradually from fully closed (0°), partially closed (120°) to the fully open position (180°).This represented a decrease in bending stiffness. In particular the fatigue-cracked shaft showed a more obvious change, which is illustrated in Fig.4.16.

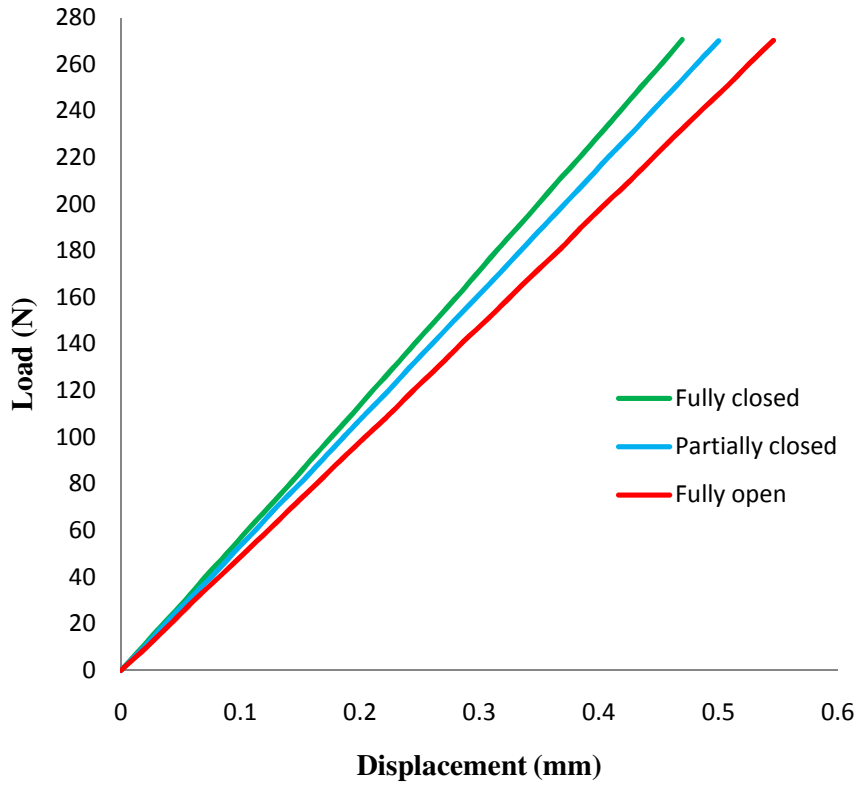

Fig.4.16. Loading force as a function of displacement for a fatigue-cracked shaft at three typical crack angular positions.

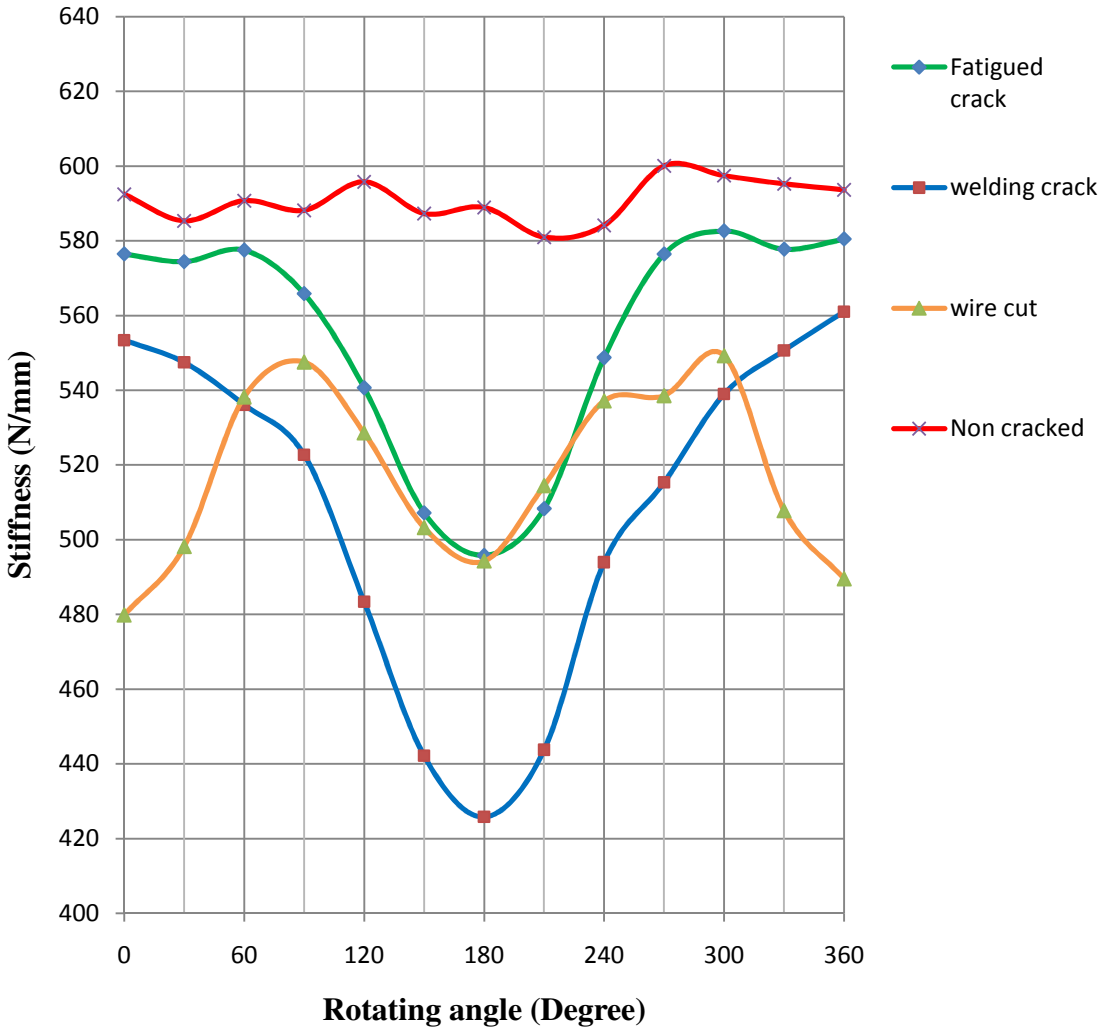

Fig.4.17.Bending stiffness (N/mm) at mid span for the four types of cracked shafts, as a function of the angular positions.

A summary of the bending stiffness of the four different crack types, as derived experimentally, is presented in Fig. 4.17. For the intact shaft, the stiffness remains independent of rotating angle with a slight fluctuation due to experimental error. The averaged stiffness was calculated to be 5.8×10^5 N/m. When a fatigue crack exists, the stiffness behaves totally differently. It can be seen clearly that stiffness at small angles is almost at the same level as that for an intact shaft. This is because the crack is fully closed. Consequently, the fatigue-cracked shaft at these angles behaves in a similar manner as an intact one. As the crack gradually rotates anticlockwise from its fully closed position at 0°, stiffness does

not show a visible change until a certain angle is reached where it starts to decrease rapidly. The minimum stiffness was 4.96×10^5 N/m and located at 180° where the crack was fully open. As the crack continued to rotate past 180°, a reverse process proceeded. It is evident that a fatigue crack shows typical crack breathing behaviour.

The welded shaft crack also showed an opening and closing behaviour, similar to that of the fatigue crack. However, the stiffness was lower than that of a fatigue crack shaft. This is likely a result of a change in the shaft material properties during the welding process, or an imperfect bonding between welded surfaces. Consequently, shaft stiffness was much lower than that indicated by the crack nominal depth. As such, to develop a quantitative breathing model, the parameter of crack depth for a welded shaft crack should be used with great care.

For the shaft with a wire cut crack, stiffness variation with rotating angle followed an "M" shape, which is again totally different from the expected normal crack breathing behaviour. Stiffness at 0° or 360° had a similar value to that at 180°. This indicates that the two surfaces of the cut do not close together under loading conditions even at 0° or 360° angular positions. Fig. 3.13 (Chapter 3) showed the cut crack gap at the shaft surface. The gap of the cut was approximately 0.15 mm while that of the welded shaft crack was only 0.05 mm (Fig. 3.12, Chapter 3). It appears the large gap of the cut prevents the two cut surfaces from closing together under load and so remains open during shaft rotation. The higher stiffness observed at 90° (or 270°) was simply due to a larger area moment of inertia of crack element cross section at these positions. This can be verified by the theoretical calculations based on published formulas in (Al-Shudeifat and Butcher, 2011). In other words, the thin direction of the uncut segment aligns with the loading direction when the crack is at 0° position. As the crack further rotates to 90° position, the thick direction is parallel to the loading direction. Observation in this study is in agreement with previous experience which has shown that even the narrowest practical machined notch cannot simulate a natural crack well enough to provide a satisfactory measurement of stiffness.

When the shaft rotates, the fatigued crack opens and closes alternatively. The tension stress, existing below the neutral axis of the cracked element tends to keep the crack open. The compression stress field that exists above the neutral axis tends to close the crack. The angle at which the crack starts to open or close depends on the shaft diameter and crack depth. Formulas to calculate these two critical angles are presented in Al-Shudeifat and Butcher (2011).

For a 40% crack depth and a shaft diameter of 15.875 mm used in this study, the two critical angles were calculated and the angular ranges in which the crack remained fully open, partially closed or fully closed, are presented graphically in Fig. 4.18. The crack starts to open at 11.5° and becomes fully open at 152.1°. As the crack continues to rotate, it starts to close at 207.9° and becomes fully closed at 348.5°. It can be seen clearly that the crack only remains fully closed within a very small angular range of 23°. On the other hand, the crack is partially closed most of the time.

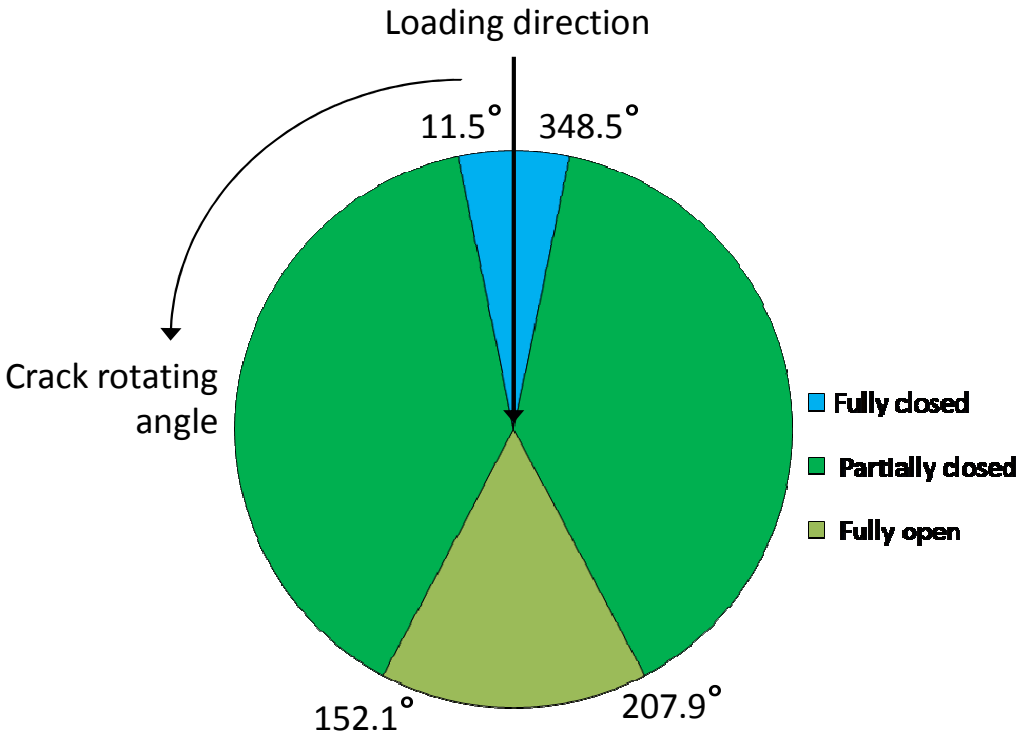

Fig.4.18. Relationship between crack angular position and its opening/closing status.

Periodic stiffness variation is usually simulated using a switch model (Jun and Eun, 1992) or a harmonic model (Mayes and Davies, 1984). The crack in the switch model was assumed to have only two states, either open or closed during each revolution. The mathematic description of the switch model is given in Equations 4.5 and 4.6, where K_o and (K_o-ΔK) are the stiffness values of a shaft when the crack is fully closed and fully open, respectively and ω is the rotating frequency of the shaft and *t* is time. The harmonic model assumed a time-variant stiffness of the shaft which can be described by Equation 4.7.

$$K = K_o 0^\circ \leq \omega t \leq 90^\circ \text{ and } 270^\circ \leq \omega t \leq 360^\circ. \quad (4.5)$$

$$K = K_o - \Delta K 90^\circ < \omega t < 270^\circ. \quad (4.6)$$

$$K = K_o - \frac{\Delta K}{2}(1 + \cos(\omega t + 180)). \quad (4.7)$$

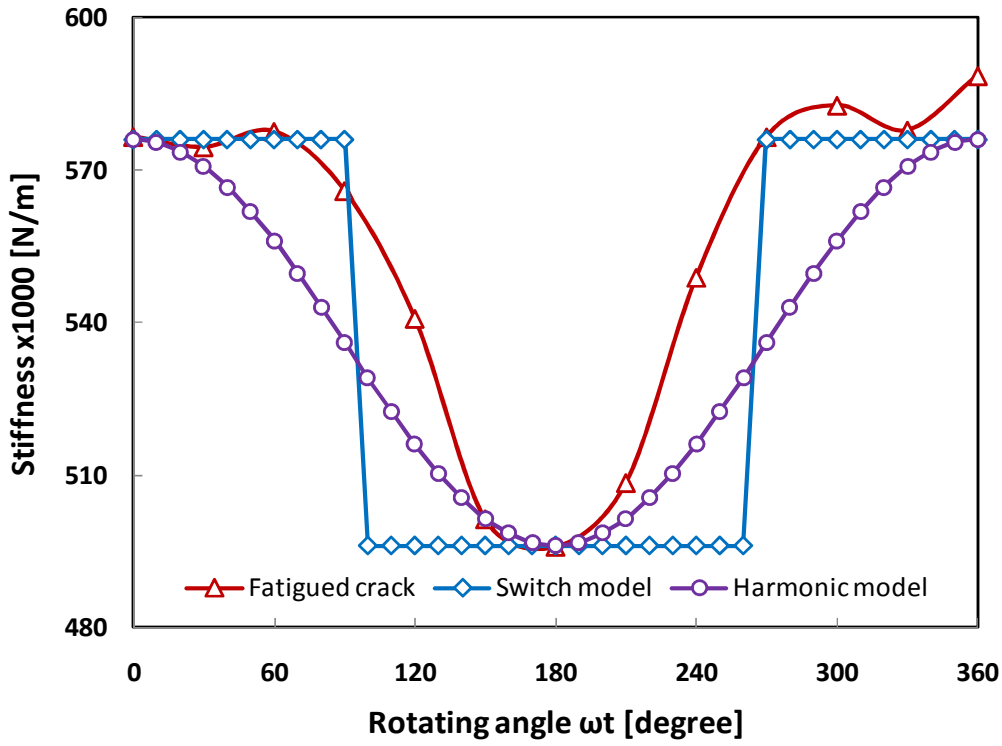

Fig.4.19. A comparison of measured periodic stiffness values and those calculated using theoretical models

Using experimental values of $K_o = 5.8x10^5$N/m and $K_o-\Delta K=4.96x10^5$N/m, respectively, stiffness values predicted by the two models were calculated and presented in Fig. 4.19, together with experimental results for a fatigue crack. It was found that the true stiffness profile due to a transverse fatigue crack could not be described accurately by either the switching model or the harmonic model. The most significant discrepancies between experimental results and theoretical models lie in the angular ranges where the crack was partially closed. In a recent study (Han, 2007) it was observed that the true shaft stiffness variation with rotating angle for a transverse shaft crack could not be described by either the switching model or the harmonic model.

4.4 Conclusion

In this Chapter the breathing mechanism for three types of shaft cracks were studied based on experimental results. It was found that the width of the crack opening gap played an important role in controlling the crack breathing behaviour. A fatigue crack without a clear gap showed a well-known opening and closing behaviour. A wider gap for a cut crack can change the periodical stiffness characteristic curve from a "V" shape to an "M" shape. Finally, a welded shaft crack does show a breathing function. However, to develop quantitative crack modelling and crack diagnostic techniques for this type of crack, the nominal crack depth must be considered carefully as the welding process tends to produce much lower measured stiffness characteristics for the shaft. This study also shows that neither the switching model nor the harmonic model can describe the periodic stiffness of a transverse shaft crack accurately.

CHAPTER 5

VIBRATION SIGNAL ANALYSIS

5.1 Experimental setup and procedures

In this chapter, vibration tests were conducted on the intact and cracked shaft specimens using SpectraQuest's rotor Machinery Fault Simulator (MFS). A tri-axis accelerometer and a disc load were mounted on the shaft near the centre of the bearing support span as shown in Fig. 5.1 below. The accelerometer formed part of the vibrational analyser tools used in the experiment. They consisted of a Brüel & Kjær, type 3050-B-060 Vibration Analyser (Fig.5.2 below) and associated software program, the Pulse Modal Test Consultant (MTC).

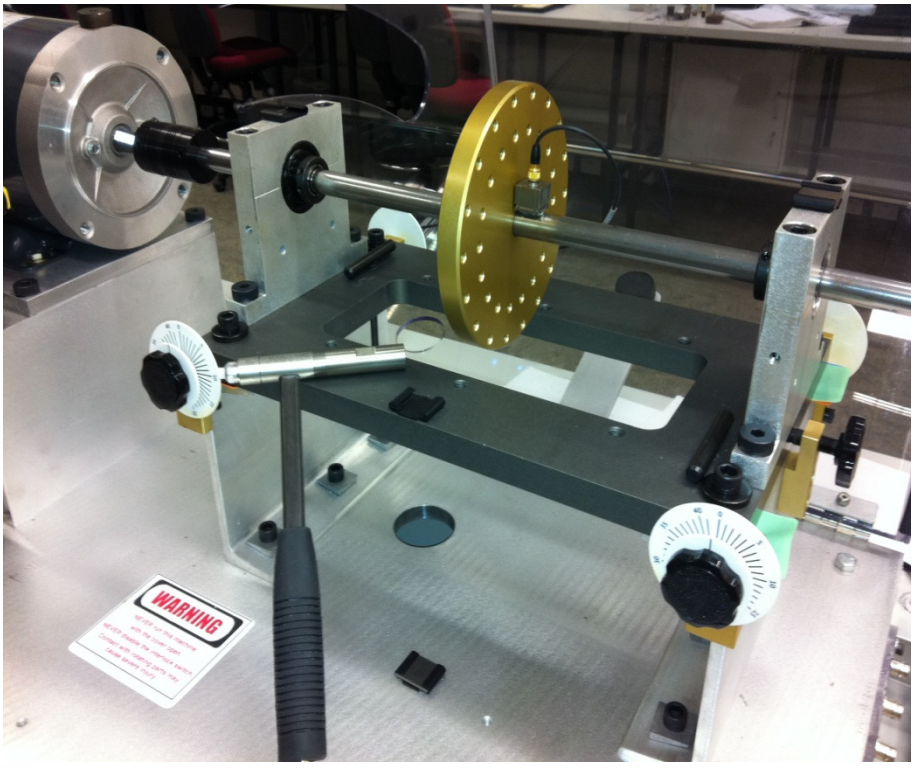

Fig.5.1 Vibration test setup on MFS

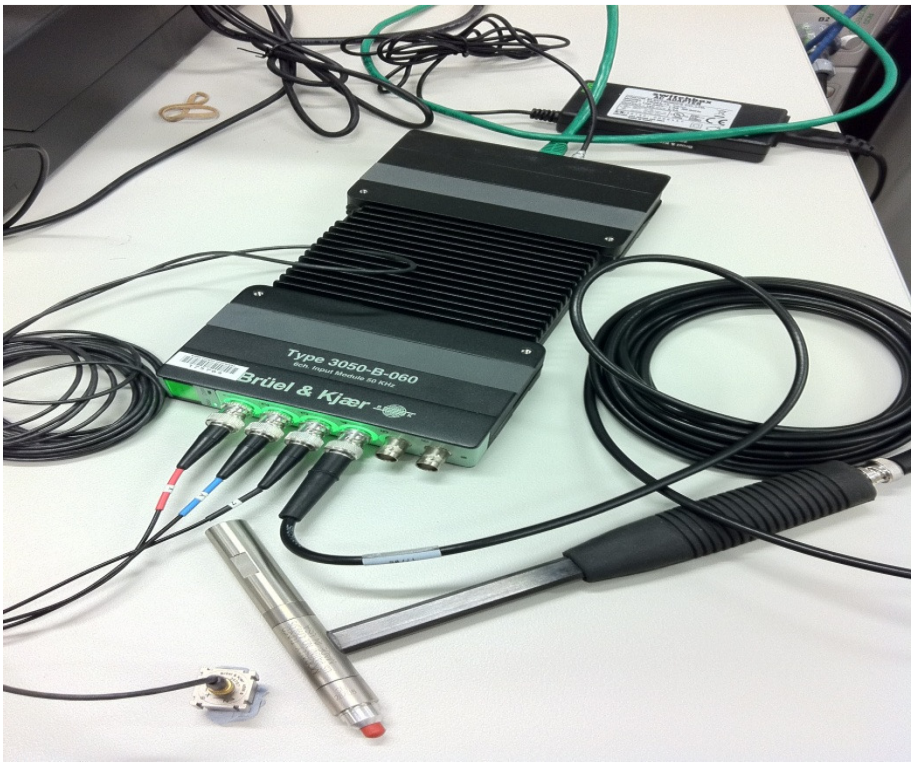

Fig. 5.2 Vibration analyser, accelerometer and hammer

Figures 5.1 and 5.2 show the Vibration Analyser accelerometer used to measure the acceleration responses of the shaft in the X, Y and Z axis directions (defined in Fig.5.3 below). They also show the impact hammer with a built-in force transducer used to apply the shaft excitation force.

The three different types of cracked shafts and one intact shaft were used to conduct the offline (Shaft stationary) vibrational experiments. Each test specimen would be hit by the hammer tool on the shaft end to create an input force that would be captured by the analyser. The MTC analyser program had pre-settable input force trigger levels that started the input force and frequency response measurement. The trigger levels in conjunction with an audible sound for feedback ensured the user could produce uniform excitation force levels in subsequent test samples. For each new shaft type placed into the MFS, the input force, the trigger levels and accelerometer responses had to be calibrated for in the MTC analyser program for measurement and analysis.

Fig.5.3 illustrates the geometry task in the MTC analyser program. The picture indicates two measurement points being selected to be analysed. Point 1 represents the hammer force input excitation, while point 2 represents the tri-axis accelerometer response, with the setup being shown in three given directions.

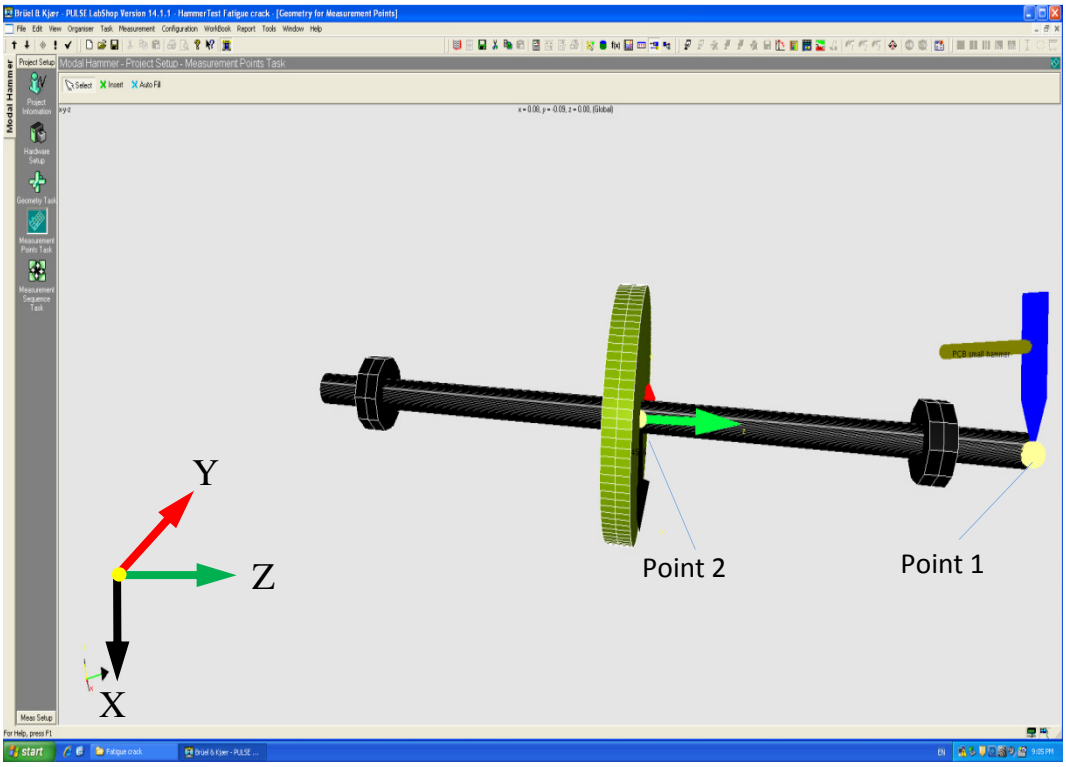

Fig.5.3A schematic geometry task and measuring point in the test.

Before conducting each experiment, the individual shaft specimen was fixed into the MFS as shown Fig. 5.1. For the cracked shaft test specimens, the crack position was placed at centre of span, and close to the disc. The crack fissure faced upward at $\theta = 0°$(the same as in chapter 4).This shaft alignment was programmed into the MTC Vibration Analyser for analysis (Fig.5.3).

The first natural frequency response of the X-axis accelerometer was used for the current vibrational analysis since the results could be directly compared to those for the previous stiffness tests (Chapter 4). The following data produced by the MTC program was used: Input (Force)-Time waveform, Transfer Function-

frequency, waterfall plot of Coherence-frequency, and the acceleration signals in three directions(X,Y, Z axes), as indicated in Figures 5.4 and 5.5 below.

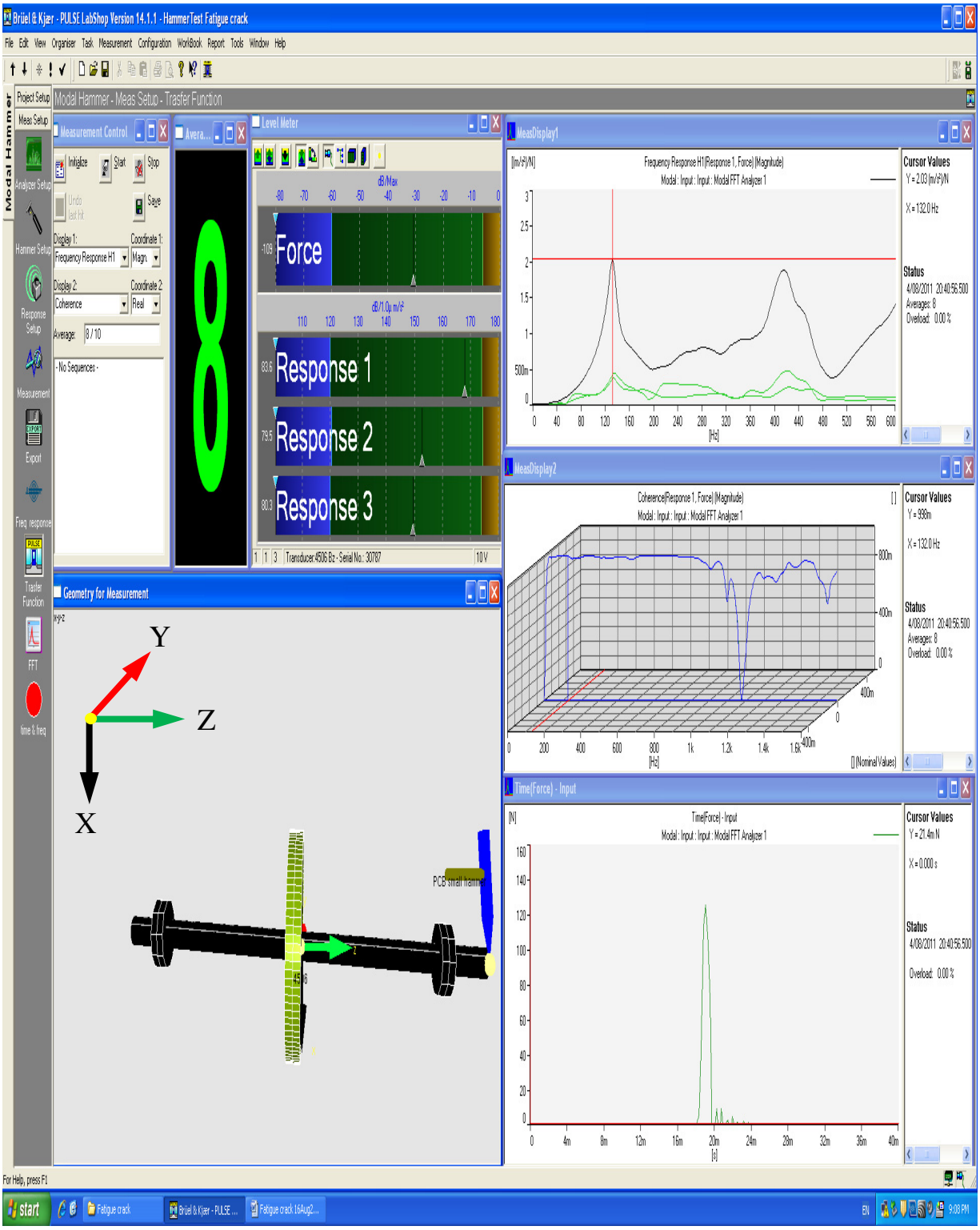

Fig.5.4 Measurement setup - Transfer function of the fatigue cracked shaft.

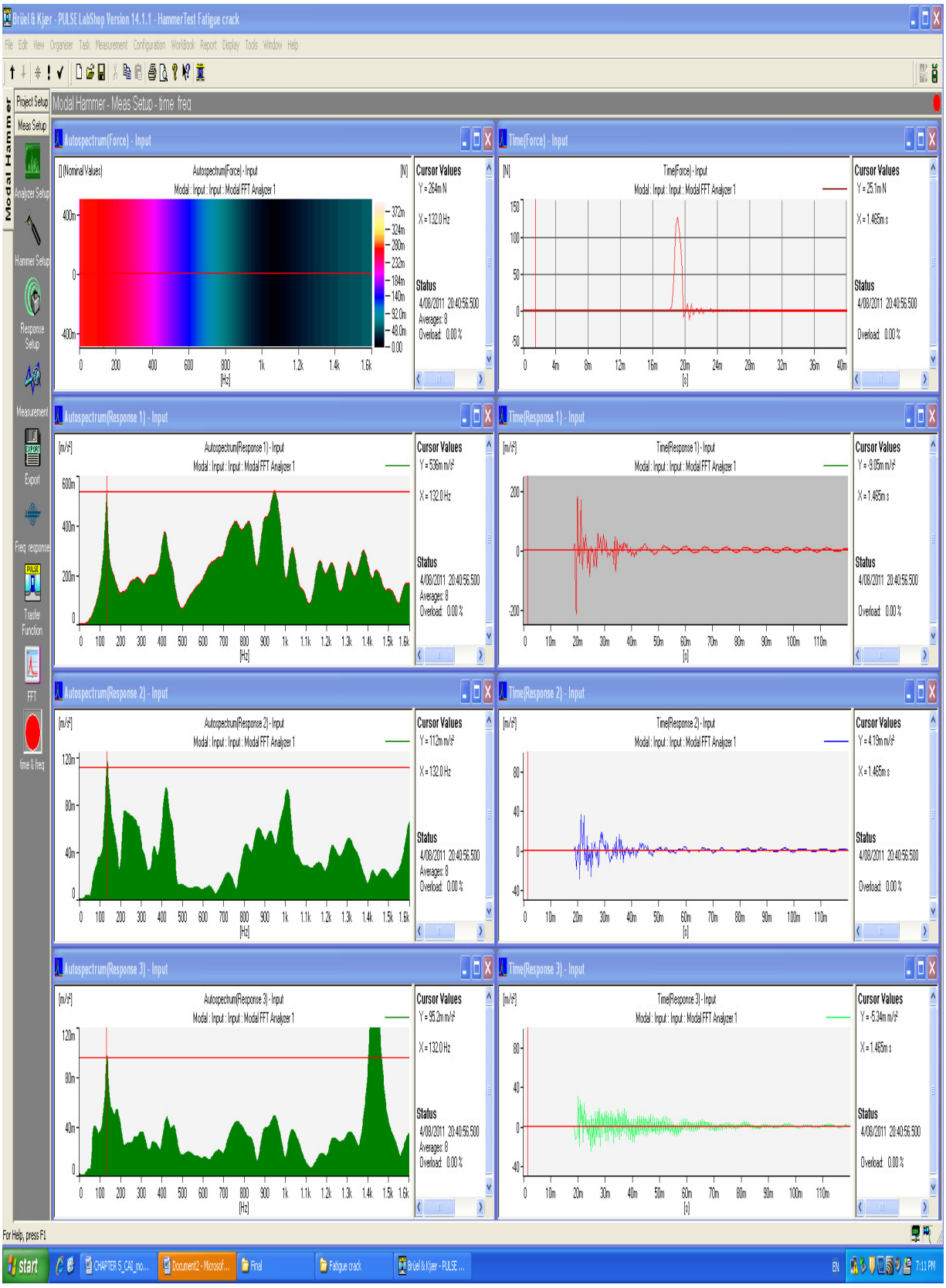

Fig.5.5 Measurement setup - Acceleration signals of the fatigue cracked shaft.

In Fig.5.4 the MTC program display shows the level meter window showing the measured input force and response trigger levels where response 1, 2 and 3 represent the X-axis, Y-axis and Z-axis accelerometer signals, respectively. The two top right analysis widows show the frequency and coherence responses of the X-axis accelerometer averaged over 8 test cycles on the specimen under test. Note the frequency response cursor showing the location of the first natural frequency of the X-axis accelerometer and corresponding cursor values on the right of the display. The final display window on the bottom RHS shows the measured input force-time waveform.

In Fig.5.5, on the left, from top, the first display shows the force input vs. frequency. The subsequent displays show the acceleration signals vs. frequency responses in the X, Y and Z axis directions. The display windows on the right hand side are the corresponding time domain signals.

Each time a test series was completed for a specimen, the raw data and the spectrograms were saved for further processing using Microsoft Excel. The specimen shaft was dismantled from the MFS, and kept for future online critical speed measurements.

The measurement procedures for all the different shaft crack type specimens were similar to the test specimen just described. However, a new MTC program measurement setup was required for each type of specimen shaft. The hammer and accelerometer response setup had to be re-calibrated in the program before proceeding with a new measurement set.

5.2 Experimental results and analysis

The first natural frequency responses (X-axis accelerometer) for different cracked conditions on the shafts in the above experiments were obtained through analysing the measured results. The obtained results of the four types of cracked shaft specimens with the crack facing up are presented in Figures 5.6 to 5.21 below.

1. *Modal test results of a fatigue cracked shaft*

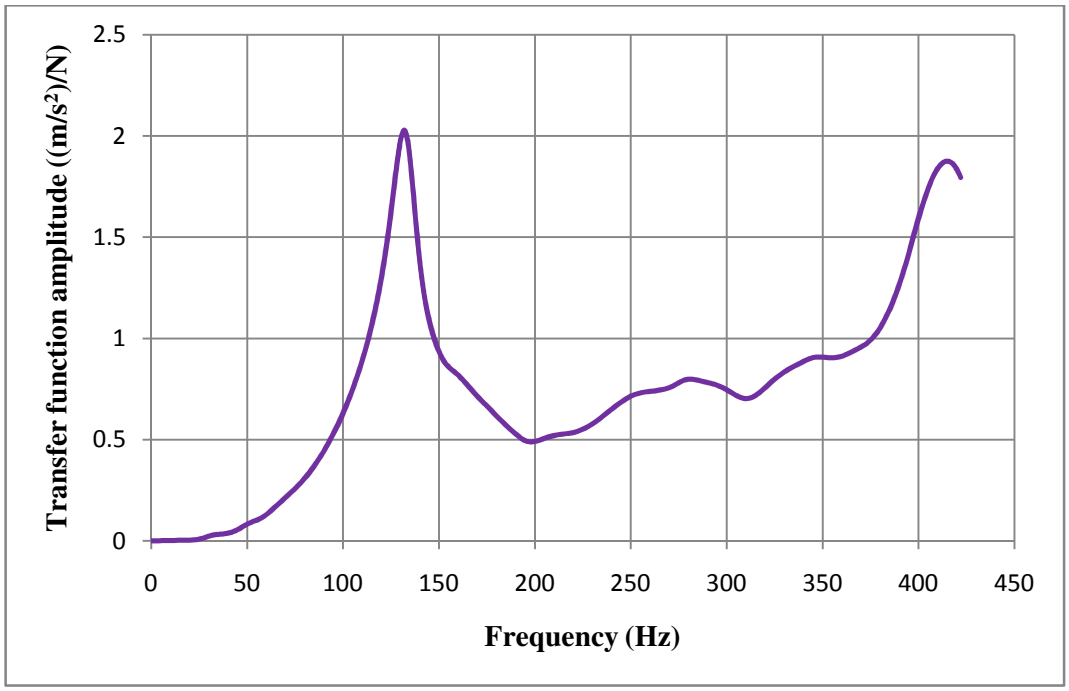

Fig.5.6. Transfer function vs. Frequency (Fatigue crack)

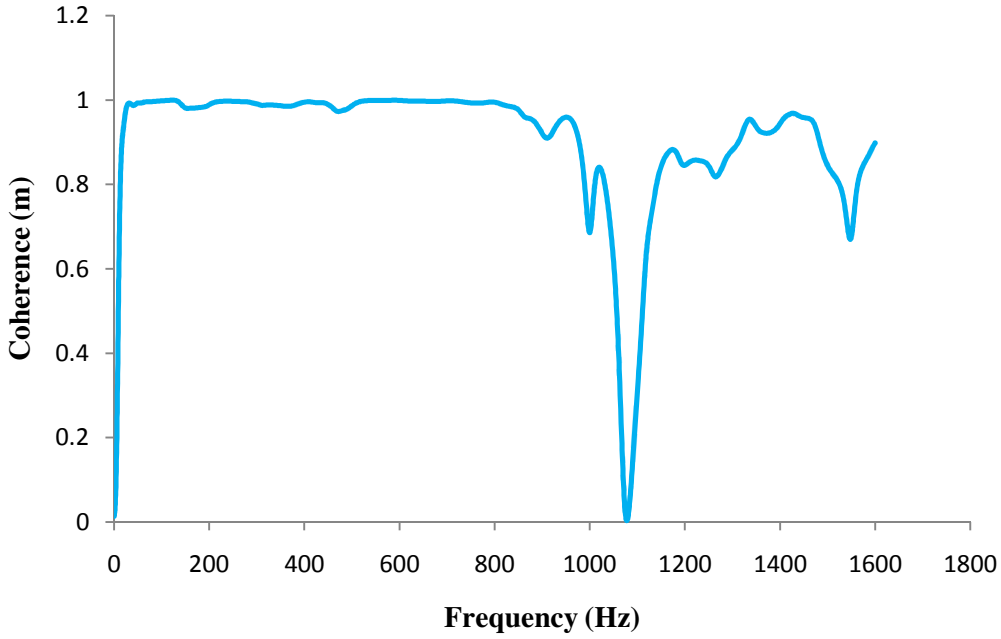

Fig.5.7. Coherence vs. Frequency (Fatigue crack)

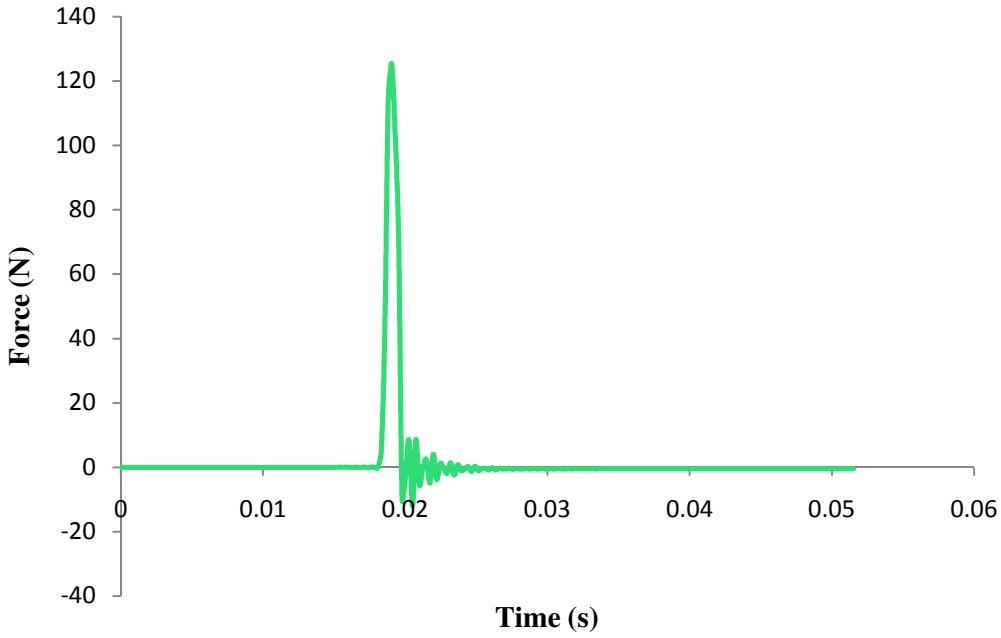

Fig.5.8. Force vs. Time (Fatigue crack)

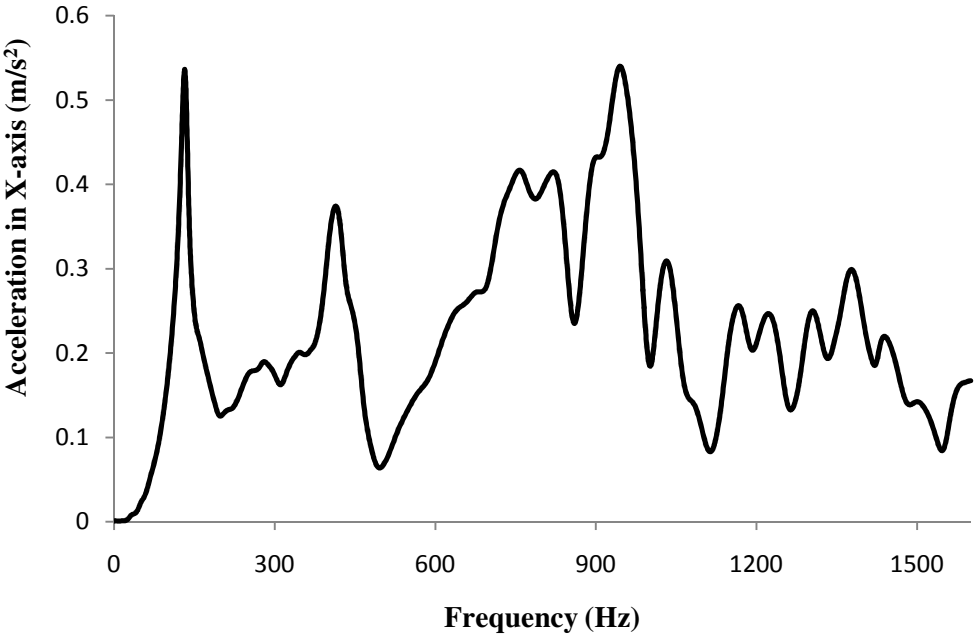

(a) - X-axis direction

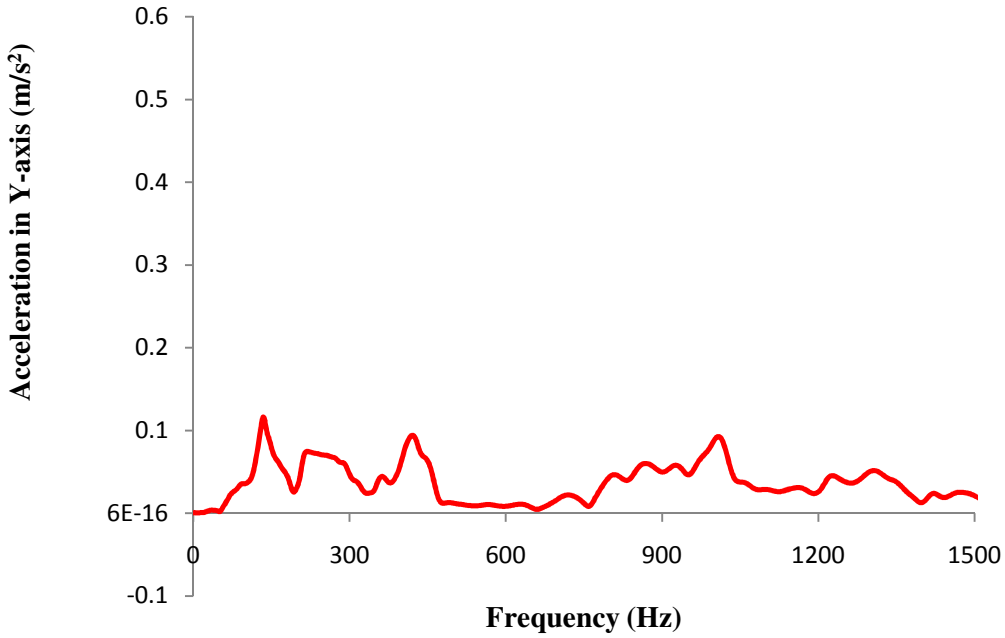

(b) -Y-axis direction

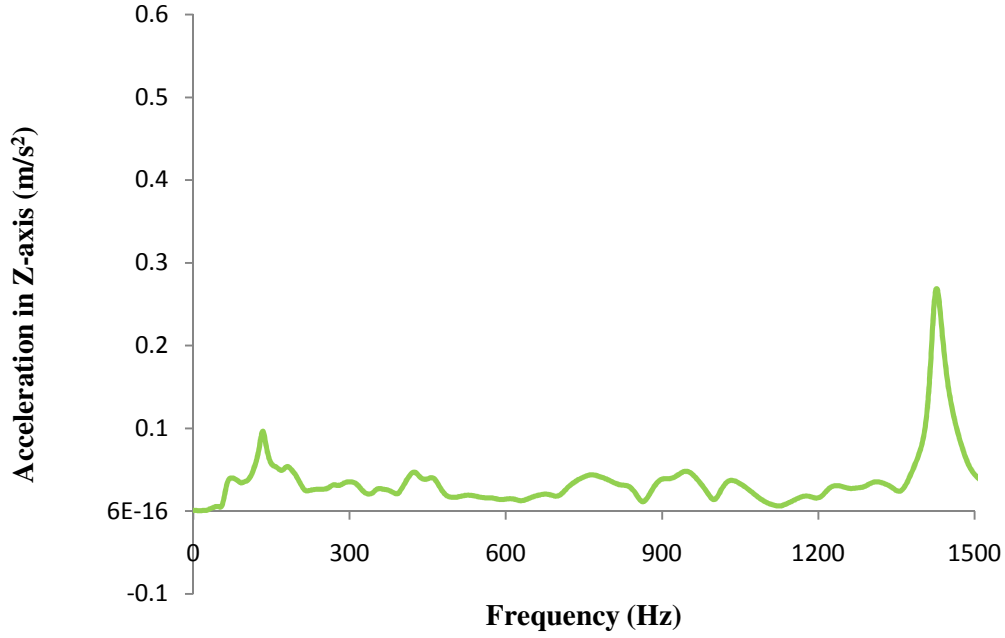

(c) -Z-axis direction

Fig.5.9. Acceleration vs. frequency in three directions (Fatigue crack).**(a),**X-axis direction; **(b),**Y-axis direction; **(c),**Z-axis direction.

2. Modal test results of a cracked welded shaft

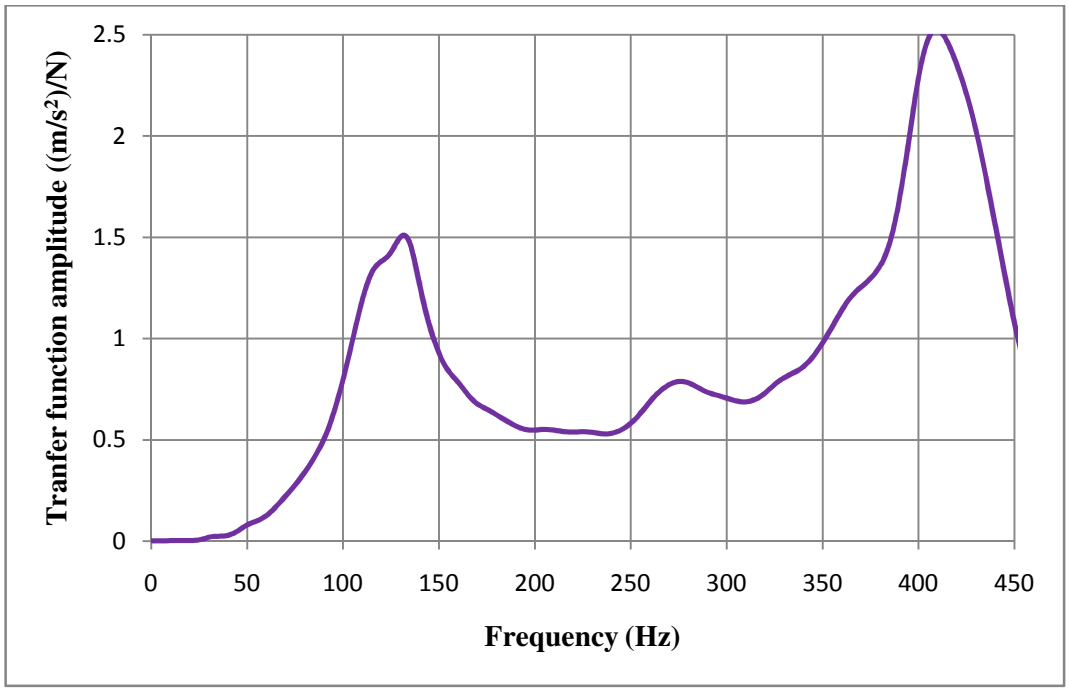

Fig.5.10. Transfer function vs. Frequency (welded shaft)

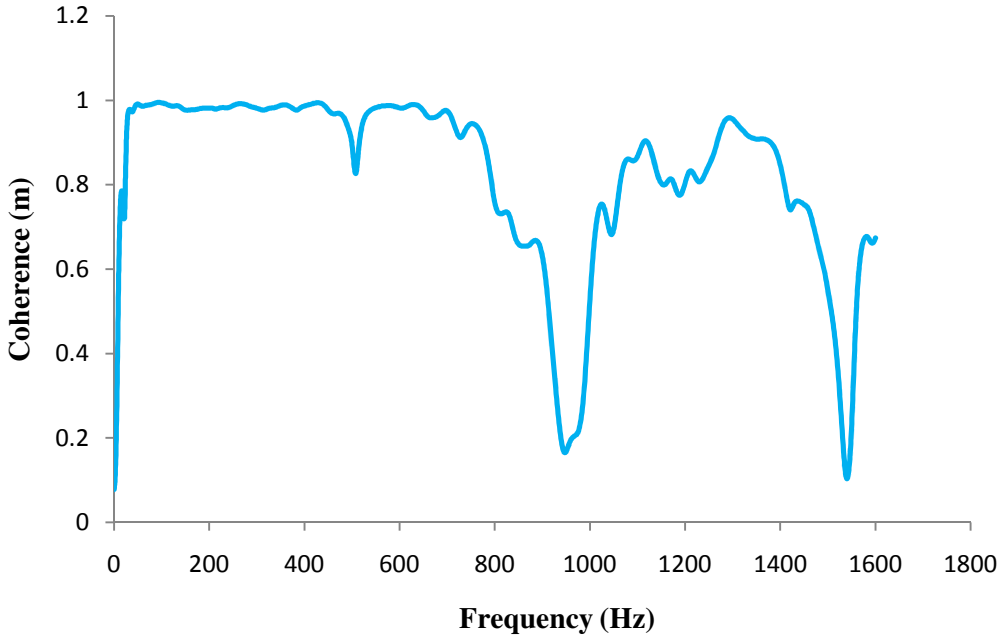

Fig.5.11. Coherence vs. Frequency (welded shaft)

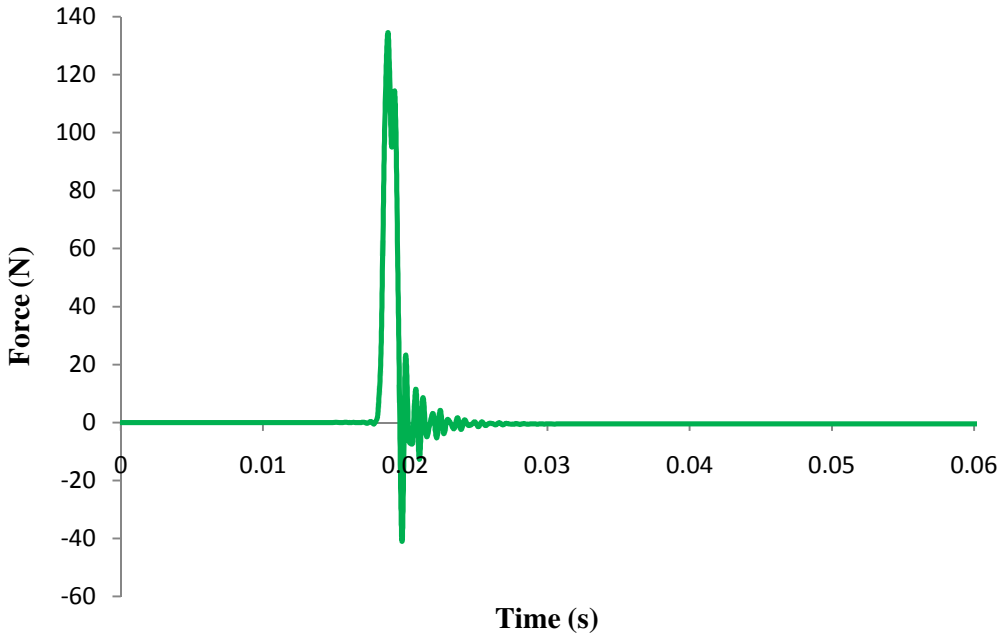

Fig.5.12. Force vs. Time (welded shaft)

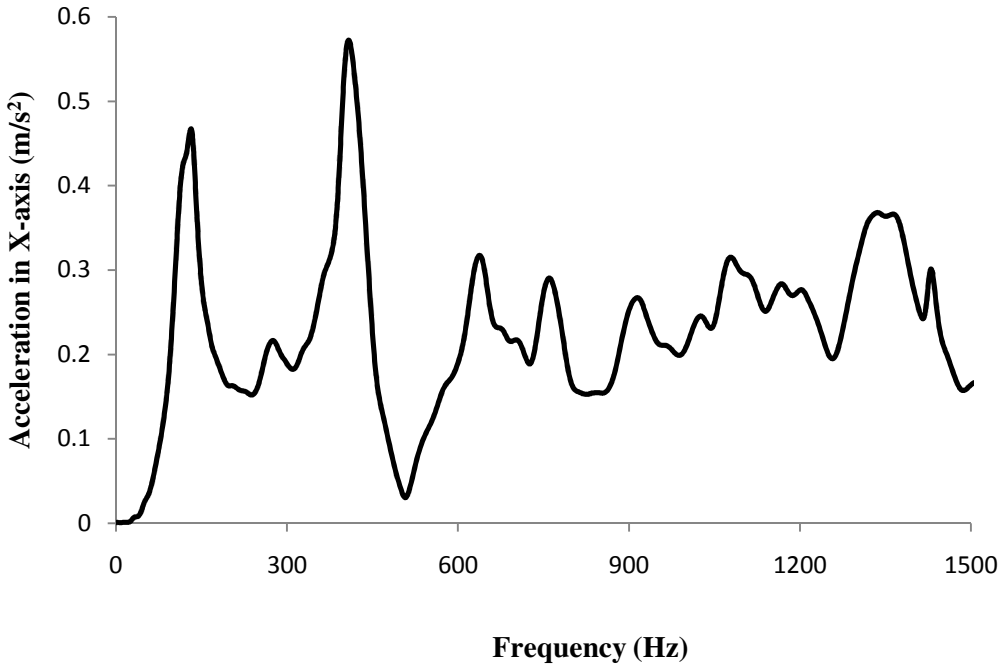

(a) - X-axis direction

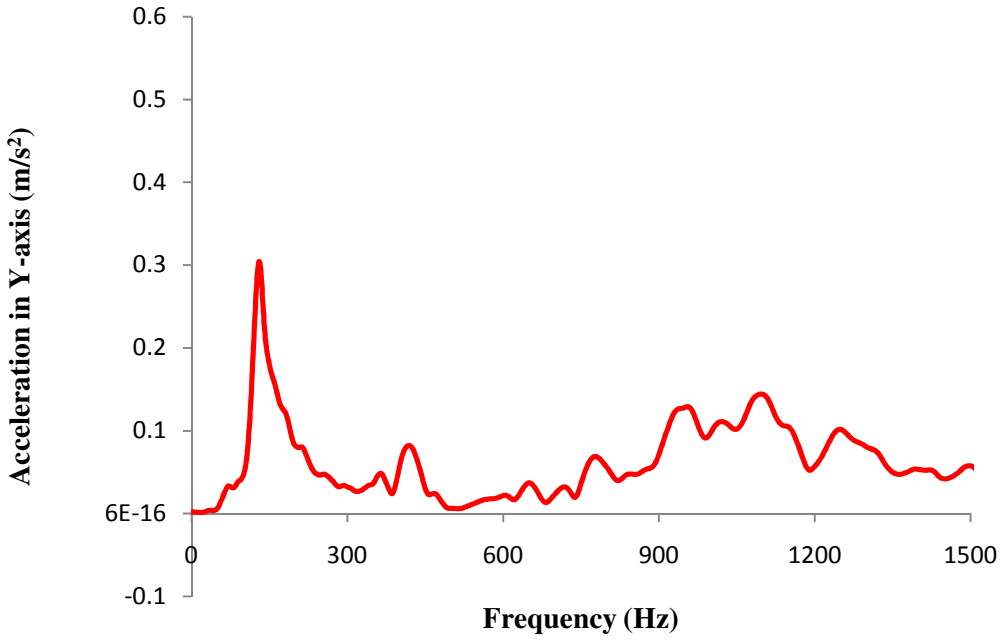

(b) - Y-axis direction

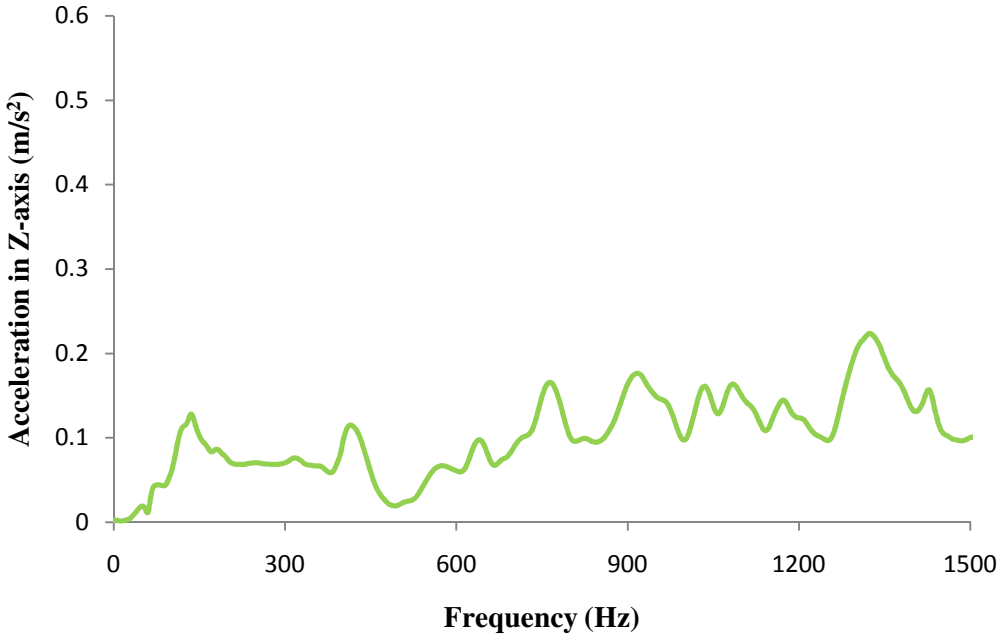

(c) - Z-axis direction

Fig.5.13. Acceleration vs. frequency in three directions (welded shaft). **(a),**X-axis direction; **(b),**Y-axis direction; **(c),**Z-axis direction.

3. *Modal test results of a Wire-cut shaft*

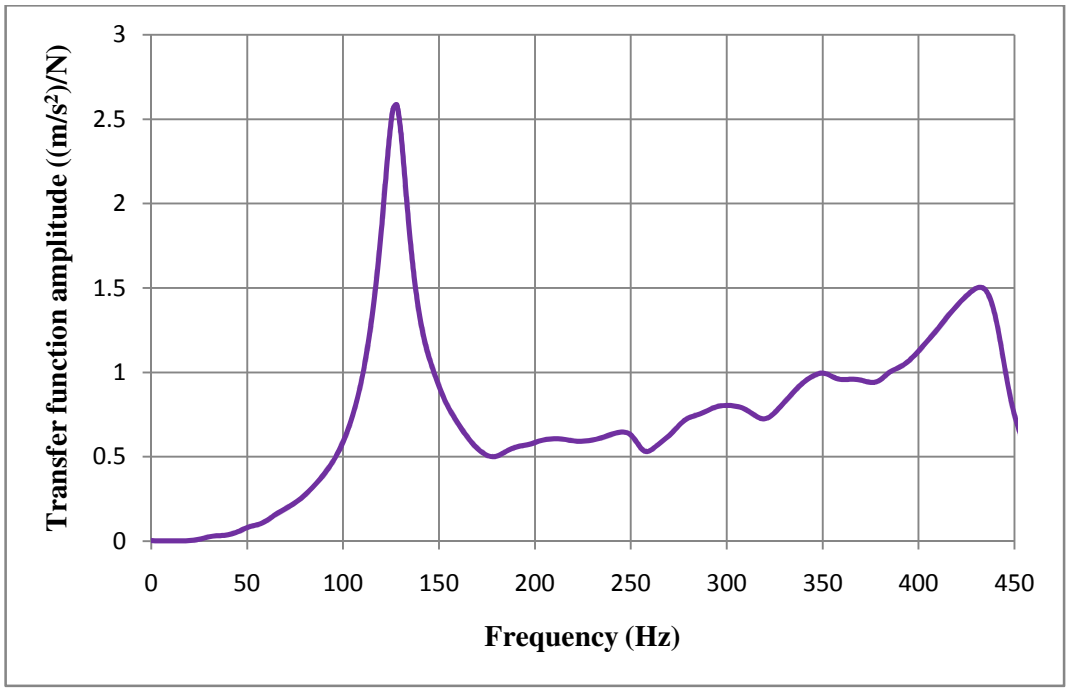

Fig.5.14. Transfer function vs. Frequency (Wire-cut)

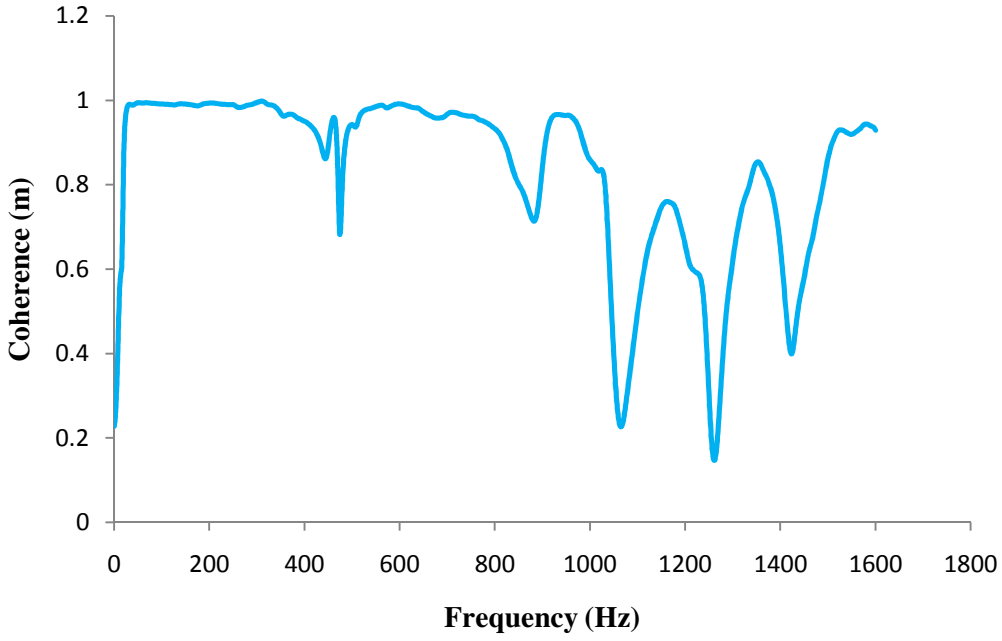

Fig.5.15. Coherence vs. Frequency (Wire-cut)

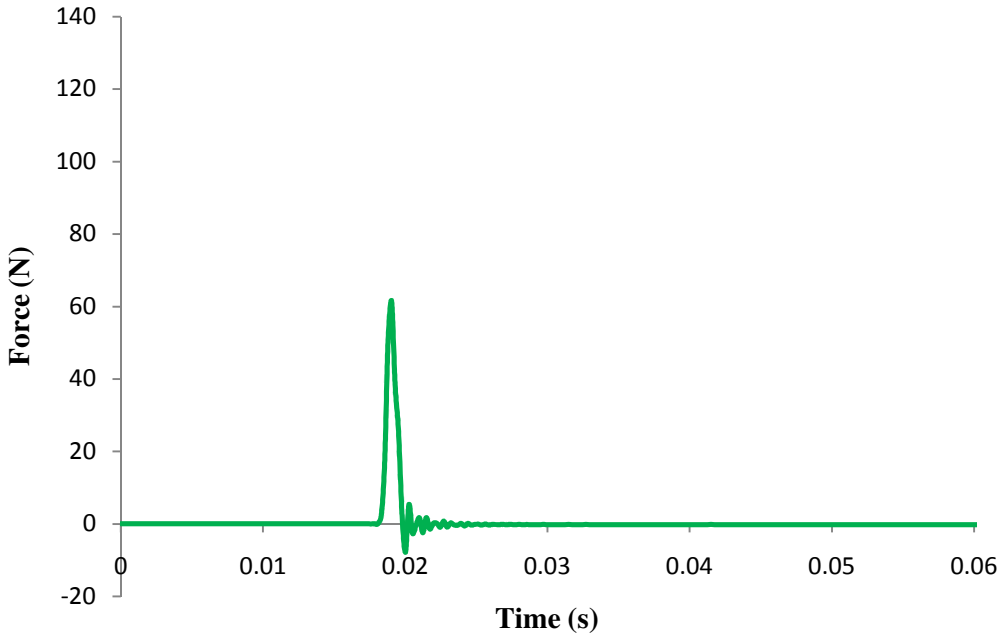

Fig.5.16. Force vs. Time (Wire-cut)

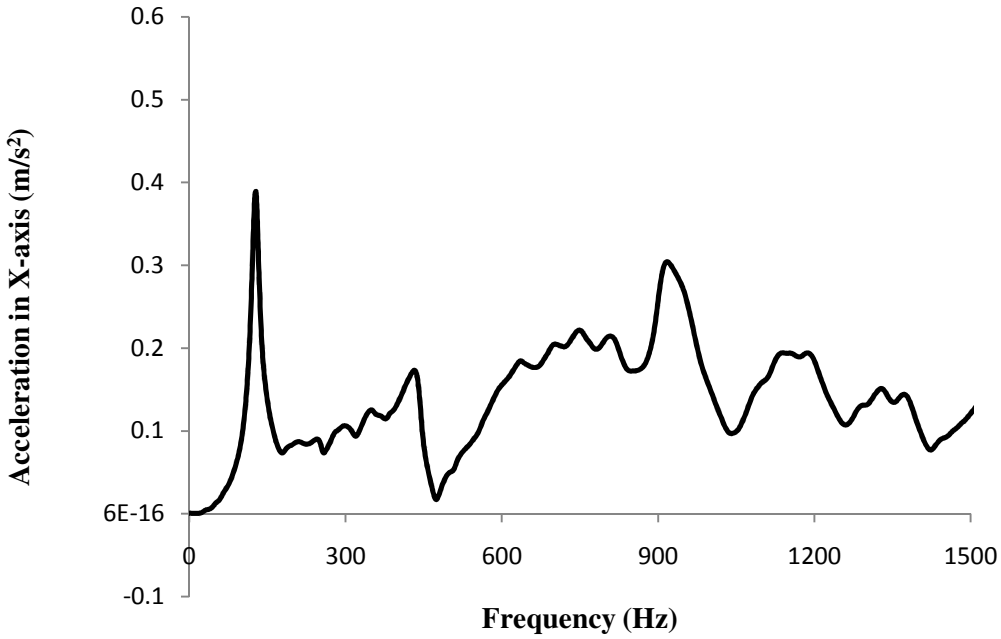

(a) - X-axis direction

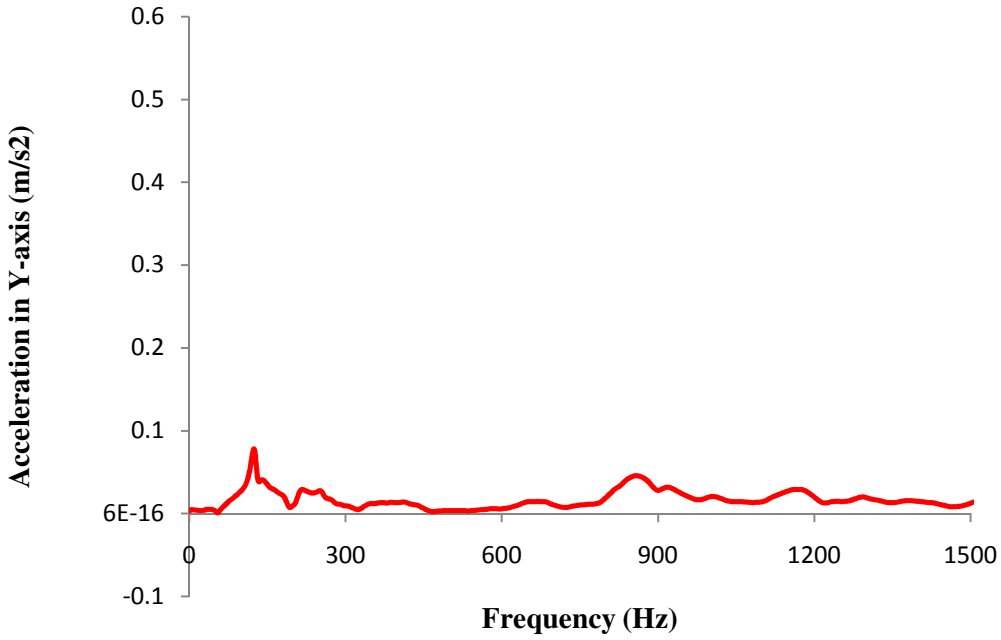

(b) - Y-axis direction

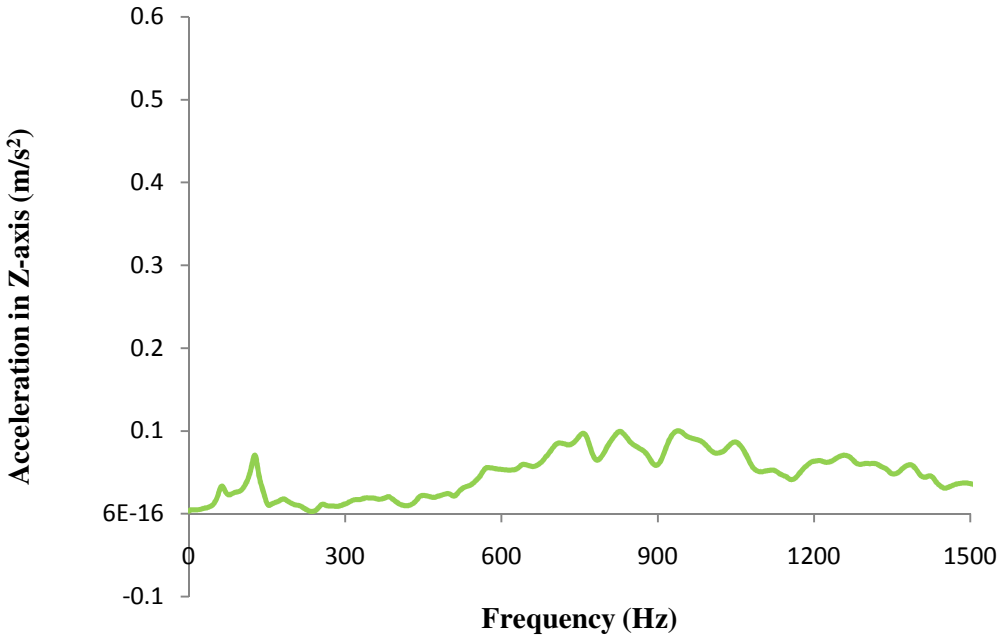

(c) - Z-axis direction

Fig.5.17. Acceleration vs. frequency in three directions (Wire-cut). **(a),** X-axis direction; **(b),** Y-axis direction; **(c),** Z-axis direction.

4. *Modal test results of an Intact shaft*

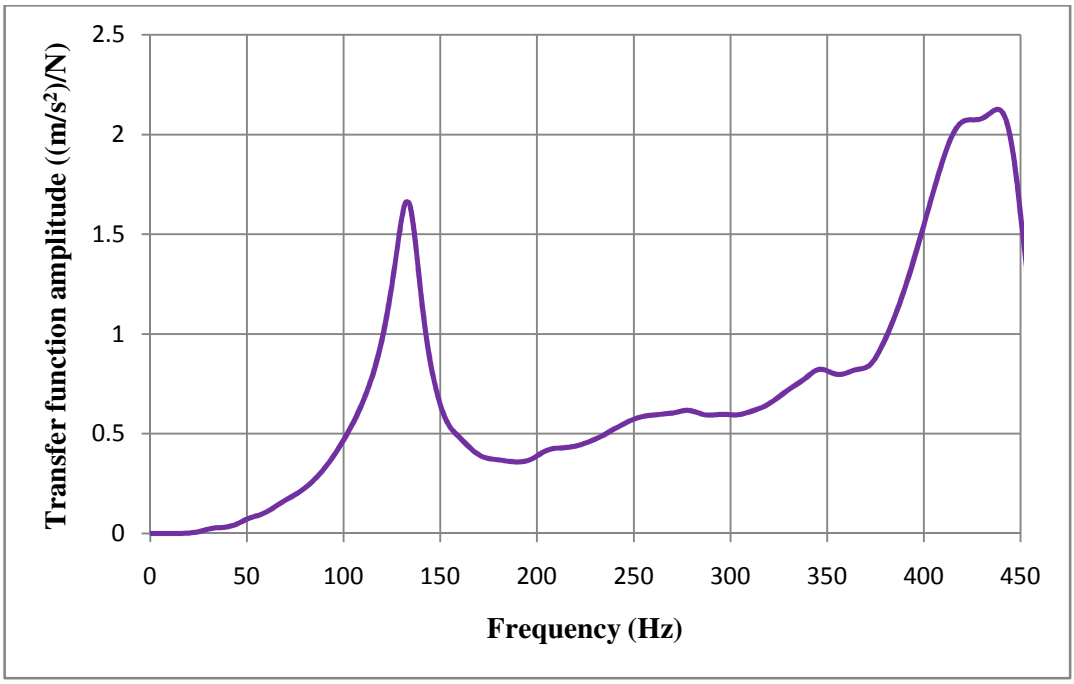

Fig.5.18. Transfer function vs. Frequency (Intact)

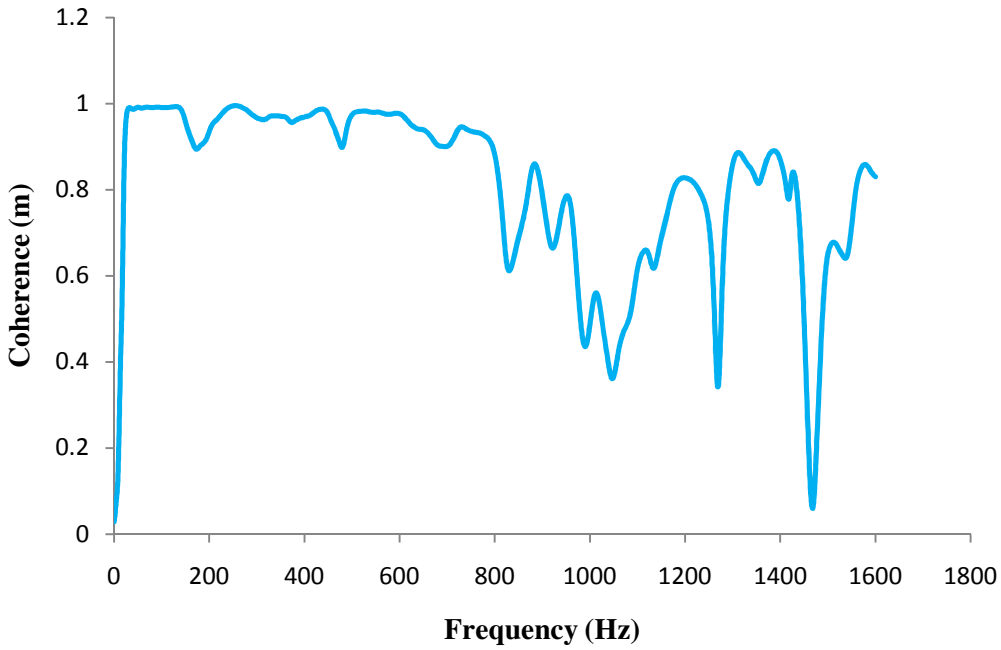

Fig.5.19. Coherence vs. Frequency (Intact)

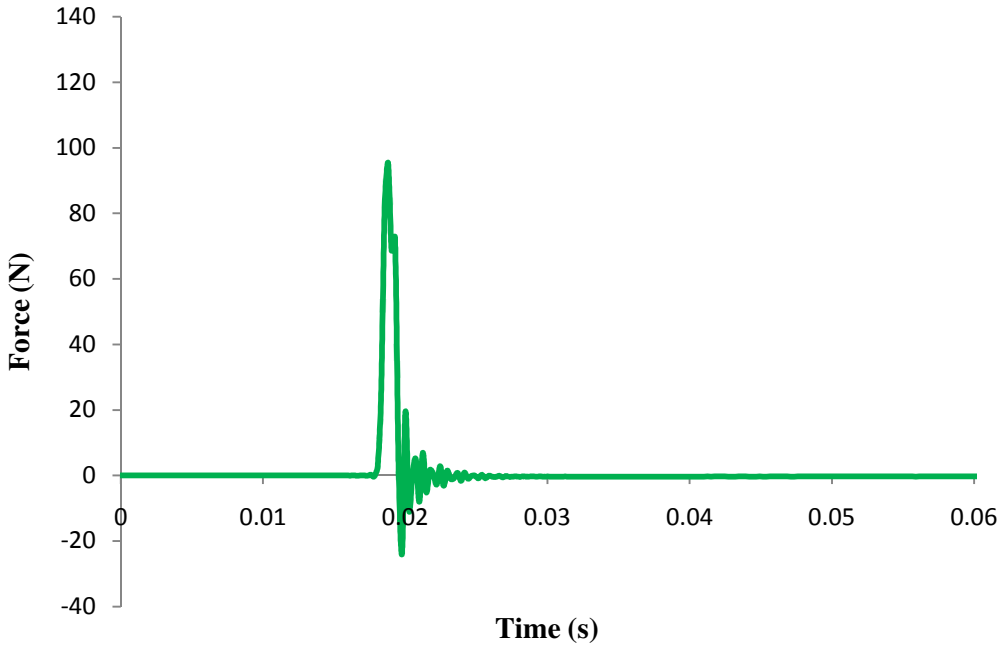

Fig.5.20. Force vs. Time (Intact)

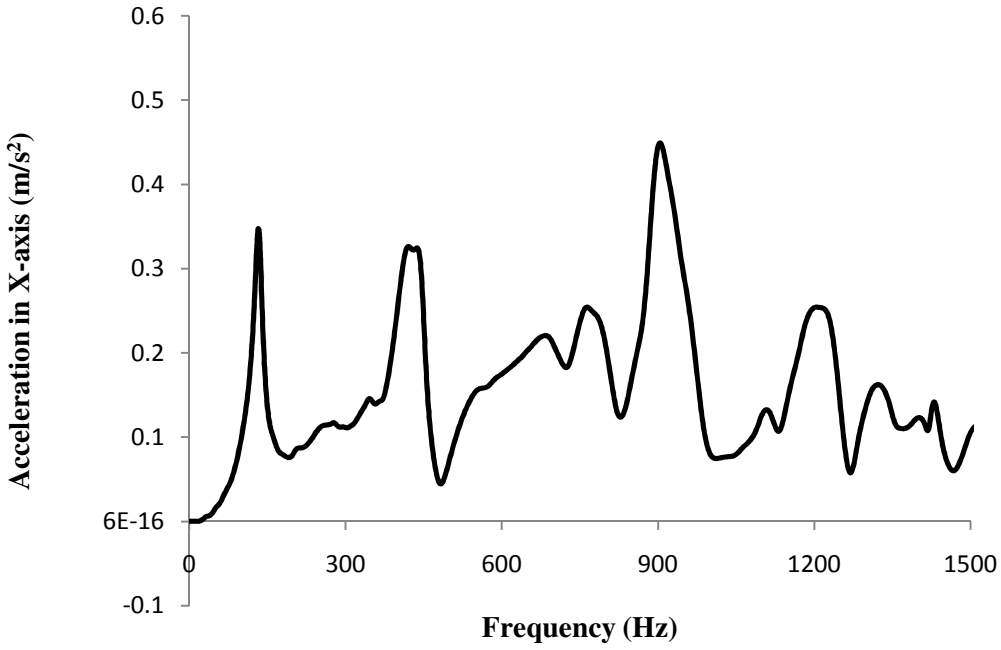

(a) - X-axis direction

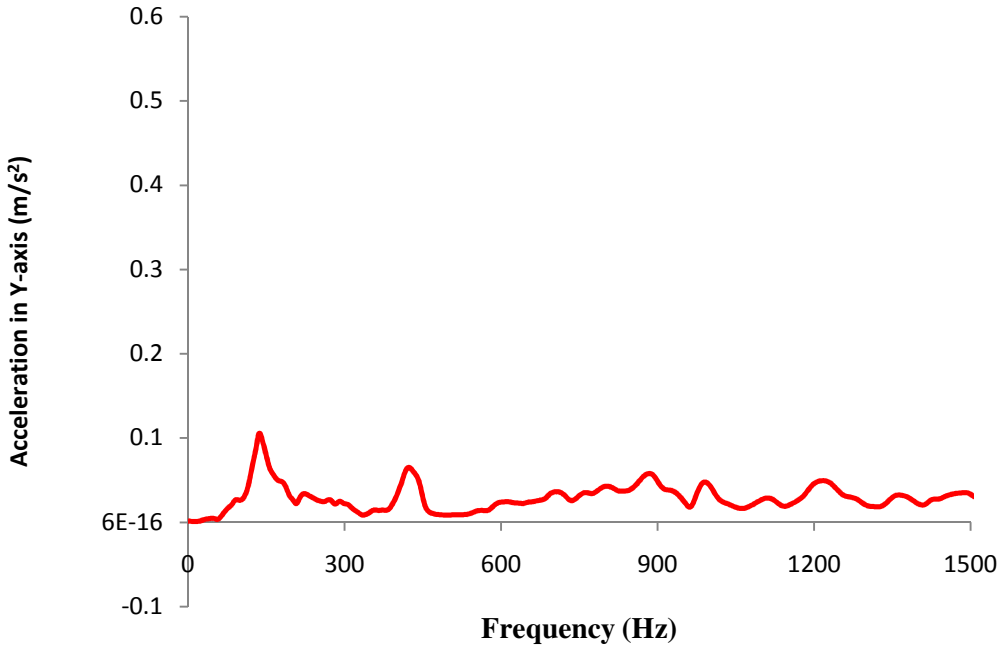

(b) - Y-axis direction

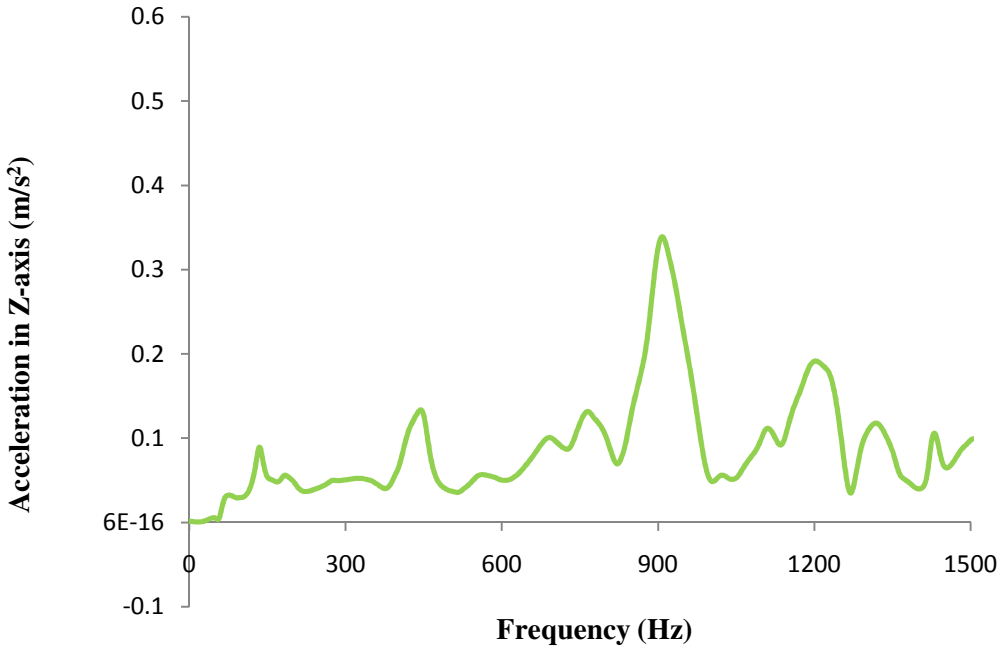

(c) - Z-axis direction

Fig.5.21. Acceleration vs. frequency in three Directions (Intact). **(a),** X-axis direction; **(b),** Y-axis direction; **(c),** Z-axis direction.

As detailed in chapter 4, the shaft bending stiffness in the X axis direction (perpendicular to shaft neutral axis) was measured and compared. Here the frequency response in the X axis direction (frequency response 1) was used for comparing and analysing the variations for different types of cracked shaft.

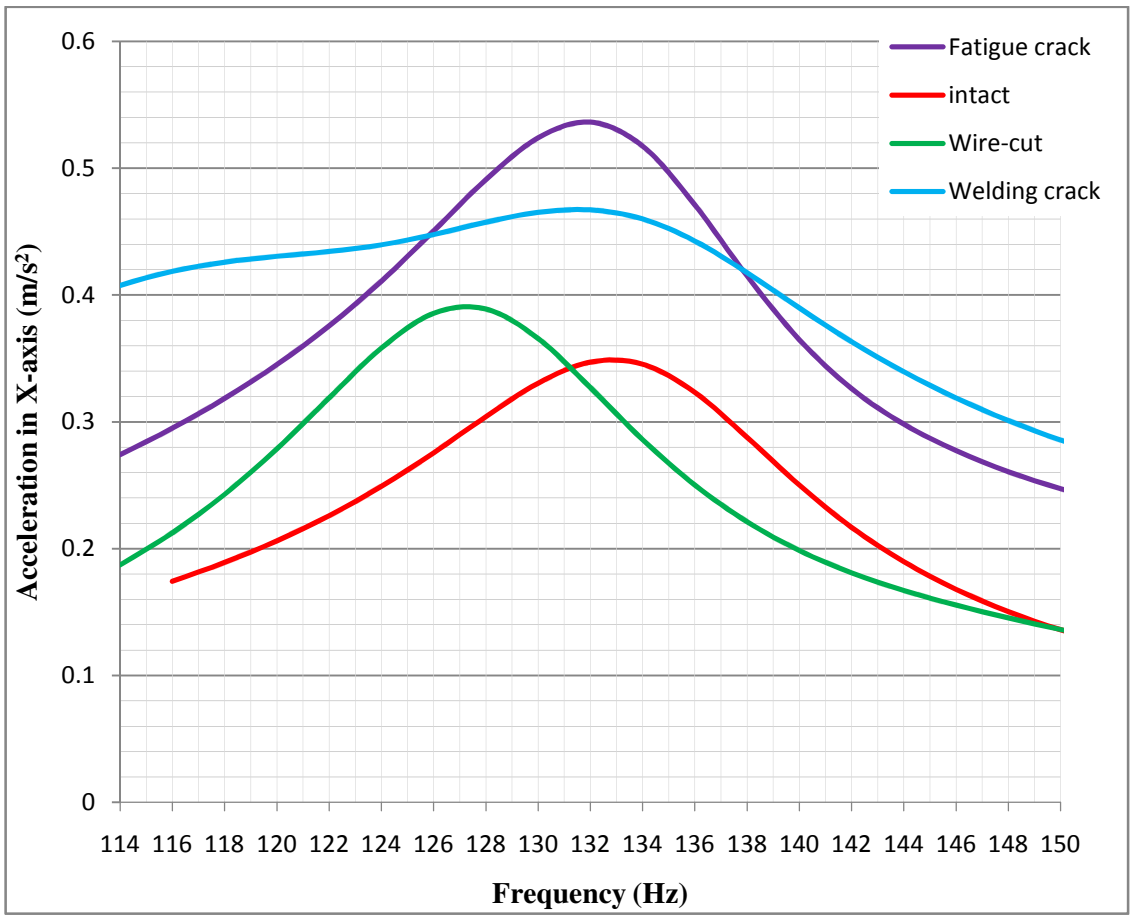

Fig.5.22.The acceleration in X-axis direction for four types of crack conditions

Based on the raw data from the experiments, the first natural frequency responses in the X-axis direction of the three different cracked shafts and the intact shaft were plotted in Fig.5.22. From the diagram, a summary of the first natural frequencies of the four specimens were listed in Table 5.1.

TABLE 5.1 The first resonant frequencies of different cracked shafts

Type of Crack	Fist resonant frequency (Hz)
Intact	133
Fatigue crack	132
Welded shaft	131
Wire-cut	127

Table 5.1 has demonstrated that the first resonance frequency decreases from 133 Hz of the intact shaft to 127 of the wire-cut cracked shaft, with the fatigue cracked shaft (132 Hz) and the cracked welded shaft (131 Hz) taking the intermediate values. The overall trend in the changes of the natural frequencies in the four types of shaft is clearly shown in Fig.5.23.

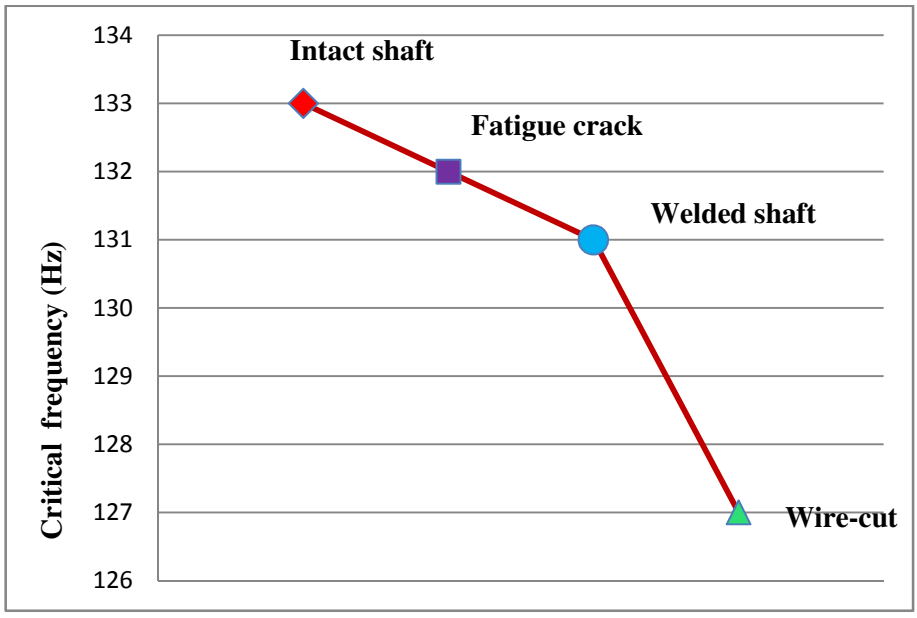

Fig.5.23. Change of the first resonant frequency in different cracked shafts

5.3 Discussion and Conclusion.

As demonstrated in Fig. 5.23, for all four types of shaft specimens with different crack conditions, the first natural frequency in the same direction as the measured shaft stiffness (Chapter 4), decreased significantly due to the presence of the crack in the shaft. The intact shaft had the highest resonance frequency, due to the fact that the bending stiffness was of the highest amongst all the shafts investigated (see Chapter 4). When a crack exists, the stiffness reduced and consequently the first natural frequency in the same measured direction would also decrease. This is consistent with the previous study by Xie *et al.*(2007).

The amount of frequency reduction in different types of cracks can also be explained by the variation in bending stiffness. As mentioned previously, these modal tests were conducted offline with the crack position at $\theta = 0°$. The bending stiffness at rotation angle $\theta = 0°$ is illustrated in Table 5.2, with the data taken from Fig 4.17 in Chapter 4.

TABLE 5.2 Different shafts' bending stiffness at rotating angle 0°

Type of Crack	Stiffness value at 0°(N/mm)
Intact	592.46
Fatigue crack	576.45
Welded shaft	553.36
Wire-cut	479.81

When a fatigue crack exists in the shaft, the stiffness would be reduced, compared to an intact shaft. However, at $\theta = 0°$, the change in stiffness was small (~2.7%). As mentioned in chapter 4, this is because the crack was fully closed. Consequently, the frequency had a slight drop to 132 Hz compared to 133Hz for an intact shaft.

The cracked welded shaft's stiffness was lower than that of a fatigue cracked shaft at the same angles of rotation. Although, the crack fully closed similar to that of the fatigue crack, from chapter 3 Fig.3.12, we knew that there was still a small gap (0.05mm) at this fully closed position. As a result, the observed frequency for the cracked welded shaft further decreased to 131Hz.

For the shaft with a wire cut crack, at $\theta = 0°$, the stiffness was much lower, even compared to the cracked welded shaft. As discussed in chapter 4, no breathing behaviour was observed for a wire-cut shaft, the large gap (0.15mm) prevented the two cut surfaces from closing. Thus, the observed frequency dropped dramatically to 127Hz.

The trend of the stiffness at rotation angle $\theta = 0°$ for the four types of shaft specimens can be illustrated in Fig.5.24.

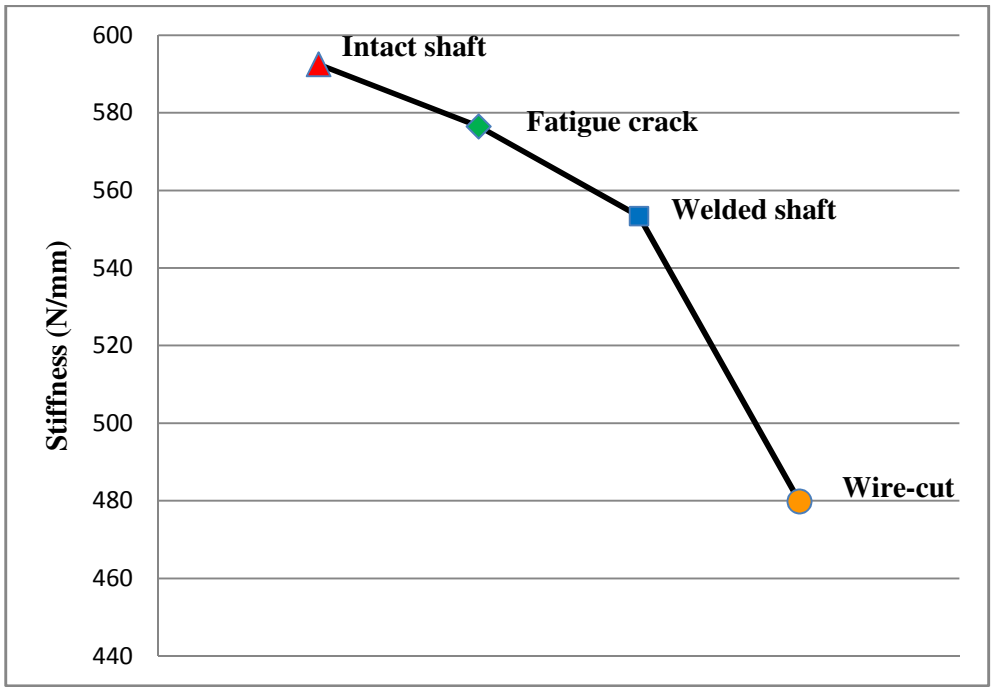

Fig.5.24. Change of the stiffness ($\theta = 0°$) in different cracked shafts

Fig.5.24 shows the same trend tendency as that of Fig.5.23. The reduction in stiffness is almost proportional to the decrease in frequency for the four different shaft crack conditions.

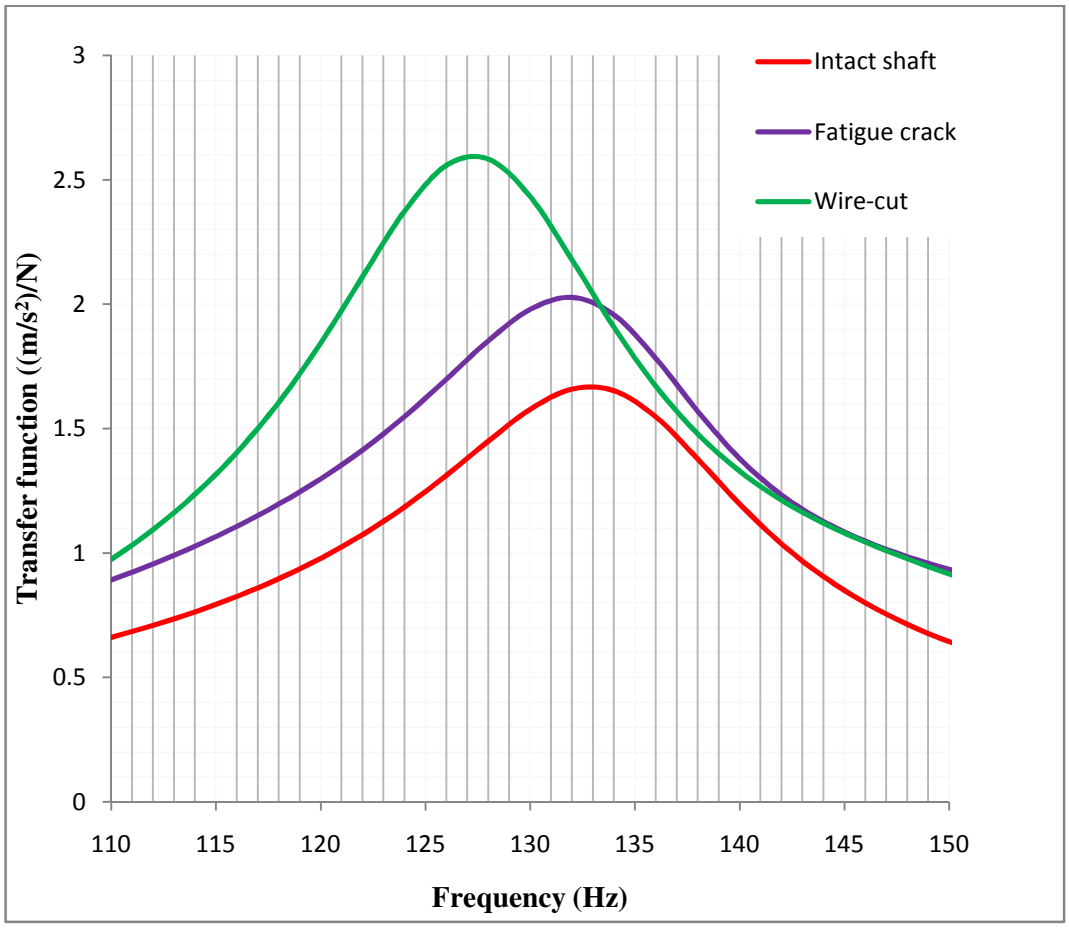

Fig.5.25.The transfer function vs. Frequency of the three typical crack conditions

As concluded in Xie *et al.* (2007), the frequency responses of the cracked shaft are larger than that of the intact shaft. The crack element changed and amplified the vibration responses. Fig.5.25 demonstrates the frequency responses of three typical types of shaft crack conditions. The frequency response of the fatigue cracked shaft is larger than that of the intact shaft. For the wire-cut shaft, the frequency response is significantly the highest among the crack types tested. This is due to the wire-cut shaft having the largest gap.

In this chapter, a number of shaft crack types were analysed using a Brüel & Kjær Pulse Modal Test Consultant (MTC) modal test analyser with hammer excitation. A series of experiments were conducted to observe the behaviour of the first natural frequency responses from all the shaft specimens in the same direction as previously performed shaft stiffness tests with the shaft crack pointing up. The results showed that, the first natural frequency in this direction decreased as the crack gap increased, on the contrary, the amplitude of the frequency responses increased while the crack gap increased. The results are consistent with the theoretical analysis and previous studies (Lee and Chung (2000), Xie et al. (2007)).

CHAPTER 6

SUMMARY AND CONCLUSIONS

6.1 Summary

Diagnosing shaft cracks in a rotating machine is one of the most challenging problems in equipment predictive maintenance today. In vibration-based methods, continuous performance monitoring allows trend analysis, for example, comparing today's vibration signals with those from a fortnight ago. Any difference is symptomatic of the existence of a fault condition, thus, early crack detection becomes possible.

A critical review of the methods adopted in the past on shaft crack detection has been attempted in this thesis. In general, shaft crack detection techniques are broadly categorized into two groups: vibration-based and model-based methods. These methods use the same principle, that the periodic stiffness variation will affect the dynamical behaviour of the shaft. Finding an efficient way to evaluate the true stiffness variation due to the crack's rotation is the key step for studying the behaviour of the cracked shaft. In terms of describing the crack element behaviour accurately, the finite element modelling approach has more potential in simulating the dynamic behaviour of one shaft having different kinds of crack. It was also noted that a combined approach (signal and model-based) for crack identification is one of the areas that relatively few works have been researched and reported on in literature.

This study has attempted a vibration-based method for cracked shaft diagnosis. The work involved crack specimen preparation (crack depth of 40% of diameter along the radial direction of the specimen shaft), in particular, fatigue crack creation. The elastic cracked shaft specimens were subjected to bending for stiffness analysis within a three point bending fixture by an Instron machine. Moreover, the cracked shafts were further studied on a SpectraQuest's rotor Machinery Fault Simulator (MFS), using Brüel & Kjær vibration analyser for studying their vibrational behaviour. The frequency responses in the X-axis direction (same direction as for the stiffness tests) were measured and analysed.

The present work demonstrated shafts with three different types of deep transverse crack (40% in depth). The characteristics of such cracks have been briefly explored. The breathing phenomenon of three transverse cracks in different rotational angles was extensively studied. The results were used to compare with that of an intact shaft and discussed, some conclusions have been drawn.

The unique vibrational behaviour due to a crack existence, and the frequency responses in the X-axis direction were presented and analysed. Furthermore, for the three different types of cracked shafts, the bending stiffness variation with different rotational angles due to crack presence has been experimentally proved. A significant change in magnitude of the stiffness, and the consequent decrease in the natural frequencies were observed and recorded. These experimental results are expected to assist with crack diagnosis in this area.

6.2 Conclusions

Based on the present study, the following general conclusions were drawn.

- ✓ Three different types of cracked shafts were carefully prepared. They represented the typical types of cracks that are being adopted for crack diagnosis in literature. Specifically the fatigue crack was properly seeded into the specimen shaft, the bending stiffness measurements and frequency response results obtained were accurate and reliable.

- ✓ In the study of shaft stiffness, the fatigue crack showed a typical breathing behaviour. This is consistent with the theoretical results reported in some published papers. The welded shaft crack also demonstrated these opening and closing characteristics. It was most probably due to the perfect contact joint the two un-welded surfaces made with each other that formed the crack. However, the cracked welded shaft stiffness was found to be much lower compared with that of a fatigue cracked shaft. This indicated that even the small gap (0.05mm) will prevent the crack gap from being fully closed, thus reducing the stiffness. As for the wire-cut crack, no breathing mechanism was observed for any rotational angle. This was because the crack gap was too big to close. The result of the wire-cut cracked shaft promoted the idea of an open crack model (papadopolous 2008) used in earlier studies which claimed the crack remained open during shaft rotation.

- ✓ Our results clearly show that existing switching model and harmonic models cannot describe the periodic stiffness of a transverse shaft crack accurately. These two models generated a much lower stiffness in the transitional regions (crack partially open) than that measured experimentally. These two models are widely used in the previous investigations to build a Finite Element model. Therefore, Crack location and depth predicted by Finite Element models are inaccurate. Further work is urgently needed to develop more accurate and reliable crack models, which are able to represent the stiffness variation in the transitional regions.

- ✓ In the modal test study, the four types of shaft resonance frequency responses in the X-axis direction had been identified, and the changes of critical frequency were addressed. The cause of reduction in frequency from intact shaft to wire-cut cracked shafts were analysed in association with their decrease in stiffness. It was experimentally proved that the decrease in frequency was almost proportional to the reduction in stiffness.

Also, the vibration responses were found to be amplified by the crack element, the wider the crack gap resulted in higher frequency responses.

6.3 Recommendations for Future Work

The topic of the present work has been one of the most important research topics in the predictive maintenance field. This area has a good research potential in view of the field requirements for the smooth operation of critical machinery and equipment. The approach of the current research work can be extended further to consider the following:

- Create shaft specimens with cracks at different locations and with various depths.
- Measure the bending stiffness as well as torsional stiffness of the cracked shafts.
- Use proximity probes to measure the shaft deflection in the x and y axis directions during rotation in the Machinery Fault Simulator (MFS).
- Analyse the shaft's bending stiffness in relation with the deflection and, the torsional stiffness in relation with the torsional frequency response.
- Investigate the rotational orbit of the cracked rotor near the first critical speed.
- Conduct an online experiment of the cracked shaft with an unbalanced fault acting simultaneously.

- Develop a finite element model (FEM) by using COMSOL software to simulate the dynamic properties of a cracked shaft based on created specimens.
- Carry out a comparative study to validate the FEM modeling algorithm with experimental results obtain from an online test.

REFERENCES

1. Al-Shudeifat, M. A., and Butcher, E. A. (2011). New breathing functions for the transverse breathing crack of the cracked rotor system: Approach for critical and subcritical harmonic analysis. *Journal of Sound and Vibration, 330*(3), 526-544.

2. Bachschmid, N., Pennacchi, P., Tanzi, E., and Vania, A. (2000). Identification of Transverse Crack Position and Depth in Rotor Systems. *Meccanica, 35*(6), 563-582.

3. Bachschmid, N., Tanzi, E., and Audebert, S. (2008). The effect of helicoidal cracks on the behaviour of rotating shafts. *Engineering Fracture Mechanics, 75*(3-4), 475-488.

4. Boyer, H. E. (2006). Atlas of fatigue curves In A. international (Eds.) section1, p.2.

5. Carden, E. P., and Fanning, P. (2004). Vibration Based Condition Monitoring: A Review. *Structural Health Monitoring, 3*, 355-377.

6. Chan, R. K. C., and Lai, T. C. (1995). Digital simulation of a rotating shaft with a transverse crack. *Applied Mathematical Modelling, 19*(7), 411-420.

7. Chen, W. J., and Gunter, E. M. (2005). *Introduction to Dynamics of Rotor-Bearing Systems*. Chapter 3, p.55.

8. Collins, K. R., Plaut, R. H., and Wauer, J. (1991). Detection of Cracks in Rotating Timoshenko Shafts Using Axial Impulses. *Journal of vibration and Acoustics, 113*(1), 74-78.

9. Darpe, A. K. (2007). Dynamics of a Jeffcott rotor with slant crack. *Journal of Sound and Vibration, 303*(1-2), 1-28.

10. Dimarogonas, A. D. (1970). Dynamic response of cracked rotors. General Electric Co. *Internal report, Schenectady,NY,USA, 1970.*

11. Dimarogonas, A. D., and Papadopoulos, C. A. (1983). Vibration of cracked shafts in bending. *Journal of Sound and Vibration, 91*(4), 583-593.

12. Dimarogonas, A. D. (1996). Vibration of cracked structures: A state of the art review. *Engineering Fracture Mechanics, 55*(5), 831-857.

13. Dirr, B. O., Popp, K., and Rothkegel, W. (1994). Detection and simulation of small trasverse cracks in rotating shafts. *Archive of Applied Mechanics, 64*(3), 206-222.

14. Dong, G. M., Chen, J., and Zou, J. (2004). Parameter identification of a rotor with an open crack. *European Journal of Mechanics - A/Solids, 23*(2), 325-333.

15. Gasch, R. (1993). A Survey Of The Dynamic Behaviour Of A Simple Rotating Shaft With A Transverse Crack. *Journal of Sound and Vibration, 160*(2), 313-332.

16. Gasch, R. (2008). Dynamic behaviour of the Laval rotor with a transverse crack. *Mechanical Systems and Signal Processing, 22*(4), 790-804.

17. Guo, D., and Peng, Z. K. (2007). Vibration analysis of a cracked rotor using Hilbert-Huang transform. *Mechanical Systems and Signal Processing, 21*(8), 3030-3041.

18. Han, D. J. (2007). Vibration analysis of periodically time-varying rotor system with transverse crack. *Mechanical Systems and Signal Processing, 21*(7), 2857-2879.

19. He, Y., Guo, D., and Chu, F. (2001). Using genetic algorithms and finite element methods to detect shaft crack for rotor-bearing system. *Mathematics and Computers in Simulation 57*, 95-108.

20. Ishida, Y., and Inoue, T. (2006). Detection of a Rotor Crack Using a Harmonic Excitation and Nonlinear Vibration Analysis. *Journal of vibration and Acoustics, 128*(6), 741-749.

21. Jun, O. S., and Eun, H. I. (1992). Modeling and vibration analysis of a simple rotor with a breathing crack, **155**(1992), 273-290.

22. Kumar, C., and Rastogi, V. (2009). A Brief Review on Dynamics of a Cracked Rotor. *International Journal of Rotating Machinery, 2009*, 6 pages.

23. Lebold, M. S., Maynard, K., Reichard, K., Trethewey, M., Bieryla, D., Lissenden, C., and Dobbins, D. (2004, 6-13 March 2004). *Using torsional vibration analysis as a synergistic method for crack detection in rotating equipment.* Paper presented at the Aerospace Conference, 2004. Proceedings. 2004 IEEE.

24. Lee, Y.-S., and Chung, M.-J. (2000). A study on crack detection using eigenfrequency test data. *Computers & Structures, 77*(3), 327-342.

25. Lissenden, C. J., Tissot, S. P., Trethewey, M. W., and Maynard, K. P. (2007). Torsion response of a cracked stainless steel shaft. *Fatigue & fracture of engineering materials & structures, 30*(8), 734-747.

26. Mayes, I. W., and Davis, W. G. R. (1984). Analysis of the response of a multi-rotor-bearing system containing a transverse crack in a rotor.

Journal of vibration, acoustics, stress, and Reliability in Design, 106, 139-145.

27. Mobley, R. K. (1999). Vibration fundamentals. In P. E. magazine (Eds.) Plant engineering maintenance series chapter 1. p.26.

28. Mohiuddin, M. A., and Khulief, Y. A. (2002). Dynamic Response Analysis of Rotor-Bearing Systems With Cracked Shaft. *Journal of Mechanical Design, 124*(4), 690-696.

29. Nagaraju, C., Rao, K. N., and Rao, K. M. (2009). Application of 3D wavelet transforms for crack detection in rotor systems. *Sadhana-Academy Proceedings in Engineering Sciences, 34*(3), 407-419.

30. Papadopoulos, C. A. (2008). The strain energy release approach for modeling cracks in rotors: A state of the art review. *Mechanical Systems and Signal Processing, 22*(4), 763-789.

31. Pennacchi, P., Bachschmid, N., and Vania, A. (2006). A model-based identification method of transverse cracks in rotating shafts suitable for industrial machines. *Mechanical Systems and Signal Processing, 20*(8), 2112-2147.

32. Penny, J. E. T., and Friswell M. I. (2003). Simplified Modelling of Rotor Cracks. *Key Engineering Materials Volumes 245 - 246*, 223-232.

33. Prabhakar, S., Sekhar, A. S., and Mohanty, A. R. (2001). Detection And Monitoring Of Cracks In A Rotor-Bearing System Using Wavelet Transforms. *Mechanical Systems and Signal Processing, 15*(2), 447-450.

34. Prabhakar, S., Sekhar, A. S., and Mohanty, A. R. (2001). Detection and monitoring of cracks using mechanical impedance of rotor-bearing system. *The Journal of the Acoustical Society of America, 110*(5), 2351-2359.

35. Sabnavis, G., Kirk, R. G., Kasarda, M., and Quinn, D. (2004). Cracked Shaft Detection and Diagnostics: A Literature Review. *The Shock and Vibration Digest, 36*(4), 287-296.

36. Sekhar, A. S., and Prabhu, B. S. (1992). Crack detection and vibration characteristics of cracked shafts. *Journal of Sound and Vibration, 157*(2), 375-381.

37. Sekhar, A. S. (2004). on-line rotor fault identification by combineed model and signal based approach. *Noise & vibration worldwide, Volume 35, Number 7* 16-30.

38. Sekhar, A. S. (2004). Crack identification in a rotor system: a model-based approach. *Journal of Sound and Vibration, 270*(4-5), 887-902.

39. Sekhar, A. S. (2005). Identification of unbalance and crack acting simultaneously in a rotor system: Modal expansion versus reduced basis dynamic expansion. [Article]. *Journal of Vibration and Control, 11*(9), 1125-1145.

40. Sekhar, A. S., Mohanty, A. R., and Prabhakar, S. (2005). Vibrations of cracked rotor system: transverse crack versus slant crack. *Journal of Sound and Vibration, Volume 279*(Issue 3-5), p. 1203-1217.

41. Sinha, J. K. (2007). Higher order spectra for crack and misalignment identification in the shaft of a rotating machine. *Structural Health Monitoring, 6*(4), 325-334.

42. Wauer, J. (1990). On the Dynamics of Cracked Rotors: A Literature Survey. *Applied Mechanics Reviews, 43*(1), 13-17.

43. Xie F., Liu L., and Ganeriwala S. (2007). Simulation and Vibration Analysis of Shaft Cracks. *SpectraQuest Tech Notes*.

44. Yu, T., Han, Q.-K., Qin, Z.-Y., and Wen, B.-C. (2006). Identification of Crack Location and Depth in Rotating Machinery Based on Artificial Neural Network. *Advances in Neural Networks - ISNN 2006, 3973/2006,*, 982-990.

45. Zou, J., Chen, J., Pu, Y. P., and Zhong, P. (2002). On the wavelet time-frequency analysis algorithm in identification of a cracked rotor *The Journal of Strain Analysis for Engineering Design, 37*(3), 239-246.